Palaeobiodiversity and Palaeoenvironments (2022) 102:1–38
https://doi.org/10.1007/s12549-021-00488-x

SENCKENBERG

ORIGINAL PAPER

Early Priabonian *Mesophyllum* dominated coralline algal assemblage from coastal upwelling settings (Central Carpathian Paleogene Basin, Slovakia)

Juraj Hrabovský[1] · Dušan Starek[1] · Katarína Holcová[2] · Kamil Zágoršek[3]

Received: 7 May 2020 / Revised: 18 August 2020 / Accepted: 15 February 2021 / Published online: 22 July 2021

Abstract

The studied transgressive deposits record the imprints of the coastal upwelling affecting the distribution of the shallow-water benthic assemblage in the early Priabonian Central Carpathian Paleogene Basin (CCPB). Our inferences are based on the study of benthic and planktonic assemblages, with special emphasis on the coralline algal (CRA) system, and the facies development at the Štrba locality. We have observed the development of cool-water carbonates on warm-water carbonate platforms. Coralline algal assemblage predominated through hapalidialids, rhodalgal and bryomol grain associations; specific microborings and calcareous nannoplankton in the Štrba locality are indicative of cool-water, while nummulite banks and hermatypic corals from adjacent and distant sites within the basin are indicative of warm-water carbonates. The last mentioned are indicative of oligotrophic and euphotic settings, while nannoplankton, bryozoans and mollusks suggest mesotrophic conditions. Given the above, our results show the heterogeneous distribution of sea water temperature and nutrients that are characteristic for recent seasonal wind or eddy-driven coastal upwelling ecosystems (e.g. in the Mediterranean Sea). Upwelled cold and nutrient-enriched water enhanced the expansion of suspension feeders and favoured the growth of cool-water CRA with gametophytic phases. In the seasons without upwelling, nummulits could thrive in warm-water settings. This mechanism well explain why extensive nummulit banks were developed in adjacent sites but were not in the Štrba locality. The section is topped by bryozoan marlstone with glaucony. This lithofacies indicates the deepening of the basin. Here we were not able to discriminate between agents causing nutrification (e.g. upwelling, river plumes or gradual cooling) and the associated mesotrophication of the environment during the climatic deterioration documented across the CCPB.

Keywords Central Carpathian Paleogene Basin · Priabonian · Coralline algae · Systematics · Palaeoecology · Upwelling

Introduction

The Central Carpathian Paleogene Basin (CCPB) of the West Carpathians was an epicontinental sea with deposition controlled by both climate and tectonics (e.g. Soták et al. 2001; Soták 2010; Starek et al. 2012). The CCPB suffered some major climatic events: the Middle Eocene Climatic Optimum (MECO) in the Lutetian–early Priabonian; climate deterioration in the Priabonian terminated with the Terminal Eocene Event at the Eocene/Oligocene accompanied by a sharp drop in temperature (Soták 2010). The studied section was correlated chronostratigraphically and lithostratigraphically with the Priabonian of the Borové Formation; therefore, the influence of the MECO, climate deterioration in the Priabonian and Terminal Eocene Event at the end of the Priabonian is expected. While MECO is characterised by the growth of warm-water carbonates with nummulites and/or corals in euphotic and oligotrophic settings, climate

✉ Juraj Hrabovský
geoljuhr@savba.sk

Dušan Starek
geolstar@savba.sk

Katarína Holcová
holcova@natur.cuni.cz

Kamil Zágoršek
kamil.zagorsek@gmail.com

[1] Slovak Academy of Sciences, Dúbravská Cesta 9, 840 05 Bratislava, Slovakia

[2] Institute of Geology and Palaeontology, Charles University, Albertov 6, 128 43 Prague 2, Czech Republic

[3] Department of Geography, Technical University of Liberec, Studentská 2, 461 17 Liberec, Czech Republic

deterioration is marked by (1) nutrient enrichment of the sea water associated with the heterotrophic assemblage expansions and (2) growth of cool-water carbonates, both commonly explained by upwelling conditions, nutrient runoff from river plumes or volcanic activity (e.g. Zágoršek 1992; Zágoršek and Kázmér 1999; Soták 2010). It is well known that all these influence the recent benthic as well as planktonic assemblages (Iryu et al. 1995; Glynn and Leyte Morales 1997; Glynn et al. 2017; Guerry and Menge 2017; Bode et al. 2017; Masotti et al. 2018; Wilson et al. 2019). However, no data are known from CCPB about the imprints of these events on the Coralline Red Algal (CRA) assemblage.

Coralline algae are predominantly marine benthic organisms, commonly investigated in early Tertiary limestones (e.g. Lemoine 1934; Johnson 1948, 1952, 1953, 1964, 1965; Bassi 2005; Ishijima 1960; Rasser 1994; Rasser and Piller 1994, 1999; Rasser 2001; Sarkar and Rao 2018; Ghosh et al. 2013; Schaleková 1962, 1963, 1964). They have wide latitudinal and depth distributions, reaching from the polar region to the tropics, and from inter-tidal settings down to depths of 268 m (Teichert et al. 2012; Adey et al. 1982; Verheij 1993; Bosence 1976; Littler et al. 1985; Basso et al. 2009; Žuljević et al. 2016). A remarkable feature of corallines is the impregnation of the cell walls by calcium carbonate (Johansen 1981; Silva and Johansen 1986; Basso 2012), strengthening the tissue and enhancing their fossilisation potential. Thus, CRA enter into the numerous biocoenosis and lithofacies that are found in the recent and ancient shelf deposits (Pérès and Picard 1964; Pérès 1982; Seneš and Ondrejčíková 1991).

There is a considerable amount of literature on the palaeoecology of the CCPB (e.g. Andrusov 1937; Mišík 1966; Samuel et al. 1972; Zágoršek 1992, 1997; Zágoršek and Kázmér 1999; Gedl 2000; Chalupová 2000; Soták et al. 2007; Garecka 2005; Soták 2010). However, modern research lacks adequate data on CRA assemblage from CCPB. What we know about CRA is largely based on the few publications from the last century (Lemoine 1934; Andrusov 1937; Schaleková 1962, 1963, 1964; Samuel et al. 1972; Mišík 1966; Moussavian 1989; Köhler 1995). Only Lemoine (1934) and Schaleková (1962, 1964) deal with the systematics, at the same time representing the last research on the CCPB coralline algal taxonomy. There are, however, two problems hampering the application of published species in the palaeoecological interpretations described below.

The first is a taxonomic problem. This phenomenon is known in many fossil groups and results from the distinct concepts used for species identification in the past versus the modern one. The CRA assemblage description from the Western Carpathians was carried out in the early twentieth century by Lemoine (1934), who studied samples from the locality Považie (e.g. Hričov, Považská Bystrica). Early Tertiary algae including Lemoine's type material were later studied by Schaleková (1962, 1963 and 1964). Although their contribution is interesting, it suffers from a lack of valuable diagnostic features for species classification in that the specimens are mostly sterile. Another striking feature emerging from the published material of CCPB algae is the lack of gametophytes. By contrast, the modern classification of CRA is based on asexuate plants (Johansen 1981; Le Gall et al. 2010; Nelson et al. 2015) as well as on gametophytes and carposporophytes (Athanasiadis and Ballantine 2014). Summarising the data on Eocene CRA from CCPB, 35 species are known, 28 are non-geniculate and 7 geniculate; however, only 10 of the non-geniculate are fertile (Schaleková 1962, 1963, 1964). Since the known CCPB fertile species bears either calcified sporangial compartments or multiporate sporangial conceptacles (Lemoine 1934; Schaleková 1962, 1964), they can be classified within the Sporolithales or Hapalidiales orders (Le Gall et al. 2010; Nelson et al. 2015), but further revision of museal collection and investigation of the new collections is required for the correct assessment of these species into certain genera.

The second problem is associated with the stratigraphic context, because there has been some disagreement concerning the age of the CRA limestones. Some of the Paleocene localities, including the CRA type locality Hričov (Köhler 1995), were known as Eocene (Lemoine 1934; Andrusov 1937; Schaleková 1962, 1964). Although the ages of most of the sites were established based on the basis of large foraminifers (e.g. Samuel et al. 1972; Köhler 1995), the stratigraphic positions of other sites remained uncertain until the publication of Buček et al. (2013) and Filo et al. (2009). The carbonate and mixed carbonate–siliciclastic deposits of some localities (e.g. Hybica) stratigraphically cover the late Bartonian, early Priabonian and late Priabonian (Buček et al. 2013). Therefore, stratigraphic position of some CRA specimens described prior to 2009 remains unknown.

In this paper, we have identified CRA species from the CCPB. Facies are examined in order to provide the proper view on CRA palaeoecology and distribution. Biostratigraphical research on the studied site enables CRA assemblage correlation and the provision of valuable information improving our knowledge about Priabonian CRA. Last but not least, the aim of our work is to extend the current knowledge of the ecological influence on limestone formation in the CCPB during this time interval.

Material and methods

In order to improve the biostratigraphic framework, we have analysed calcareous nannoplankton from 12 samples (Table 1). The slides for optical microscopy were prepared according to the methods described in Zágoršek et al. (2008, p. 387). The slides were studied using an Olympus optical microscope with a ×1000 magnification. Usually 300 nannofossils were counted to determine the relative abundance of taxa. At least 100 coccoliths were counted per slide in coccolith-poor samples. A tentative

Table 1 Abundance and preservation state of the calcareous nannoplankton.

Species Sample	B0	B1	B2	B2lateral	B3	B3b	B4	B4a	B4b	B5	B6	B6a	Stratigraphical range from Young et al. 2019
Reticulofenestra bisecta (Hay, Mohler and Wade, 1966) Roth, 1970	27.78	31.30	34.67	37.40	34.62	48.70	45.45	28.57	22.37	43.70	21.13	17.31	NP17-NN1
Coccolithus pelagicus (Wallich 1877) Schiller, 1930	13.89	13.91	21.33	15.45	11.54	10.43	5.45	4.39	6.58	21.01	7.04	0.00	NP2-Recent
Reticulofenestra stavensis (Levin and Joerger, 1967) Varol, 1989	0.00	1.74	4.00	0.00	0.58	2.61	0.91	10.71	2.63	3.36	2.82	4.03	NP17-NN1
Lanternithus minutus Stradner, 1962	25.00	26.96	12.00	21.14	10.00	6.96	14.55	7.14	9.21	10.08	18.31	13.46	NP14-NP23
Cyclicargolithus floridanus (Roth and Hay, in Hay et al., 1967) Bukry, 1971	22.22	17.39	4.00	8.13	26.92	16.52	15.45	14.29	22.37	9.24	22.54	7.69	NP15-NN6
Reticulofenestra westerholdii Bown and Dunkley Jones, 2012	2.78	0.87	4.52	3.25	10.77	11.30	6.36	0.00	19.74	0.00	8.02	17.31	NP16-NP20
Reticulofenestra erbae (Fornaciari et al., 2010) Bown and Newsam 2017	2.78	0.00	0.00	0.00	0.00	1.74	0.91	10.71	0.00	0.00	0.82	3.85	NP17-NP20
Reticulofenestra reticulata (Gartner and Smith, 1967) Roth and Thierstein, 1972	0.00	0.00	0.00	0.00	0.77	0.43	0.00	0.00	0.00	0.84	0.00	0.00	NP16-NP20
Reticulofenestra minuta Roth, 1970	0.00	4.35	14.67	0.00	0.00	0.00	1.82	0.00	11.84	3.70	9.86	30.77	NP13-Pliocene
Zygrhablithus bijugatus (Deflandre in Deflandre and Fert, 1954) Deflandre, 1959	0.00	1.74	2.67	11.38	0.00	0.00	0.00	17.86	0.00	0.84	0.00	0.00	NP9-NN1
Micrantholithus vesper Deflandre 1950	0.00	0.00	1.33	0.00	0.00	0.00	0.00	0.00	0.00	0.00	0.00	0.00	NP10-NN4
Sphenolithus moriformis (Brönnimann Stradner, 1960) Bramlette and Wilcoxon, 1967	0.00	0.00	0.59	2.44	2.31	0.00	1.53	2.81	0.00	3.36	0.00	0.00	NP5-NN15
Thoracosphaera sp.	5.56	0.00	0.00	0.00	0.00	0.87	4.55	0.00	2.63	0.00	4.23	2.21	Mesozoic_Recent
Reticulofenestra daviesii (Haq, 1968) Haq, 1971	0.00	0.87	0.00	0.00	1.54	0.00	0.00	0.00	0.00	0.00	0.00	0.00	NP14-NN2
Sphenolithus spiniger Bukry, 1971	0.00	0.00	0.00	0.00	0.95	0.00	0.00	0.00	0.00	0.00	0.00	0.00	NP14-NP17
Chiasmolithus solitus (Bramlette and Sullivan, 1961) Locker, 1968	0.00	0.00	0.00	0.00	0.00	0.00	0.00	0.00	0.00	0.84	0.00	0.00	NP9-NP16
Hayella simplex Bown and Dunkley Jones, 2006	0.00	0.00	0.00	0.00	0.00	0.00	0.00	0.00	0.00	1.68	1.41	0.00	NP14-NP16
Chiasmolithus grandis (Bramlette and Riedel, 1954) Radomski, 1968	0.00	0.00	0.00	0.00	0.00	0.00	0.00	0.00	0.00	0.00	0.46	1.92	NP11-NP17
Reticulofenestra hillae Bukry and Percival, 1971	0.00	0.00	0.00	0.00	0.00	0.00	0.43	0.00	0.00	0.00	0.00	0.00	NP17-NP22
Reticulofenestra hampdenensis Edwards, 1973	0.00	0.00	0.00	0.00	0.00	0.00	1.25	0.00	0.00	0.00	0.00	0.00	NP14-NP20
Braarudosphaera bigelowii (Gran and Braarud 1935) Deflandre, 1947	0.00	0.00	0.00	0.00	0.00	0.00	0.91	0.00	0.00	0.00	0.00	0.00	Mesozoic-Recent

Table 1 (continued)

Species Sample	B0	B1	B2	B2lateral	B3	B3b	B4	B4a	B4b	B5	B6	B6a	Stratigraphical range from Young et al. 2019
Chiasmolithus modestus Perch-Nielsen, 1971	0.00	0.00	0.00	0.00	0.00	0.00	0.00	0.00	0.00	0.00	0.00	1.32	NP15-NP17
Helicosphaera compacta Bramlette and Wilcoxon, 1967	0.00	0.94	0.00	0.81	0.00	0.00	0.00	0.00	0.00	0.00	2.38	0.00	NP16-NP24
Calcidiscus bicircus Bown, 2005	0.00	0.00	0.00	0.00	0.00	0.00	0.00	3.57	0.00	0.00	1.04	0.00	NP12-NP17
Reticulofenestra umbilicus (Levin, 1965) Martini and Ritzkowski, 1968	0.00	0.00	0.00	0.00	0.00	0.00	0.00	0.00	1.32	0.00	0.00	0.00	NP16-NP22
Syracosphaera tanzanensis Bown, 2005	0.00	0.00	0.00	0.00	0.00	0.00	0.00	0.00	0.00	2.50	0.00	0.00	NP16-NN4
Abundance of calcareous nannoplankton	Very rare	Rare	Rare	Rare	Common	Common	Abundant	Rare	Common	Rare	Rare	Common	
Preservation of nannoplankton	Moderate	Moderate	Moderate	Moderate	Good	Good	Moderate	Moderate	Poor	Moderate	Moderate	Poor	

abundance of nannoliths in the rock were expressed semiquantitatively as numbers of nannoliths/visual field of microscope (abundant: more than 10 specimens in the visual field; common: 3–10 specimens in the visual field; rare: 1–2 specimens in the visual field; very rare: 1 specimen in two or more visual fields). The preservation of the calcareous nannoplankton was evaluated using the simplified classification of Steinmetz (1979): good, no evidence of etching or overgrowth; moderate, etching or overgrowth is apparent; poor, significant etching or overgrowth (Table 1).

Thirty-four thin sections were analysed for the study of the following: grain associations, abrasion degree of large foraminifera, endolith associations, taxonomy and quantification of CRA. The analyses were performed with an AXIOZEISS scope A1 light microscope equipped with an AXIOCAM 105 Color camera and a Leica MZ6 stereomicroscope equipped with a Leica EC3 camera. Quantification was performed using a point-counting method in Jmicrovision (Roduit 2001) software. Scanning electron microscope (SEM) analyses were done in order to study the fine-scale diagnostic characteristics of CRA and bryozoans. For this purpose, two thin sections and two polished slabs were etched in one percent HCl for 40–60 s, in the case of the CRA. This method is the modified approach of Braga et al. (1993). Samples were analysed with SEM JEOL JSM-3690LV. We have found that all of the CRA thalli show a diagenetic structure that prevents fine-scaled diagnostic characteristics from being used in a systematic description (Fig. 1).

Endoliths were studied in thin sections; hence, the boring structures can be observed only in 2D slides. The infilling of structures and cementation of rock caused that the application of the vacuum cast-embedding technique was unsuccessful (Golubic et al. 1983; Wisshak 2012). This hampered the detailed reconstruction of the 3D morphology of the boring structures. We have classified the borings according to their size as follows: (1) macroborings of more than 300 μm and (2) microborings of less than 300 μm in diameter (Checconi et al. 2010).

We followed the extended Wright (1992) classification of carbonates for microfacies description. In the description of grain association, we follow Carannante et al. (1988), Nelson et al. (1988) and Flügel (2004). We think that this approach is strongly subjective, especially when considering rhodalgal and bryomol grain association. The first assemblage type is dominated by CRA (typically >80%) but locally can also contain abundant bryozoans (~uo to 50% in transitional types) (Carannante et al. 1988; Hayton et al. 1995), while the second assemblage type is dominated by bryozoans (>50%) and mollusks are frequent, and CRA are typically below 10% (Nelson et al. 1988; Hayton et al. 1995). From this point of view, some assemblages observed in our study, i.e. bryozoans and mollusks are frequent but CRA still attain ~30% are transitional between bryomol and rhodalgal types. In order to facilitate the interpretations, the samples with CRA exceeding ~20–30%

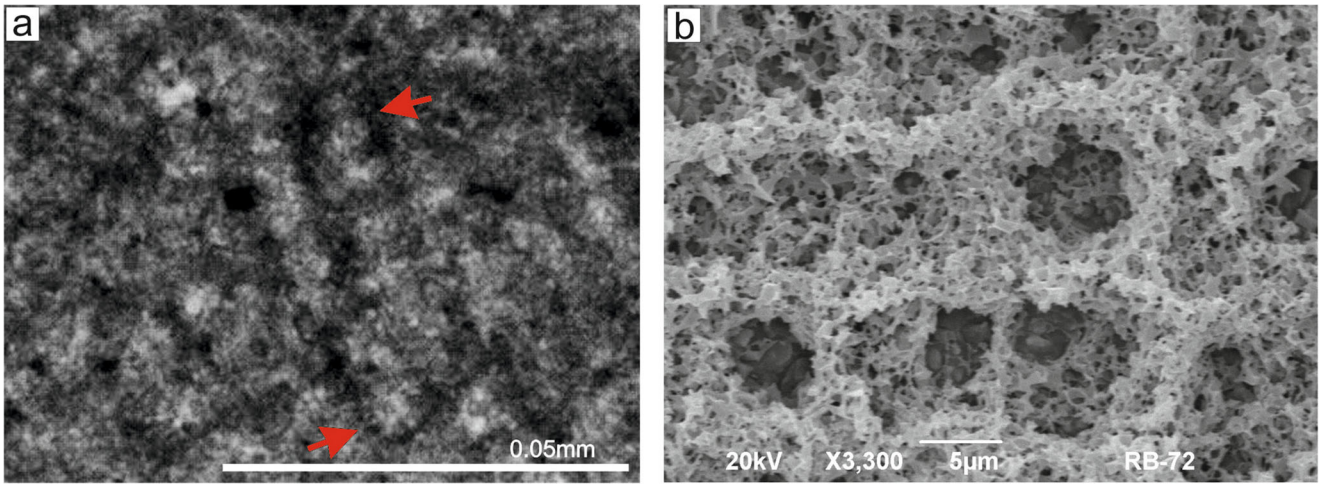

Fig. 1 Detailed photographs of the coralline algal thalli. **a** Photograph of the thallus pointing to the thick and irregular cell wall structure; **b** SEM photograph shows diagenetically altered cell walls

are still assigned to the rhodalgal assemblages whereas the samples with dominant bryozoans and rare CRA (<10%) are assigned to the bryomol assemblage in our study. The determination of biogenic limestone components was necessary. Excluding calcareous nannoplankton, CRA and SEM studied bryozoans, the identification of others in the thin sections follows the common morphological characteristics, e.g. in Flügel (2004), Hageman et al. (1998), Mišík (1966) and Samuel et al. (1972). Special attention was given to (1) CRA description where we follow Hrabovský et al. (2015), and to (2) Bryozoa description, where we follow the method described in Zágoršek and Vávra (2000). However, the approaches in bryozoan identification using SEM and Microscopy markedly differ, as the latter does not provide valuable diagnostic data. Therefore, we determine morphologies only, following the figures of sectioned and polished 3D specimens in Zágoršek (1996), Figs 4, 6, p. 526 erect colonies; Figs 3, 5, p. 528 globular colonies). Coralline algal growth forms of Woelkerling et al. (1993), Sola et al. (2013) and Beavington-Penney et al. (2004) were used. The thickness of the thalli and subsequent determination of the CRA morphology used in the palaeoecological interpretations follow Steneck (1986). The abrasion degree of large foraminifera proposed by Beavington-Penney (2004) was also used, so that we were able to analyse the palaeoecological influence on the biogenic assemblages found in the Štrba section.

Geological settings

The CCPB lies inside the Western Carpathian Mountain chain (Fig. 2(a)). It belongs to the basinal system of the Peri- and Paratethyan seas. The CCPB opening and evolution is probably related to crustal thinning, either as a result of subcrustal erosion (Kázmér et al. 2003), or due to the extensional collapse of the overthickened Central Western Carpathian crust and the pull of the External Western Carpathian oceanic lithosphere retreating subduction (Kováč et al. 2016).

The basin covered a large part of the Central Western Carpathian area (Fig. 2(a–b)) and is mainly filled with marine deposits which overlap the older nappe units. Their ages range from the Middle Eocene (Samuel and Fusán 1992; Gross et al. 1980) to the Late Oligocene (Olszewska and Wieczorek 1998; Gedl 2000; Soták et al. 2001, 2007; Garecka 2005). The CCPB sediments are preserved in many structural sub-basins (Fig. 2(b)), located in the Žilina, Rajec, Turiec, Orava, Podhale, Liptov, Poprad and Hornád regions as well as in the Spišská Magura, Levočské vrchy and Šarišská vrchovina Mountains.

The CCPB deposits ("Podtatranská skupina Group" according to Gross et al. 1984; Gross 2008) are divided commonly into the following formations (Fm): the lowermost Borové Fm. (including Hornád Member (Mb), Chrastianske Mb. and Tomášovce Mb., according to Filo and Siráňová 1996, 1998); they consist of breccia, conglomerates, lithic sandstones to siltstones, marlstones, organodetrital and organogenic limestones. They represent basal terrestrial, fluvial-deltaic and shallow marine transgressive deposits (Marshalko 1970; Kulka 1985; Gross et al. 1993; Baráth and

Fig. 2 **a** Location of study area within the Alpine-Carpathian orogen; **b** ▶ the Central Carpathian Paleogene Basin system depicting structural sub-basins, basement massifs and surrounding units; **c** simplified geological sketch of a part of the Liptov and Poprad regions (after Biely et al. 1996; modified) with the studied locality. **d** Situational geological map of the wider area of the studied locality (Geological Map of Slovakia M 1:50,000 [online] ŠGÚDŠ 2013); key: *1 a* roads and railway, *b* rivers, *c* town. *2 a* fluvial deposits (Pleistocene), *b* fluvial deposits (Holocene), *c* glaciofluvial gravels (Pleistocene). *3* diluvial deposits, landslides (Pleistocene-Holocene). *4* Zuberec Formation: turbidite mudstones, siltstones and sandstones (Oligocene). *5* Huty Formation: mudstones in absolute predominance over sandstones and conglomerates (Eocene-Oligocene). *6* Borové Formation: carbonate breccias, conglomerates, sandstones, limestones, marlstones (Eocene). *7* Gutenstein limestones (Triassic). *8* Dolomites (Triassic). *9* Location of studied outcrop (Štrba section: N49°03′44.28″, E20°05′48.39″)

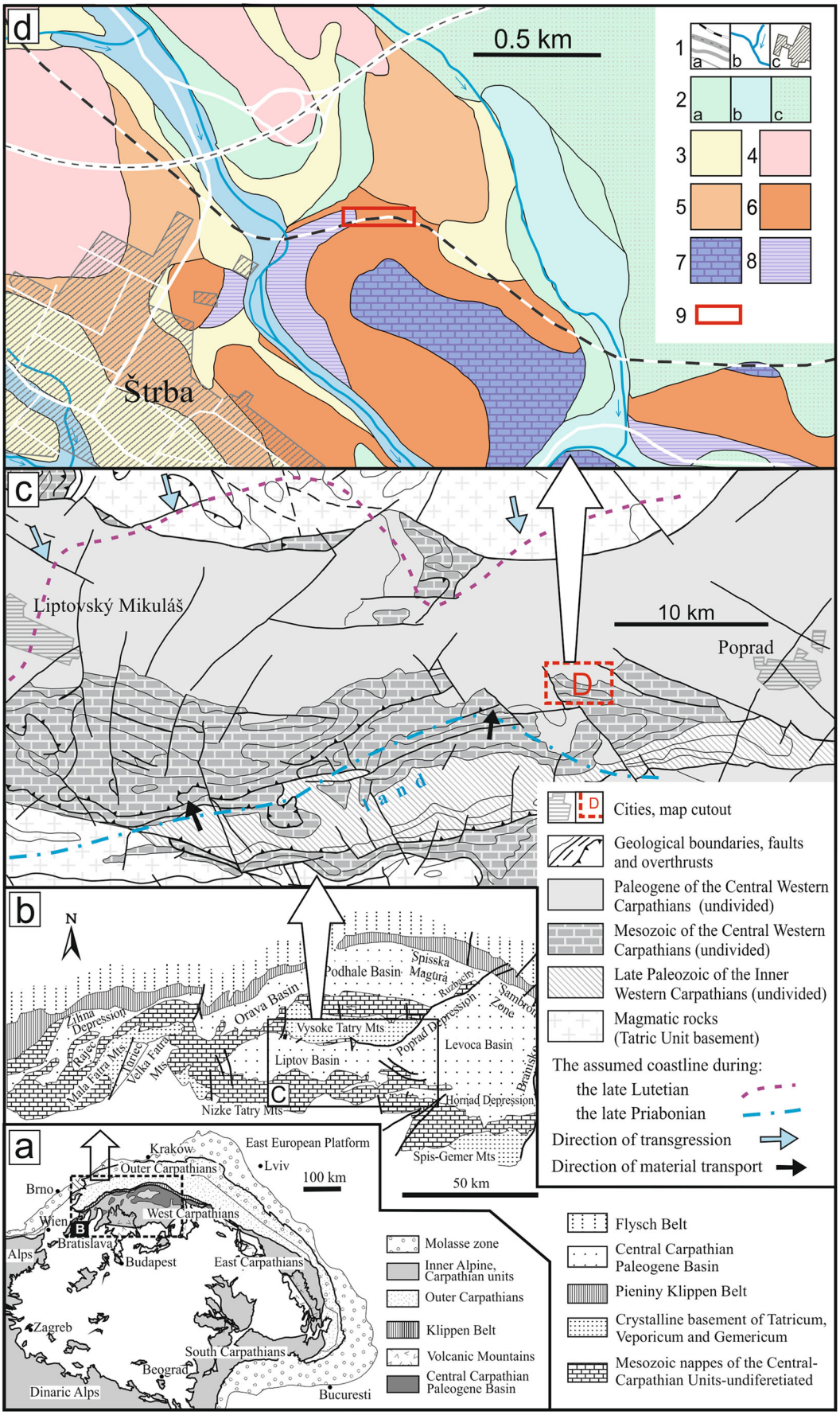
d
0.5 km
Štrba
1 a b c
2 a b c
3
4
5
6
7
8
9
c
Liptovský Mikuláš
10 km
Poprad
D
Tatra Mts
b
N
Podhale Basin
Spisska Magura
Ruzbachy
Sambron Zone
Orava Basin
Zilina Depression
Rajec
Mala Fatra Mts
Tonec
Velka Fatra Mts
Vysoke Tatry Mts
Poprad Depression
Levoca Basin
Liptov Basin
C
Nizke Tatry Mts
Hornad Depression
Branisko
Spis-Gemer Mts
50 km
a
Kraków
East European Platform
Outer Carpathians
Lviv
100 km
Brno
Wien
West Carpathians
B
Bratislava
Alps
Budapest
East Carpathians
Zagreb
South Carpathians
Beograd
Dinaric Alps
Bucuresti
Molasse zone
Inner Alpine, Carpathian units
Outer Carpathians
Klippen Belt
Volcanic Mountains
Central Carpathian Paleogene Basin
Flysch Belt
Central Carpathian Paleogene Basin
Pieniny Klippen Belt
Crystalline basement of Tatricum, Veporicum and Gemericum
Mesozoic nappes of the Central-Carpathian Units-undiferetiated
Cities, map cutout
Geological boundaries, faults and overthrusts
Paleogene of the Central Western Carpathians (undivided)
Mesozoic of the Central Western Carpathians (undivided)
Late Paleozoic of the Inner Western Carpathians (undivided)
Magmatic rocks (Tatric Unit basement)
The assumed coastline during:
the late Lutetian
the late Priabonian
Direction of transgression
Direction of material transport

Kováč 1995; Filo and Siráňová 1996, 1998; Šurka et al. 2012). The ages of the marine deposits range from the late Lutetian to the late Priabonian. The latter is documented only in the Tomášovce Mb. However, the age of the predominantly continental Hornád Mb. was recently established as Paleocene to Middle Eocene (Marshalko 1970; Filo and Siráňová 1996). The Borové Fm. is overlaid by the Huty Fm., which mainly includes various mud-rich shelves to deep marine deposits (Janočko and Jacko 1999; Soták et al. 2001; Starek et al. 2004) intercalated with sandstone megabed events (Starek et al. 2013). The Zuberec Fm. and Biely Potok Fm. (including Kežmarok Mb.) compose the CCPB up-section, predominantly consisting of rhythmically bedded turbidites and massive sandstones, which represent the various sand-rich submarine fans facies associations (Westwalewicz-Mogilska 1986; Wieczorek 1989; Soták 1998; Starek et al. 2000; Sliva 2005; Starek and Fuksi 2017a, 2017b; Starek et al. 2019). The age of the Huty Fm. ranges from the late Priabonian to early Oligocene, and the age of the Zuberec and Biely Potom Fms. was established to be within the Oligocene (Olszewska and Wieczorek 1998; Gedl 2000; Starek et al. 2000; Soták et al. 2001; Garecka 2005; Filipek et al. 2017).

The study area is situated on the border of the Liptov and Poprad depressions (Fig. 2(c)) on the northeastern edge of the village of Štrba (Fig. 2(d)). Quaternary deposits of variable thickness overlay CCPB deposits in its northern part, while the southern border consists of Mesozoic Central Carpathian units (Fig. 2(d)). The evaluated and interpreted deposits are exposed in a railway cut, about 100 m north of Kolombiarok Hill (899.6 m) and about 700 m east of the road connecting the villages of Tatranská Štrba and Štrba (Fig. 2(d)). They are a part of the Borové Fm., represented by basal carbonate breccia and conglomerate, biodetrital limestones and marlstones. These deposits are unconformingly overlying Triassic limestones and dolomites (Fig. 3), and their age is estimated to the early Priabonian, based on the shallow-water benthic foraminifers (Buček et al. 2013).

Results

Biostratigraphy

Calcareous nannoplankton is generally rare, showing common corrosion and the recrystallisation of nannoliths. The highest abundance of nannoplankton was recorded in sample 4. The diversity of assemblages is low in samples 1–3 (the values are 7–10 species per sample) and increases in samples 4–6 (the values are 10–13 species per sample). Reticulofenestras strongly dominate in assemblages; *Coccolithus pelagicus* (Wallich) Schiller, 1930 is common, as well as *Lanternithus minutus* Stradner, 1962, and *Zygrhablithus bijugatus* (Deflandre) Deflandre, 1959 (Table 1, Fig. 3(a)—calcareous nannoplankton distribution).

The stratigraphical ranges of calcareous nannoplankton species from Young et al. (2019) and Gradstein et al. (2012) were used for biostratigraphical interpretations (Fig. 4). The common occurrence of species with First Occurrence (FO) in the NP17 Zone (*Reticulofenestra bisecta* (Hay, Mohler and Wade) Roth, 1970; *R. stavensis* (Levin and Joerger) Varol, 1989; *R. erbae* (Fornaciari et al.) Brown and Newsam, 2017) enables us to correlate the top of the studied section with the NP17 and younger zones. Together with these taxa, the species with the Last Occurrence (LO) in the NP17 Zone were also recorded (*Sphenolithus spiniger* Burky, 1971; *Chiasmolithus grandis* (Bramlette and Riedel) Radomski, 1968; *Ch. modestus* Perch-Nielsen, 1971; *Calcidiscus bicircus* Bown, 2005). This means that the Štrba section can be correlated with the NP17 Zone (Bartonian to early Priabonian). However, the species with the LO in the NP17 Zone are very rare and their reworking cannot be excluded, as is the case for the taxa with LO in the NP16 Zone (*Chiasmolithus solitus* (Bramlette and Sullivan) Locker, 1968; *Hayella simplex* Bown and Dunkley Jones, 2006), which rarely occur in the uppermost part of the section. Then the section might be deposited somewhere over a longer period of time (NP17-NP20 Zone, latest Bartonian to Priabonian). On the other hand, the absence of the common species *Isthmolithus recurvus* Deflandre in Deflandre and Fert, 1954, with the FO in the NP19-20 Zone indicates a possible correlation with the NP17-NP18 Zone.

Sedimentary description

On the basis of the prevailing lithology, the following lithofacies could be allocated within the studied section: (1) basal conglomerate, (2) bioclastic bedded limestone and (3) marlstone (Fig. 3). Basal conglomerates occur at the bottom of the section where they infill uneven erosive relief and directly overlap Mesozoic rocks (Fig. 3(a)). The conglomerate contains clastic material derived from these rocks. Basal conglomerates are poorly sorted with clasts of different size in a range from boulders to pebbles, as well as with a varied degree of clast shaped from angular to oval. They are matrix supported. The sandy carbonate matrix contains CRA, bivalves and bryozoans visible to the naked eye (Fig. 3(g)). Debris, mostly pebbles, are coated with CRA. The conglomerates are no longer present within the overlying beds.

Succession above the basal conglomerate is formed by bioclastic bedded limestone. Thin sandy marlstones are also part of the limestone lithofacies. They are very sporadic in the lower part of this lithofacies, but gradually increase upwards where limestones irregularly intercalate, or they thinly cover the bedforms. The limestone contains a large amount of bioclasts and abundant large marine mollusks arranged in

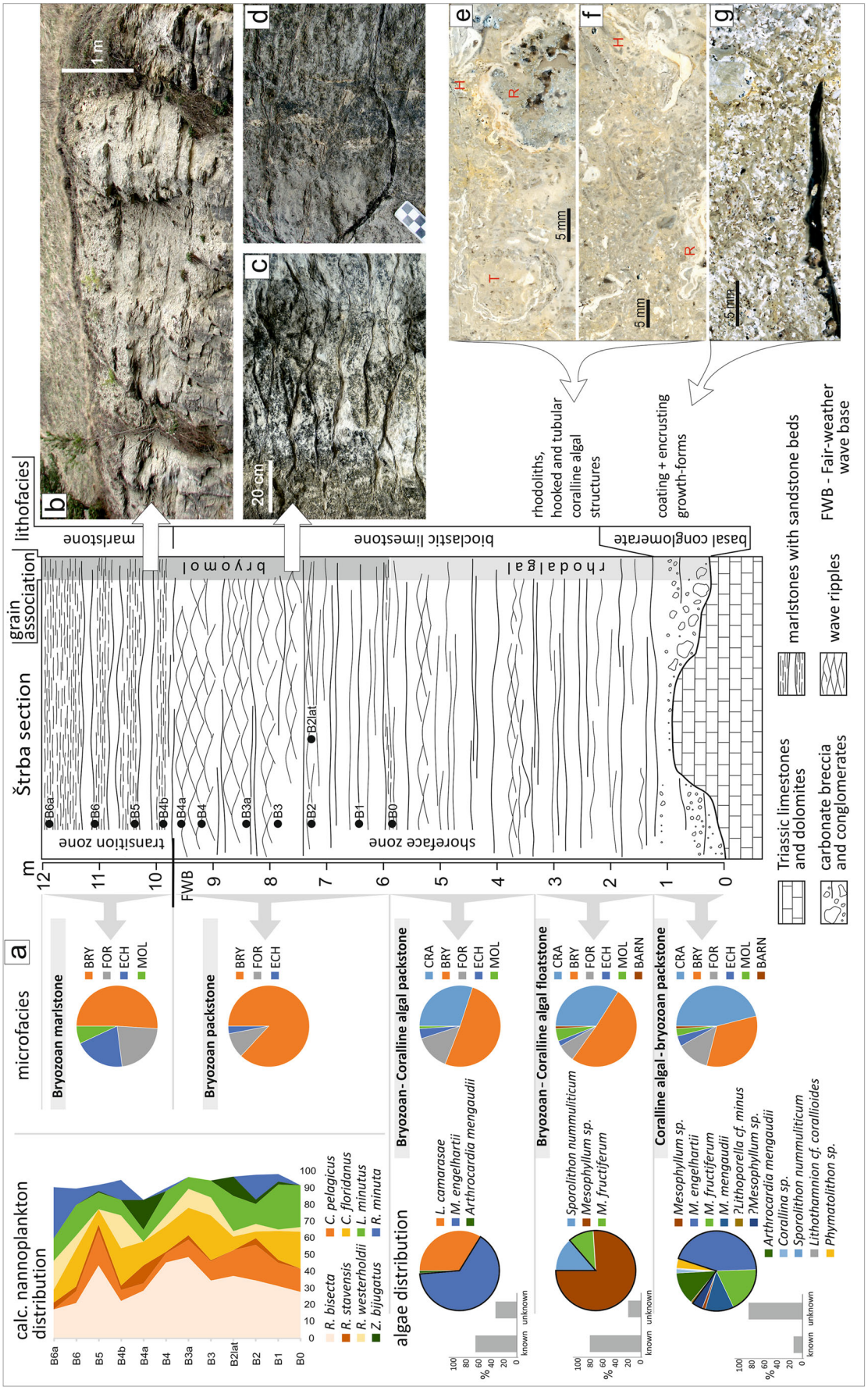
a
microfacies
Štrba section
grain association
lithofacies
m
transition zone
FWB
bryomol
shoreface zone
rhodalgal
marlstone
bioclastic limestone
basal conglomerate
b
c
d
e
f
g
1 m
20 cm
5 mm
rhodoliths, hooked and tubular coralline algal structures
coating + encrusting growth-forms
Triassic limestones and dolomites
carbonate breccia and conglomerates
marlstones with sandstone beds
wave ripples
FWB - Fair-weather wave base
Bryozoan marlstone
Bryozoan packstone
Bryozoan - Coralline algal packstone
Bryozoan - Coralline algal floatstone
Coralline algal - bryozoan packstone
BRY
FOR
ECH
MOL
CRA
BARN
calc. nannoplankton distribution
algae distribution
C. pelagicus
C. floridanus
L. minutus
R. minuta
R. bisecta
R. stavensis
R. westerholdii
Z. bijugatus
L. camarasae
M. engelhartii
Arthrocardia mengaudii
Sporolithon nummuliticum
Mesophyllum sp.
M. fructiferum
?Lithoporella cf. minus
?Mesophyllum sp.
Corallina sp.
Lithothamnion cf. corallioides
Phymatolithon sp.
known
unknown

◀ **Fig. 3** **a** Sedimentary logs of the Štrba section represented by basal carbonate breccia, conglomerate, limestones and marlstones. The chart depicts the vertical distribution of distinguished lithofacies, grain associations and microfacies. Black dots are sampling points for calcareous nannoplankton analyses. Calcareous nannoplankton distribution represents the distribution of the identified species in the section. Microfacies are described in the pie charts where the following abbreviations are used: *CRA* coralline algae, *BRY* bryozoans, *FOR* foraminifera, *ECH* echinoids, *MOL* mollusks, *BARN* barnacles. Algae distribution points to the distribution of CRA in the microfacies where they are documented. The pie charts are supplemented by a volume of identified (known) and unidentified (unknown) thalli. **b** The marlstones with thinner carbonate sandstone beds in the uppermost part of the studied succession; **c** wave-rippled limestones with large amount of bioclasts; **d** small-scale erosional structures documented within shoreface deposits. The scale corresponds to 10 cm. **e**–**g** The limestones of rhodalgal lithofacies with large amounts of corallines, bivalves and bryozoans visible to the naked eye: *R* rhodoliths, *H* hooked structures, *T* section through the proposed three dimensional tubular structures

sub-parallel sets of evenly laminated and wave-rippled beds. Towards the top of this lithofacies, the wave-ripple structures (Fig. 3(c)) are more abundant, and sometimes small-scale erosional structures occur (Fig. 3(d)). Rhodoliths (Fig. 3(e)) along with hooked and proposed tubular CRA growths (Fig. 3(e–f)) are present at the base of this limestone. The rhodoliths have loose internal structure with primary voids and are developed around a muddy core (Fig. 3(e)). Bioclasts including CRA and large bryozoans float in the greyish carbonate matter. Upward, CRA are limited to sporadic debris and rhodoliths. Both decrease and subsequently vanish in the middle part of the bioclastic bedded limestones, and bryozoans with mollusks predominate. However, bryozoans are a significant component of the whole lithofacies.

The uppermost part of the section is formed by marlstone lithofacies with thinner carbonate sandstone beds (Fig. 3(b)). Marlstone is formed by bryozoan colonies that have become visible on its weathered surface. These lithofacies do not contain CRA.

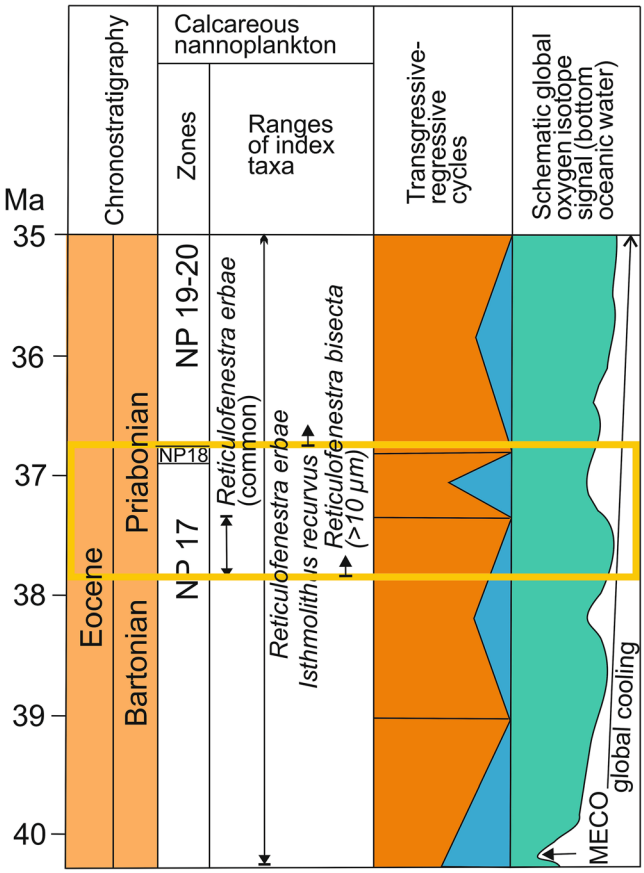

Fig. 4 Stratigraphical correlation of the Štrba section. Chronostratigraphy, calcareous nannoplankton biostratigraphy, oxygen isotopic data and T-R cycles from Gradstein et al. (2012)

Grain association

In general, the fossil assemblage consists of bryozoans, CRA, bivalves, foraminifers, echinoids, barnacles, brachiopods and serpulids. However, the proportion of components significantly differs in the studied lithofacies. On average, basal conglomerates consist of CRA (46%), bryozoans (33%) with a smaller amount of benthic foraminifers (13%) and minor echinoids (4%), bivalves (3%) and barnacles (1%). It is worth noting that the amount of bryozoans in the bioclastic bedded limestone differs in samples with and without CRA. Therefore, in its lower part, the bioclastic bedded limestone contain bryozoans (51%), a variable amount of CRA (30–34%), benthic foraminifers (7–14%), minor echinoids (2–4%) and bivalves (1–5%). In its upper part, the limestone consists of bryozoans (87%), benthic foraminifers (10%) and echinoids (3%). Although bivalves are sporadic in the thin section material, their accumulation in the sub-parallel sets above the rippled structures points to their much higher abundance. The bryozoan marlstone contains bryozoans (51%), foraminifers (22%), echinoids (20%) and bivalves (7%).

We were able to recognise two grain associations—rhodalgal and bryomol. While the rhodalgal is documented in the basal conglomerate and lower part of the bioclastic bedded limestone, the bryomol characterises the upper part of the bioclastic bedded limestone and bryozoan marlstone (Fig. 3). The transition from rhodalgal to bryomol grain association is characterised by the vanishing of CRA and does not match the lithofacies transition because its location is approximately in the middle of the bioclastic bedded limestone.

Microfacies

We have identified five microfacies within the studied section: (1) coralline algal-bryozoan packstone, (2) bryozoan-coralline algal floatstone, (3) bryozoan-coralline algal packstone, (4) bryozoan packstone and (5) bryozoan marlstone.

Coralline algal-bryozoan packstone (Figs. 3(a), 5a) matches with the basal conglomerate. The grain association is rhodalgal. The microfacies contain lithoclasts derived from the underlying

Mesozoic limestones and dolomites. Coralline algae are represented by geniculate forms and encrusting to encrusting-layered growth forms that predominate above the accessory fruticose to warty protuberant growth forms. The latter are represented by two specimens only. Two morphological groups of CRA thalli are recognised in encrusting species—thin and thick. The pebbles are coated by algal species with thin thalli. These thalli are either monostromatic or consist of the thick hypothallus and thin perithallus. Both the thalli and developed crusts are thin, i.e. their thickness is less than 500 μm (Steneck 1986). The prevailing thickness of other thalli is also < 500 μm. The exception is represented by some fertile specimens thicker than 500 μm that occur on the places where conceptacles are present. Thick crusts are developed by species with the thin thalli (1) when multiple overgrowths of a few species occurs or (2) where the thalli of the single specimen show a thickening through the development and fusion of applanate branches. Both types of these thicker crusts are present as fragments. Most of the thin thalli were more robust than those we measured because the upper filaments that usually bear epithallial and meristematic cells were abraded or bioturbated. Other dominant components of this microfacies are bryozoan colonies that are encrusting, globular or erect. The last mentioned are sporadic. However, most of the documented bryozoans are fragments of colonies. Interactions between CRA and bryozoans are exceptional. Among the benthic foraminifera, *Nummulites* is the most abundant genus, while others are represented by agglutinated forms and miliolids. Tests of nummulits show different degrees of abrasion, from generally undamaged or having outer walls damaged on one side of the test to small fragments or damaged tests with shallow pits and holes penetrating them. Bivalves, barnacles, plates and spines of sea urchins and segments of crinoids are minor components. Brachiopods and serpulids are subordinate elements. All kinds of bioclasts are bored by microendolithic organisms. The bioclast s surface is abraded and occasionally pyritized. Pyrite is present in the form of framboids with variated diameter. The pores are incompletely filled with mud. Because the mud is irregularly distributed, its amount can vary in the samples. Empty pores are filled with cement. On average, the muddy compounds form 12%, while cement forms 5% of the sample s volume.

Bryozoan-coralline algal floatstone (Figs. 3(a), 5b–c) consists of globular and encrusting bryozoan colonies, and CRA. It shows rhodalgal grain association. Corallines are present in the form of monospecific rhodoliths with loose internal structure. Corallines forming rhodoliths are of thin thalli; thicker rhodoliths develop after their multiple overgrowth. Other specimens have encrusting growth forms with tubular and hooked morphologies. The same growths have some large encrusting bryozoans. Thin encrusting CRA thalli are formed around large bioclasts; sporadic geniculate specimens are also present. Succession in rhodoliths shows interaction between different competitive sessile organisms such as foraminifers, bryozoans and barnacles that encrusted and settled at the CRA thallus. Minor limestone components include benthic foraminifers, bivalves and echinoids. Thereof, the nummulits are far less common than those in the former microfacies. Coralline algae, bryozoans and bivalves are the largest allochems that float in the muddy matrix. However, detrital compound is also abundant. The muddy matrix and undefined fine-grained detritus are present in 34% and 21%, respectively. Cement was detected in a wide range of hollows after boring activity, inside conceptacles, or bryozoan zoeciae. All kinds of bioclasts are bored by microendolithic organisms, while only rhodoliths, thick coralline algal thalli and bivalves bear traces of macroendoliths. The detected pyrite framboids are variable in diameter.

Bryozoan-coralline algal packstone (Figs. 3(a), 5d) shows rhodalgal grain association. The microfacies consists of densely packed bryozoan colonies; less common are CRA. Bryozoans are present mainly as erect colonies; globular and encrusting ones are not as abundant. The prevailing colonies, however, are damaged. Coralline algae are present as fragments with two exceptions. These are monospecific fruticose-warty protuberant rhodolith and monospecific rhodolith formed by an encrusting layered specimen. The first appears as non-nucleated, while the second overgrows the bryozoan colony. One large fragment of layered CRA above the fragment of massive but damaged CRA specimens was also observed. In general, only scarce large CRA occur in this microfacies. Among the benthic foraminifers, agglutinated and large flat *Operculina*-like specimens predominate, while nummulits tests are highly damaged or present as fragments only. The limestone in this microfacies exposed rippled structures with many bivalves deposited in sub-parallel sets on their planes but was not detected in the thin section material. Poorly preserved bivalves are distributed along the whole length of section but their greatest abundance is in the bioclastic bedded limestone, including both bryozoan–CRA and bryozoan packstone microfacies. All the identified specimens are either *Chlamys* or *Spondylus* genera. Unfortunately, the state of preservation does not allow us to identify the bivalves to the species level. Nevertheless, both are suspension feeders (Temelkov and Andreev 2005; Vokes 2017). Although the echinoids are a minor component of the limestone, echinoid plates can be 2–3 mm in diameter. Other remains are represented by small spines of sea uechins or small skeletal fragments with syntaxial cement around the clasts. The muddy matrix, fine-scaled undefined bioclasts and cement represent 12%, 15% and 1%, respectively. Some micro-fractures are infilled by pyrite, which is also present as framboids of variable diameters in this microfacies.

Bryozoan packstone (Figs. 3(a), 5e) contains predominantly bryozoan colonies represented by erect growth forms. Bryozoans with abundant mollusks deposited in sub-parallel sets above the rippled structures, and with the absence of CRA, define this microfacies as a bryomol grain association. Benthic foraminifers and echinoids are less common. The muddy matrix represents 19%, while fine-scaled undefined bioclastic material and

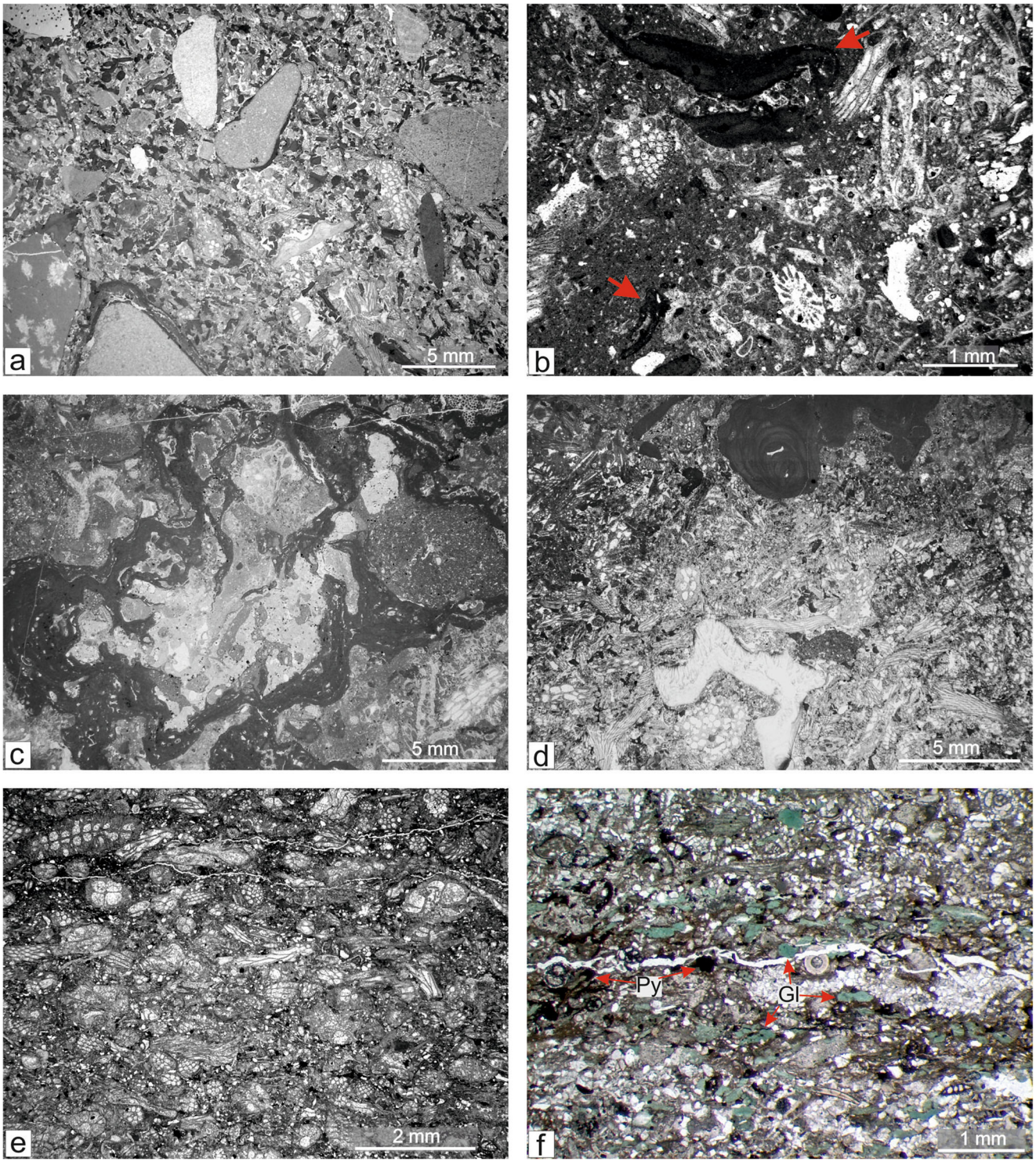

Fig. 5 **a**–**d** Rhodalgal grain association from the Štrba section; **a** basal conglomerate limestone with numerous coralline-coated pebbles in the coralline algal-bryozoan packstone matrix; **b** hooked growth forms of coralline algae from coralline algal-bryozoan packstone (arrows); **c** monospecific rhodolith with loose internal structure and numerous borings caused by endoliths; **d** bryozoan coralline algal packstone. **e**–**f** Bryomol grain association; **e** bryozoan packstone; **f** bryozoan marlstone with glaucony (arrows). Note the common pyrite (arrows) and pyritized foraminiferal tests, as well as the lithoclasts enrichment

lithoclasts are present at 17% and 3%, respectively. The detected pyrite framboids are of variable sizes.

Bryozoan marlstone (Figs. 3(a), 5f) is formed by erect bryozoan colonies, benthic foraminifers, echinoids and

bivalves, therefore, a bryomol grain association. The most remarkable character of bryozoan marls is the glaucony that occurs as intraclast or infill of the bryozoan colonies and foraminifer tests. Pyrite is also common. The detected framboids are variable in diameter. Other pyrite occurrence is spotty or in pyritized foraminiferal tests. Lithoclastic input is relatively high in this part of the section. The volumes of the muddy matrix, fine-sized undefined bioclasts, lithoclasts and cement are 19%, 23%, 6% and 1%, respectively.

Endoliths

The boring structures were observed practically in all the bioclacts, and their diversity is relatively high (Fig. 6a–f). Most of them are less than 300 μm in diameter hence classified here as microborings. The exception is the large rounded to ellipsoidal or irregular sack-like boring structure with a diameter of about 0.5 mm connected to the shell surface by a narrow neck (Fig. 6d–e). The structure is infilled by material similar to the matrix. As causative organisms of these structures could be Porifera, structures resemble final chambers of *Entobia* (e.g. Shweta and Kantimati 2018).

Microborings are identified in different substrates (Fig. 6). Rhodoliths exhibit meandering tunnels with diameters of 20–25 μm, and 40–60 μm; they are rarely bifurcated and partly filled by pyrite (Fig. 6a, c). Larger tunnels (70–90 μm) are filled with the matrix-surrounding bioclasts. Thecideid brachiopods (Fig. 6b) show microborings that are dominated by circular to elliptical structures with diameters between 50 and 75 μm; the peripheral cavities are of variegated and gradually increased diameter from 5 to 25 μm. The infilling of cavities is with pyrite. There are also bioclasts bored with tunnels of variegated diameters between 50 and 100 μm and with branching to narrower tunnels (5–10 μm). The mollusks exhibit corroded surfaces (Fig. 6d). Moreover, they show shallow pits with diameters of about 0.2 mm. Large foraminifera show numerous bifurcating tunnels with diameters of the central tunnels reaching values of 20–25 μm (Fig. 6f); after bifurcation, the tunnels are narrower with diameters of around 10 μm.

Coralline algae

The distribution of identified CRA in defined microfacies differs. However, the identification and quantification of CRA species were limited by the elevated fragmentation of their thalli (Fig. 3—algae distribution). The amounts of non-identified specimens vary in the microfacies from about 86% in coralline algal-bryozoan packstone, and 34% in bryozoan-coralline algal packstone to about 20% in bryozoan-coralline algal floatstone. The remaining two microfacies are barren of CRA. The results below refer to the identified CRA species that represent 14%, 66% and 80% of their total abundance, respectively.

The identified species are from the orders Sporolithales—single species *Sporolithon nummuliticum* (Rothpletz) Ghosh and Maithy, 1996; Hapalidiales—most diversified order with *Lithothamnion camarasae* Pfender, 1926, *Lithothamnion* cf. *corallioides* (Crouan and Crouan) Crouan and Crouan, 1867, *Phymatolithon* sp., *Mesophyllum engelhartii* (Foslie) Adey, 1970, *Mesophyllum fructiferum* Airoldi, 1932, *Mesophyllum mengaudii* (Lemoine) Aguirre, Braga and Bassi, 2011, *Mesophyllum* sp., ?*Mesophyllum* sp., other non-geniculate Corallinales such as ?*Hydrolithon* sp., *Lithoporella* cf. *minus*, and geniculate *Arthrocardia mengaudii* (Lemoine) Aguirre, Braga and Bassi, 2011, and *Corallina* sp. We have identified the gametophytes of the *Lithothamnion camarasae*, *Mesophyllum engelhartii*, *Mesophyllum mengaudii* and ?*Mesophyllum* sp. In general, encrusting coralline algal assemblage is dominated by Hapalidiales, with minor Sporolithales and Corallinales. Gametophytes are known from the hapalidialid species only. Our results suggest that *Mesophyllum* has represented the most diverse and abundant genus of the documented CRA assemblage in Štrba (Table 3, Fig. 3—algae distribution).

Coralline algal-bryozoan packstone predominantly contains encrusting growth forms of *Mesophyllum engelhartii* (45%), *Mesophyllum fructiferum* (19%), *Mesophyllum mengaudii* (12%), ?*Mesophyllum* sp. (4%) and encrusting protuberant *Phymatolithon* sp. (4%). Other species of non-geniculate coralline algae are *Lithoporella* cf. *minus*, *Sporolithon nummuliticum* and *Mesophyllum* sp., each representing 1% of volume. *Lithothamnion corallioides* is present in less than 0.5%. What is striking is the abundance of the geniculate species *Arthrocardia mengaudii* (13%) and *Corallina* sp. (1%).

Bryozoan-coralline algal floatstone consists predominantly of *Mesophyllum* sp. (61%), while *Sporolithon nummuliticum* (11%) and *Mesophyllum fructiferum* (8%) are less common. However, fragments of other species not detected during the point-counting could be present as well. These are *Lithoporella* cf. *minus*, *Phymatolithon* sp. and *Arthrocardia mengaudii*, which are present in very low amounts.

Bryozoan-coralline algal packstone contains two species of non-geniculate corallines *Lithothamnion camarasae* (34%) and *Mesophyllum engelhartii* (65%), as well as single geniculate *Arthrocardia mengaudii* (1%).

Historical collection

Despite the number of outcrops in the Priaboian of CCPB, the assemblages from the Tichá dolina locality were investigated and published exclusively by Schaleková (1962). The dominant rock building components of the limestones are large foraminifera and coralline algae. Schaleková (1962) also reported less common bryozoans and echinoids, and fragments of hermatypic corals. Because of the dominance of phototrophic organisms–nummulites, we classify the assemblage as photozoan. We can

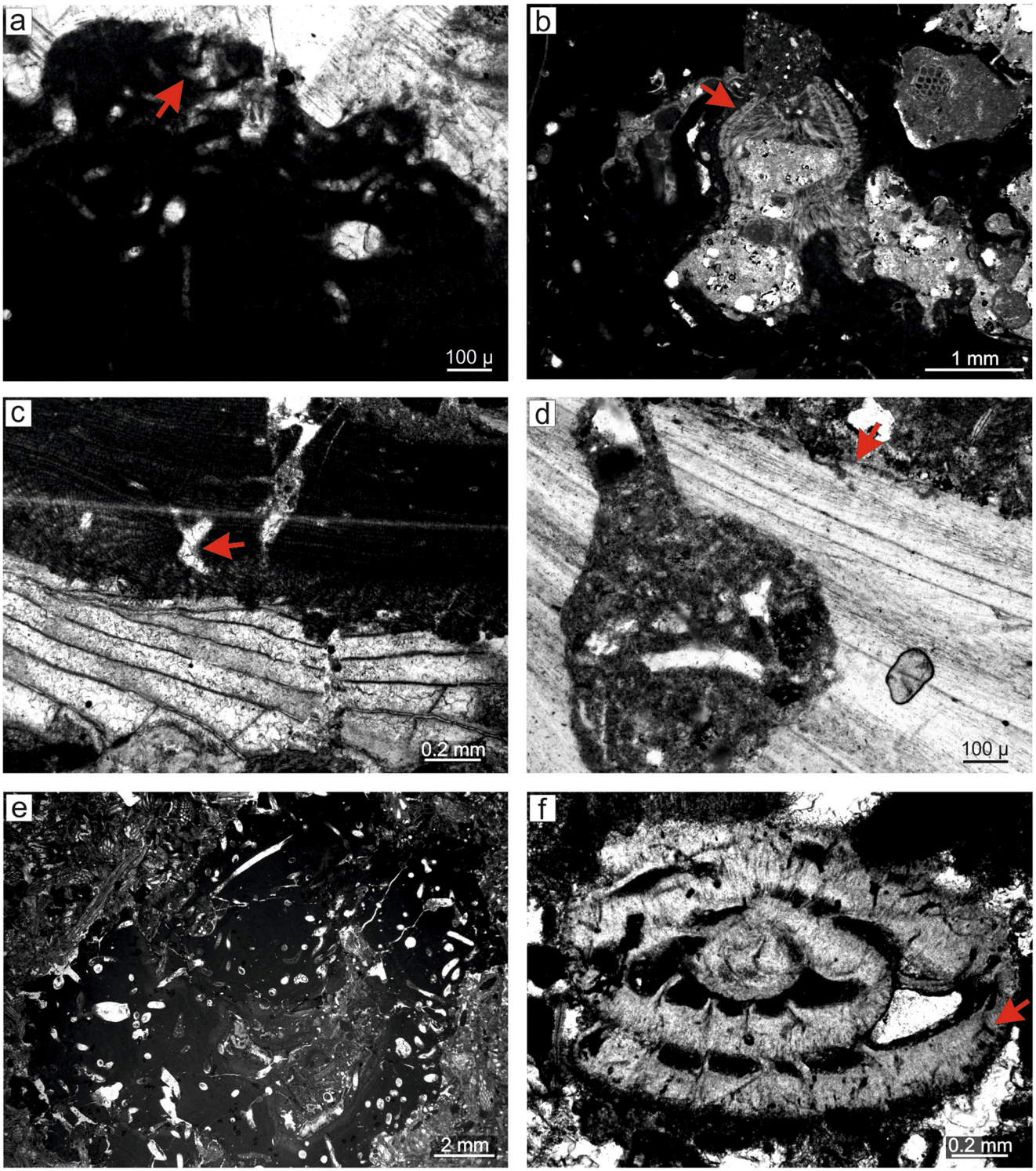

Fig. 6 Endoliths documented on a different biogenic substrate; **a** coralline algal thallus bored by microendoliths producing tunnels (arrow); **b** thecideid brachiopod bored by *Fossichnus solus* (arrow); **c** coralline alga. Same tunnel producer as in **a**. **d** Bivalve with corroded surface (arrow). Note large and sac-like boring with neck-like structure filled with fine sediment. **e** Fragment of monospecific rhodolith intensively bored by endoliths producing rounded, elongated or bifurcating tunnels; **f** benthic foraminifera bored by microendoliths

confirm the presence of the genera *Sporolithon*, *Lithoporella*, *Mesophyllum* and *Lithothamnion*. The assemblage consists of *Sporolithon nummuliticum* (Gümbel) Ghosh and Maithy, 1996 with gametophytes, *Sporolithon* sp. with gametophytes,

M. fructiferum Airoldi, 1932, *Lithothamnion ramosissimum* (Reuss) Piller, 1994, *L.* cf. *corallioides*, other uncertain *Lithothamnion* sp., *Lithoporella* cf. *minus* and gametophyte of *Hydrolithon lemoinei* (Miranda) Aguirre et al. 2011 (Tab. 4, Supplementary Material).

We could not find any lithophylloid coralline alga that should represent the most diversified genus in the Tichá dolina locality based on the published material (Schaleková 1962). The identification of sterile lithophylloid thalli is possible to some degree in well-preserved thalli because the cells of the adjacent filaments in lithophylloid algae are not laterally joined by fusions and the epithallial cells are not flared (Braga et al. 1993). Fertile bi/tetrasporic thalli bear conceptacles with roofs formed by filaments that are perpendicularly oriented to the chamber (Braga et al. 1993). All of the studied specimens bear cell fusions and are either sterile specimens, *Sporolithon* gametophytes or *Hydrolithon* species. One could argue that the observed lateral cell fusions are results of diagenetic processes. However, diagenetic processes are not selective and occur in patches within the thalli (Braga et al. 1993) or alter the complete fossils (Pisera 1985 p. 139, fig.16; Flügel 2004 p. 94, fig.4.5), hence could be well-recognised. The presence of the genus *Melobesia* is also questioned because of the absence of multiporate conceptacles in the thalli that Schaleková (1962) attributed to this genus. However, we observed fertile thalli identical to Schaleková's *Melobesia*, and found only uniporate conceptacles. We identified these specimens as *Lithoporella* cf. *minus*. *Hydrolithon lemoinei* which was not known until now in such old limestones (compare Aguirre et al. 2011, Hrabovský 2019); its occurrence in Tichá dolina locality is its oldest record.

Systematic palaeontology

Phylum Rhodophyta Wettstein, 1901
Subphylum Eurhodophytina Saunders and Hommersand, 2004
Class Florideophyceae Cronquist, 1960
Subclass Corallinophycidae Le Gall and Saunders, 2007
Order Sporolithales Le Gall and Saunders in Le Gall et al., 2010
Family Sporolithaceae Verheij, 1993
Genus *Sporolithon* Heydrich, 1897
Type species: *Sporolithon ptychoides* Heydrich, 1897, El Tor, Sinai Peninsula, Egypt, Recent.

Sporolithon nummuliticum (Gümbel) Ghosh and Maithy, 1996
(Figure 7a-d)

Material: Bi/tetrasporic plant description is based on the specimen from the thin section 2019-SL-3.
Description: Growth form is encrusting to warty protuberant (Fig. 7a), up to 1 mm thick with a protuberance of 2 mm L and 1.5 mm D. Thallus is pseudoparenchymatous with dorsiventral internal organisation. The hypothallus is monomerous non-coaxial (Fig. 7b), with 4–15 filaments and 30–101 μm thick. The cells are 10–37 μm L (25 μm mean, 5.9 sd.) and 7–12 μm D (10 μm mean, 1.4 sd.). The cells in the perithallus are 8–23 μm L (14 μm mean, 3.9 sd.) and 7–14 μm D (11 μm mean, 1.4 sd.). Lateral fusion of the cells is present in the hypothallus and perithallus (Fig. 7b). Trichocytes, meristematic and epithallial cells were not observed.

Sporangial compartments are grouped in 10–40 per sorus (Fig. 7a), and flush with the thallus surface. The chambers are 49–69 μm D (58 μm mean, 5.4 sd.) and 84–116 μm H (104 μm mean, 8.2 sd.) with a D/H ratio of 0.5–0.7. The paraphyses separating the compartments are 4–6-celled. The compartments are developed above the layer of elongated cells 16–31 μm long (Fig. 7c). We have observed the possible remains of the single stalk cell (Fig.7c) and the secondary infilling of cavities by multi-celled filaments (Fig. 7d). Gametophytes were not observed.
Remarks: The species was observed in three thin sections. The specimen description overlaps with *A. nummuliticum*, which is shown and described by Schaleková (Schaleková 1962, p. 89, pl. 8, fig 16) from the Tichá dolina locality to be of early Priabonian age. Her specimen shows cell elongation below the compartments. However, such cells occur only in some spots, while normal cells prevail. We did not study the type material of *S. nummuliticum*. Nevertheless, we refer to Aguirre et al. (2011), who assessed the type material of *S. lugeonii* (Pfender) Ghosh and Maithy, 1996, and compared it with a species attributable to *S. nummuliticum* from its type locality (Aguirre et al. 2011, p. 275). According these authors, *S. lugeonii* bears compartments that are developed above the relatively elongated cells and differs from *S. nummuliticum* based on its smaller compartments only. Therefore, we expect that the elongation of the cells most likely occurs in both species. This is consistent with our observations as well as with the characteristics recognised in the figures provided by Schaleková (1962). Some important findings are (1) the single stalk cell, which is characteristic for genus *Sporolithon*, and (2) the secondary infilling of the compartments. The second mentioned characteristic was shown in *S. glangeaudii* by Aguirre and Braga (1998) and in *S. lugeonii* by Aguirre et al. (2011); it is known in some extant species, e.g. *S. molle* (Verheij 1993). On the contrary, the single stalk cell suggests that only one single sporangium is produced in each compartment—a characteristic known in the genus *Sporolithon* but unknown in *Heydrichia* (Townsend et al. 1994).

Order Hapalidiales Nelson et al. 2015
Family Lithothamniaceae Haas, 1886
Genus *Lithothamnion* Heydrich, 1897

Type species: *Lithothamnion muelleri* Lenormand ex Rosanoff, 1866, Western Port Bay, Victoria, Australia, Recent.

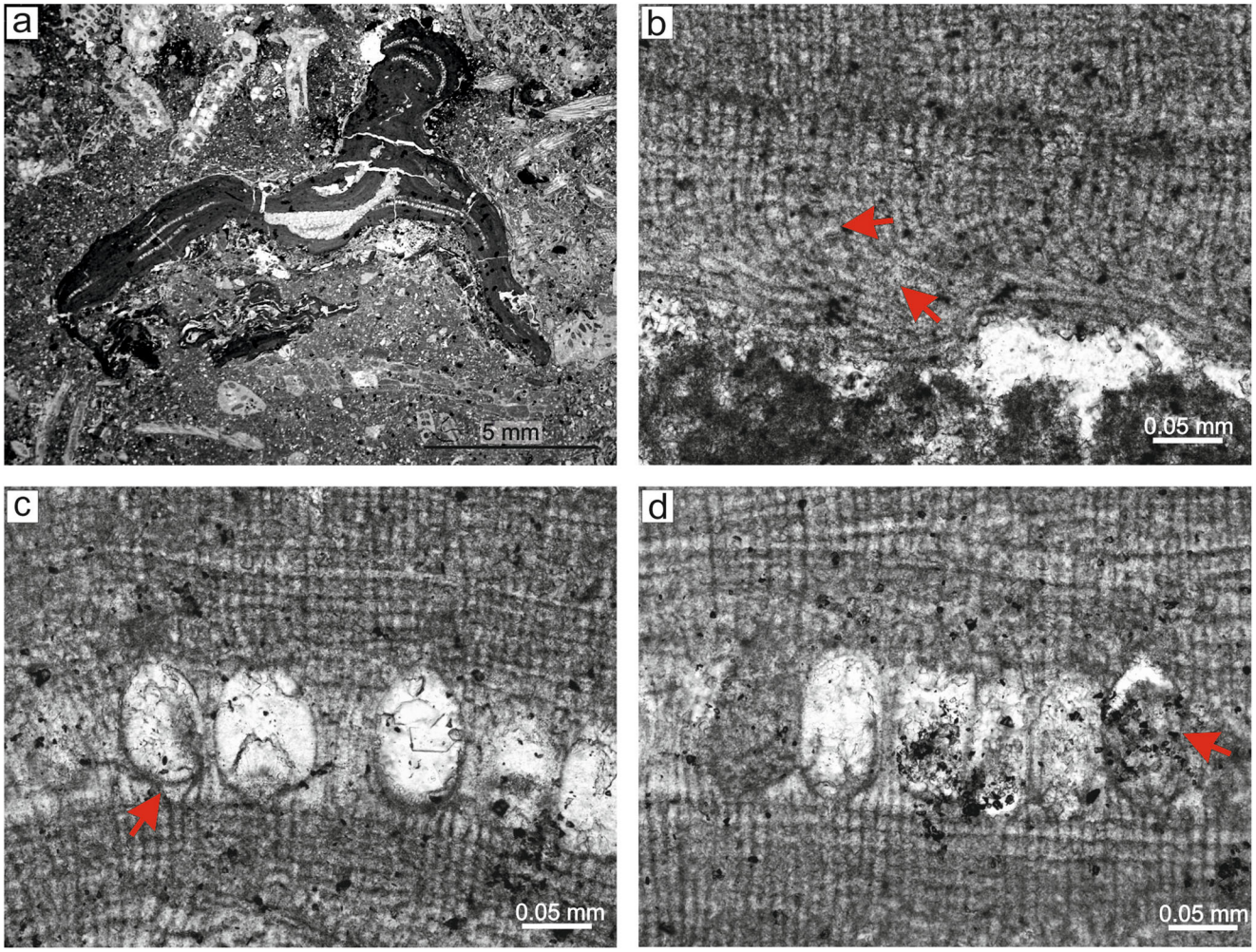

Fig. 7 *Sporolithon nummuliticum* (Rothpletz) Ghosh and Maithy, 1996, thin section 2019-Sl-3, bryozoan-coralline algal floatstone; **a** encrusting growth form with warty protuberance; **b** monomerous thallus with non-coaxial ventral core. Note the cell fusions (arrows). **c** Fertile portion of the thallus with calcified sporangial compartments developed above a layer of elongated cells. The arrow points to the single stalk cell. **d** Secondary infill of the compartments by vegetative cells (arrow)

Lithothamnion camarasae Pfender, 1926
(Figure 8a-f)

Material: Bi/tetrasporophyte and gametophyte-carposporangial plants are described based on specimens from thin section 2019-S3 and 2019-S3a, respectively. The two specimens are known from Štrba only.

Description: The growth form is fruticose protuberant (Fig. 8a). The thallus is pseudopyrenchymatous with dorsiventral internal organisation and monomerous non-coaxial construction (Fig. 8b). Cells in the hypothallus are 13–17 μm L (15 μm mean, 1.7 sd.) and 7–9 μm D. Cells in the perithallus are 6–16 μm L (12 μm mean, 2.4 sd.) and 6–10 μm D (8 μm mean, 1.1 sd.). The perithallus is zoned (Fig. 8c). Secondary overgrowths above the damaged thallus occurs in some spots (Fig. 8d). The trichocytes, epithallial cells and cells of the meristem not observed.

Gametophyte bears two types of conceptacles (Fig. 8e). The small conceptacle is 111 μm D and 42 μm H and tentatively described here as carpogonial. The large one, proposed carposporangial conceptacle, is 197–561 μm D and 96–181 μm H, without a central pedestal and most likely developed from the carpogonial through the enlargement and destruction of roof-forming cells (Fig. 8e). The bi/tetrasporic conceptacle is buried in the thallus. The chamber is rectangular with rounded corners filled with large cells and measures 430 μm D and 181 μm H, (Fig. 8f). The chamber D/H ratio is 2–4. The roof is 43–50 (69) μm thick with thin pores enlarged at the base. At the base, the pores are 10–18 μm D. The pore canals are lined with cells that are the same as other roof cells (Fig. 8f). The roof vanishes after the spore release. For this reason, we were not able to detect the roof surface clearly. Therefore, the detected roof filaments are only approximately 4–5(6)-celled (Fig. 8f).

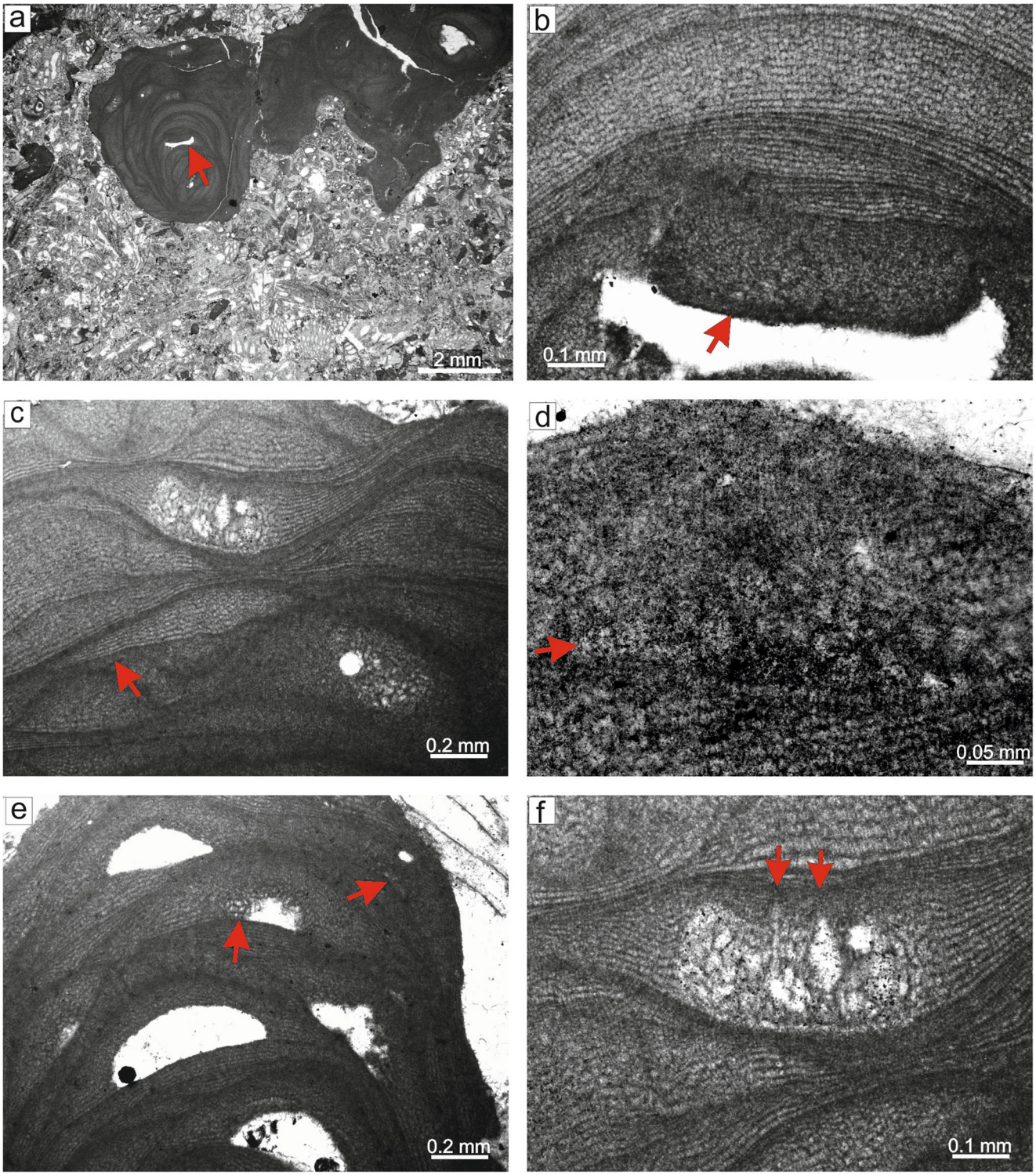

Fig. 8 **a–c** *Lithothamnion camarasae* Pfender, 1926, bi/tetrasporic life cycle, thin section 2019-S3, bryozoan-coralline algal packstone; **a** fruticose to warty protuberant growth form. Arrow points to the portion of single occurrence of the ventral core. **b** Monomerous thallus with non-coaxial ventral core; **c** fertile thallus. Note the distinct zonation pattern. **d–e** *Lithothamnion camarasae* Pfender, 1926, gametophyte, thin section 2019-S3a, bryozoan-coralline algal packstone; **d** secondary overgrowths above the damaged thallus (arrow); **e** gametophyte, arrows point to the carpogonial conceptacle (right) and enlarged conceptacle after the karyogamy (left). Large conceptacles mostly at the base of the figure are considered carposporangial. **f** *Lithothamnion camarasae* Pfender, 1926, bi/tetrasporic life cycle, thin section 2019-S3, bryozoan-coralline algal packstone. Arrows point to the pore canals that are bordered by cells that are the same dimensions as other roof cells. Growth zones indicate that the conceptacles were most likely slightly raised above the thallus surface during their maturity. Subsequent renewal meristematic activity of the roof cells resulted in the vanishing of the conceptacle roof

Remarks: The anatomical and reproductive characteristics match with those given by Pfender (1926) and Aguirre et al. (2011); nevertheless, the neotype specimen shows empty sporangial conceptacles (Aguirre et al. 2011, figs 4e-f). Moreover, the conceptacles in both the neotype and the specimen described in Pfender (1926, pls 10 and 14) protrude above the thallus surface. Their emergence is inconsistent and differs between conceptacles. Therefore, one could propose that these two characters would point to different species from the *L. camarasae* found in the Štrba locality. However, (1) the specimen described in the original publication by Pfender (1926) bears sporangial conceptacles that are mostly filled by large cells, and (2) the conceptacles in the Štrba locality specimen were probably raised above the thallus surface, as is suggested by the perithallus growth zones (Fig. 8a). In contrast to the neotype, we did not observe any epithallial cells. Their morphology is important in the assessment of the specimen to the genus *Lithothamnion* (Braga et al. 1993). Nevertheless, we did not find other morphological differences between the type material and our species; hence, we consider the alga to be *L. camarasae*.

Lithothamnion cf. *corallioides* (Crouan and Crouan) Crouan and Crouan, 1867
(Figure 9a-d)

Material: The description is based on specimens from a thin section 2019-SL-5. This is a single occurrence of the species in Štrba, as no other specimens were detected.
Description: The growth form is fruticose protuberant with protuberances of 1.3 mm L and 0.7 D (Fig. 9a). The thallus is pseudopyrenchymatous with dorsiventral internal organisation and monomerous non-coaxial construction. The cells in the

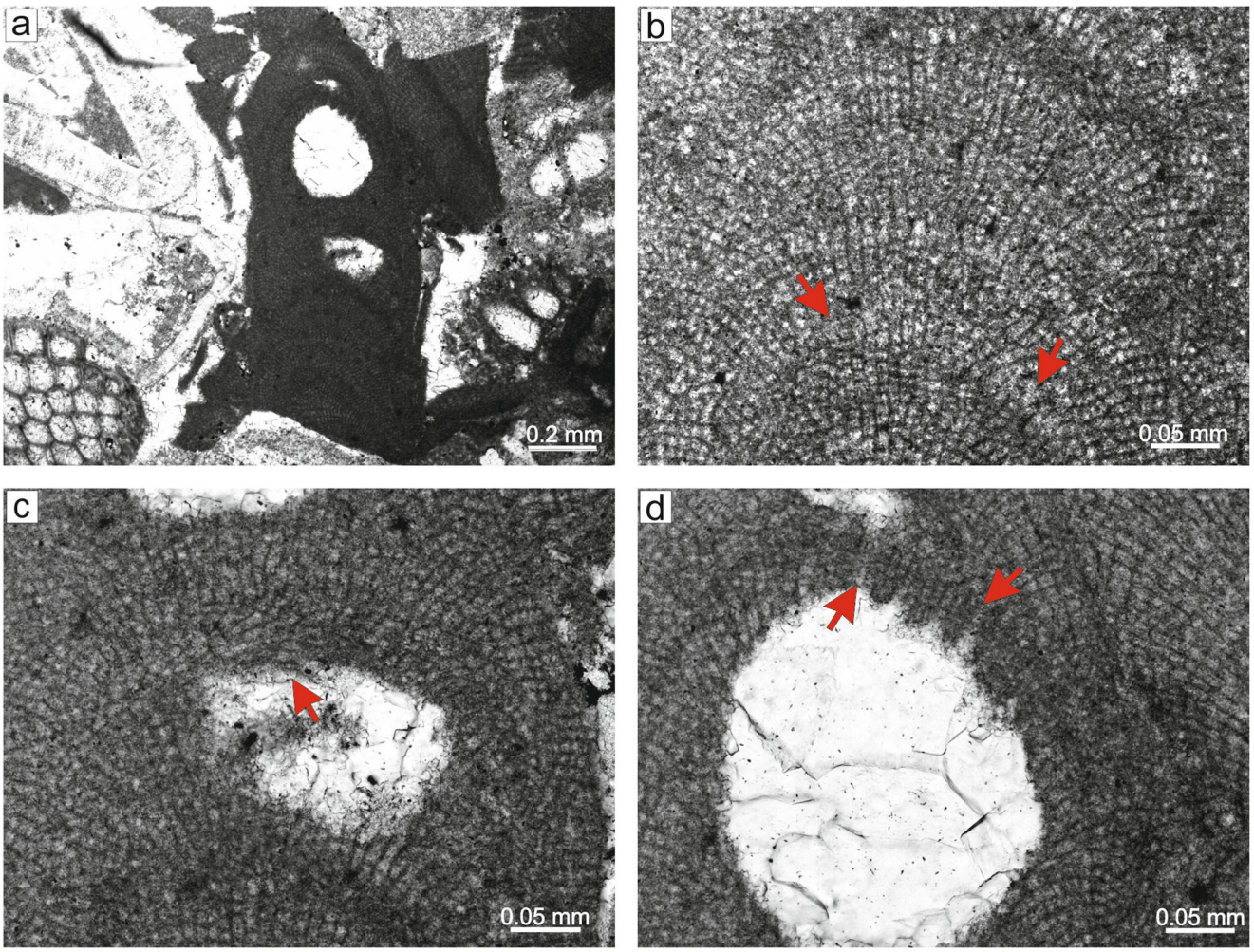

Fig. 9 *Lithothamnion* cf. *corallioides* (Crouan and Crouan) Crouan and Crouan, 1867, thin section 2019-SL-5, coralline algal-bryozoan packstone; **a** fragment of the thallus with fruticose protuberant growth form; **b** cells of adjacent filaments are laterally joined with fusion (arrows); **c** empty cavity and secondary non-coaxial ventral core (arrow) developed above; **d** empty bi/tetrasporic conceptacle with preserved roof. Pore canals are lined with cells that are the same as other roof cells (arrows)

hypothallus are 12–19 μm L (14 μm mean, 2.3 sd.) and 5–9 μm D. The cells in the perithallus are 6–21 μm L (14 μm mean, 4.1 sd.) and 7–11 μm D (8 μm mean, 1.1 sd.). The fusion of cells in adjacent filaments is common and more frequent in distinct parts (Fig. 9b). The secondary hypothallium can develop above the damaged thallus (Fig. 9c). Trichocytes, epithallial cells and meristem are not observed.

The bi/tetrasporic conceptacles are developed at the tips of the protuberances (Fig. 9a). The complete bi/tetrasporic conceptacle is 242 μm D and 225 μm H. The roof is 35–44 μm thick with many pores of 8–10 μm W. The D/H ratio is 1.1. The pore canals are cylindrical and lined by cells that are the same as other roof cells (Fig. 9d). The roof filaments and pore canal filaments are 5-celled.

Remarks: The anatomical and growth form characteristics match with the description of the species in Irvine and Chamberlain (1994) and overlap with the description of Basso (1995). However, the complete conceptacle in the specimen is much higher; hence, the overall shape is rounded rather than low-elliptical (according to Irvine and Chamberlain 1994). Absence of epithallial and meristematic cells makes generic placement of the specimen impossible (see remarks for *L. camarasae*). However, the pore canal anatomy, dimensions of hypothallial and perithallial cells, and also the growth form match with the diagnosis of *L. corallioides*. Therefore, we consider the specimen from Štrba as *L.* cf. *corallioides*.

Genus *Phymatolithon* Fosle, 1898

Type species: *Phymatolithon calcareum* (Pallas) Adey and McKibbin ex Woelkerling and Irvine, 1986, Falmout Harbour, Cornwall, England, Recent.

Phymatolithon sp.
(Figure 10a-d)

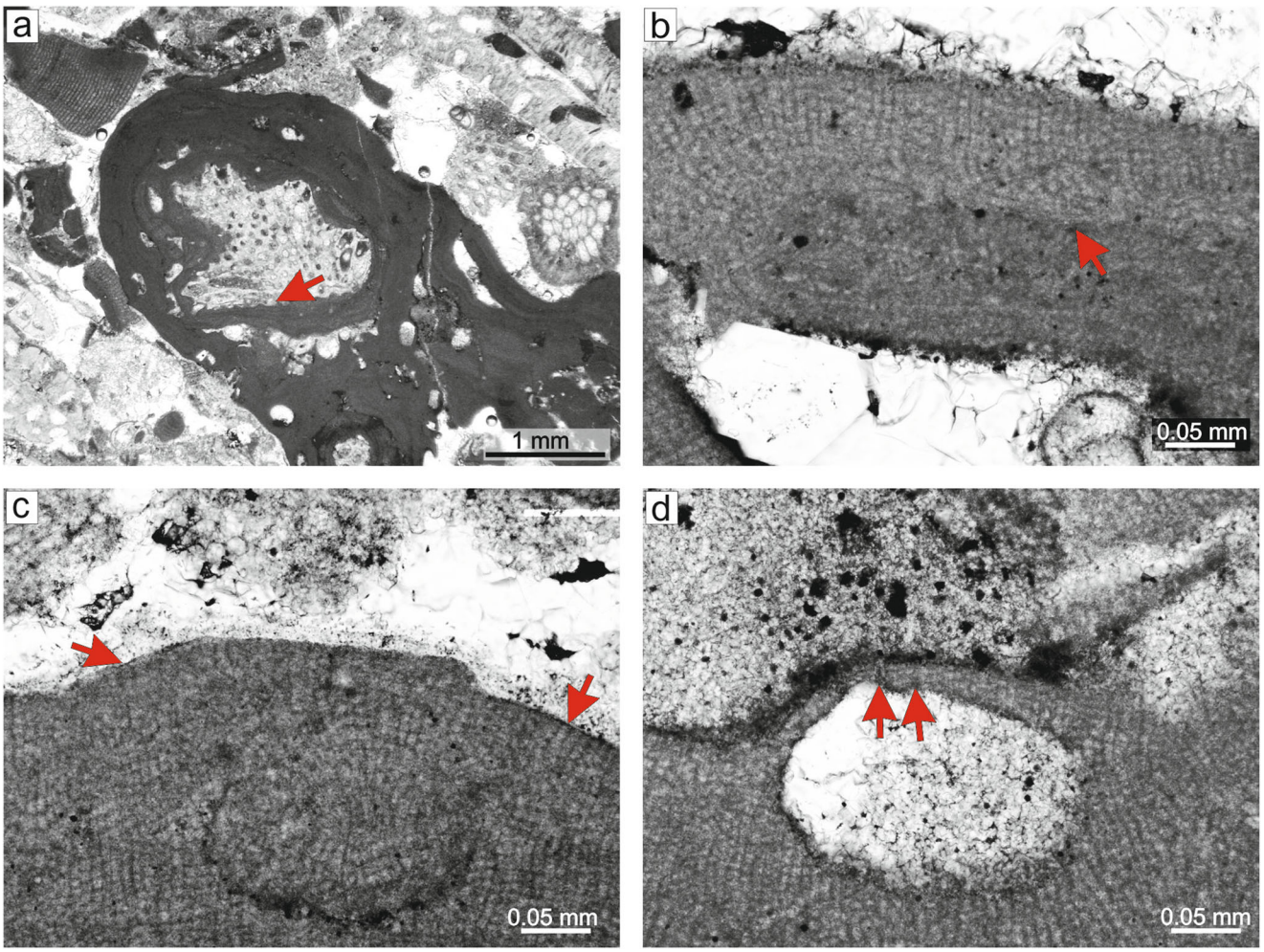

Fig. 10 *Phymatolithon* sp., thin section 2019-S1, coralline algal-bryozoan packstone; **a** encrusting growth form. Multiple overgrowth of thalli developed lumpy protuberances. **b** Non-coaxial hypothallus (arrow); **c** epithallial cells (arrows). Meristematic cells are as long as or shorter than cells immediately subtending them. Note the secondary infill of the empty conceptacle with a broken-off roof. **d** Raised bi/tetrasporic conceptacle. Arrows point to the pore canals. Cells lining the pore canals are the same as other roof cells

Material: Only two specimens were identified. The smaller one is a fragment while the larger is an unattached monospecific rhodolith. The description is based on a large specimen from a thin section 2019-S1.

The growth form is encrusting layered with an uneven wavy surface (Fig. 10a). Multiple thallus overgrowths (Fig. 10b) around a bryozoan colony form a monospecific rhodolith (Fig. 10a). The thallus is pseudoparenchymatous with dorsiventral internal organisation and monomerous construction (Fig. 10b). The hypothalus is non-coaxial and 24–84 μm and 5–11 filaments thick. The cells are 11–23 μm L (15 μm mean, 2.8 sd.) and 5–9 μm D (6 μm mean,1 sd.). The perithallus consists of cells of 6–11 μm L (8 μm mean, 1.4 sd.) and 5–9 μm D (7 μm mean, 1.1 sd.). The cells of adjacent filaments are laterally joined with fusions. The proposed meristematic cells are as long as or shorter than the cells immediately subtending them (Fig. 10c). The meristematic cells are 5–6 μm L (6 μm mean, 0.6 sd.) and 5–7 μm D (6 μm mean, 0.7 sd.). The cells above proposed meristematic cells are tentatively described as epithallial cells. Epithallial cells are flattened or rounded but not flared (Fig. 10c), measuring 3–4 μm L (3 μm mean, 0.5 sd.) and 5–8 μm D (6 μm mean, 1.1 sd.).

The multiporate sporangial conceptacles protrude above the thallus surface (Fig. 10d) or are flushed with the surface (Fig. 10a). Some conceptacles have broken out roofs and the empty chambers are filled with the new thallus (Fig. 10c). The conceptacles are raised 57 μm above thallus surface and their external D reaches 314 μm. The chambers are 183–215 μm D (199 μm mean, 18 sd.) and 79–148 μm H (107 μm mean, 29.8 sd.). The roof filaments are 3–4-celled and 20–27 μm L. The cells are 3–7 μm L (5 μm mean, 1.1 sd.) and 4–6 μm D (5 μm mean, 0.8 sd.). The pore canals are cylindrical and about 7 μm W (Fig. 10d). The pore canals are lined by 3–4-celled filaments (Fig. 10d). The cells in the pore canal filaments are more or less the same as the other roof cells and measure 3–4 μm L (4 μm mean, 0.5 sd.) and 3–4 μm D (4 μm mean, 0.4 sd).

Remarks: Based on the traditional concept used by palaeontologists, two genera *Phymatolithon* and *Leptophytum* Adey, 1968, cannot be separated in the fossil record (Braga et al. 1993). As far as known, only fossils of *Phymatolithon* are recognised in limestones (Hrabovský et al. 2015; Basso et al. 1998). Extant species of the genus *Phymatolithon* are morphologically similar to *Leptophytum* both having a mostly non-coaxial hypothallus, multiporate sporangial conceptacles, non-flared epithallial cells and meristematic cells that are as long as or shorter than the cells immediately subtending them. However, the two genera could be differentiated by the morphology of the pore canal cells, which are normal and same as other roof cells in *Phymatolithon*, while a specialised variation could occur in *Leptophytum* (Athanasiadis 2001; Adey et al. 2001). Therefore, at least some of the *Leptophytum* should be recognised as fossil. The specimens from Štrba rather match with the diagnosis of the genus *Phymatolithon* because the pore canal lining cells are similar to the other roof cells. *Lithothamnion* cf. *corallioides* described above bears similar characteristics of the pore canal. As mentioned in the description, epithallial cells are absent in the *L.* cf. *corallioides* and cannot be used to separate the two genera. Therefore, the question arised whether the *Phymatolithon* sp. and *L.* cf. *corallioides* represent the same species. However, our observations suggest that the conceptacles are smaller, the roof filaments are shorter and the pore canal and the roof filaments are 3–4-celled in the proposed *Phymatolithon* sp., hence distinguish specimen from the *L.* cf. *corallioides*. Also, the growth form of *L.* cf. *corallioides* is fruticose-protuberant while the one of the *Phymatolithon* sp. is encrusting-layered.

Family Mesophyllaceae Athanasiadis, 2016
Genus *Mesophyllum* Lemoine, 1928

Type species: *Mesophyllum lichenoides* (Ellis) Lemoine, 1928, Cornwall, England, Recent.

Mesophyllum engelhartii (Foslie) Adey, 1970
(Figure 11a-f)

Material: Bi/tetrasporophyte was described in a thin section 2018-S-4, gametophyte with proposed carpogonial and carposporangial conceptacles are from a thin section 2019-S6.
Description: The growth form is encrusting layered (Fig. 11a). The thalli develop applanate branches which can subsequently be fused. The thallus is pseudoparenchymatous with dorsiventral internal organisation and monomerous construction (Fig. 11b). The hypothallus is only non-coaxial (Fig. 11b). The cells are 13–33 μm L (22 μm mean, 4.6 sd.) and 6–13 μm D (8 μm mean, 1.7 sd.). The hypothallus is up to 100 μm and 5–12 filaments thick. The perithallus is a few cells thick. Growth zones are present. The cells are 7–14 μm L (10 μm mean, 2 sd.) and 7–11 μm D (9 μm, 1.2 sd.). Lateral fusion of cells is present in the hypothallus and perithallus. The meristematic cells are 8–12 μm L (10 μm mean, 1.7 sd.) and 7–8 μm D (8 μm mean, 0.5 sd.), elongated and terminated by a single rounded epithallial cell (Fig. 11b). The epithallial cells are 4–6 μm L (5 μm mean, 0.6 sd.) and 7–8 μm D (8 μm mean, 0.5 sd.). Trichocytes are not observed.

The gametophyte bears two type of conceptacles. Proposed carpogonial conceptacle has a triangular shape. The roof and the pore canal are developed from the initials peripheral to the fertile area (Fig. 11c). Its external D is 575 μm and is raised 181 μm above the thallus surface. The chamber is 162 μm D and 62 μm H. The pore canal is 98 μm L and 58 μm W (Fig. 11c–d). The proposed carposporangial conceptacle develops through the enlargement and destruction of the cells on the sides of the

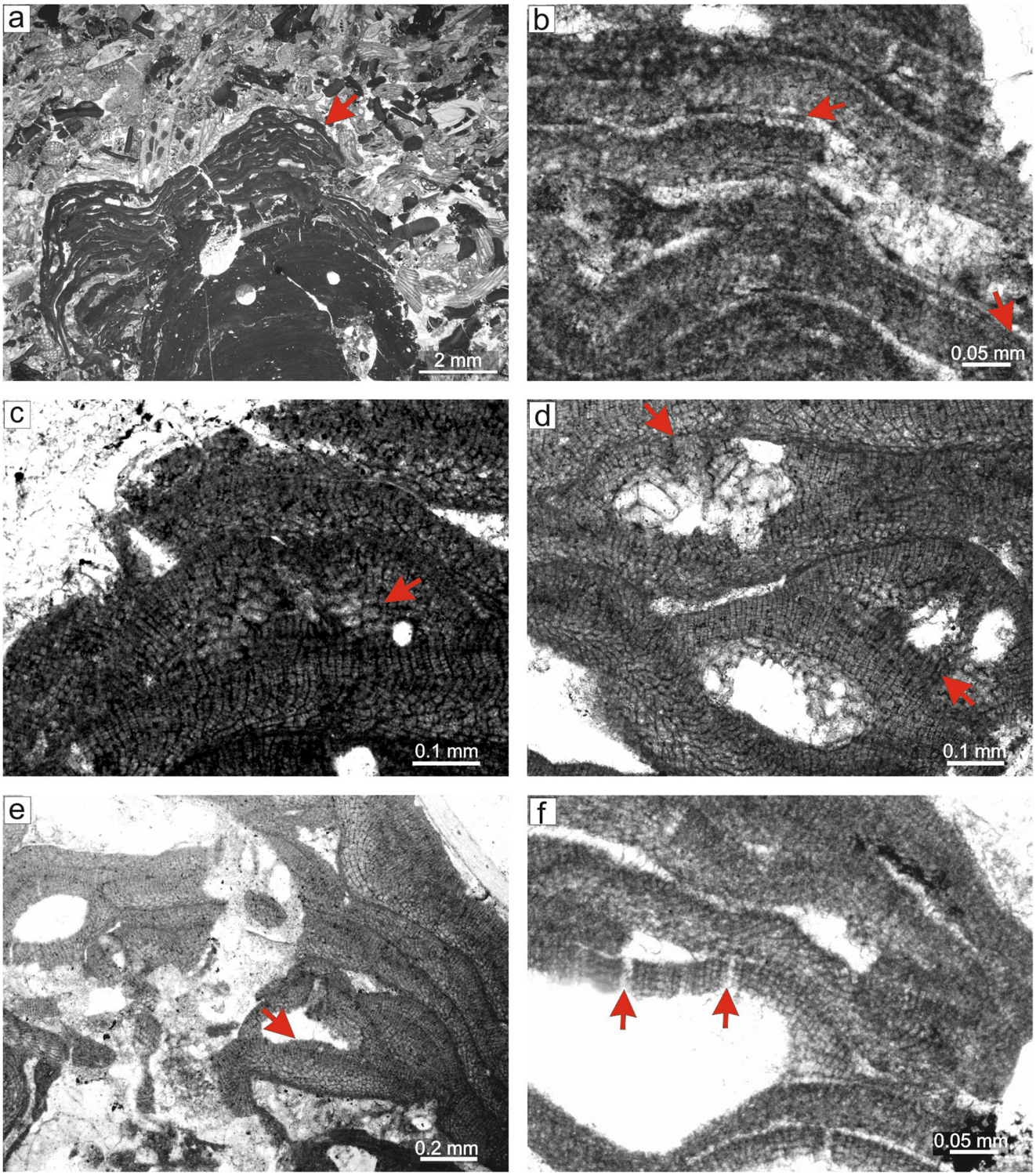

Fig. 11 **a**, **b** *Mesophyllum engelhartii* (Ellis) Lemoine, 1928, bi/tetrasporic plant, thin section 2018-S4, coralline algal-bryozoan packstone; **a** encrusting layered growth form (arrow) with applanate branches. Multiple overgrowths and fusion of applanate branches produce primary voids. **b** Portion of the thalli with detected epithallial cells (arrows). Cells below them are meristematic cells and are longer than cells immediately subtending them. Ventral core filaments appear non-coaxially arranged. **c–e** *Mesophyllum engelhartii* (Ellis) Lemoine, 1928, gametophyte, thin section 2019-S6, bryozoan-coralline algal packstone; **c** proposed carpogonial conceptacle. Arrow points to the enlarged cells at the sides of the conceptacle. **d** Enlarged conceptacle after the karyogamy and the development of the carposporangial conceptacle. Conceptacle at the left (arrow) has distinct pore canal with cells protruding inside. Conceptacle at the right shows transitional stage in the process of enlargement. **e** Fully developed carposporangial conceptacle with central pedestal (arrow). **f** *Mesophyllum engelhartii* (Ellis) Lemoine, 1928, bi/tetrasporic plant, thin section 2018-S4, coralline algal-bryozoan packstone. Bi/tetrasporic conceptacle. Arrows point to the cylindrical pore canals linned with cells that are the same as other roof cells. Some of the pore canal cells appear only a little wider than the adjacent roof cells

carpogonial conceptacle (Fig. 11d). The carposporangial conceptacle is 506–561 μm in external D and protrudes 85–265 μm above the thallus surface. The chambers are 327–363 μm D and 123–131 μm H. The pore canal is 51–128 μm L and 49–68 μm W with roof cells protruding inside. The floor of the carposporangial conceptacle possesses a central pedestal (Fig. 11e).

The multiporate sporangial conceptacles can markedly protrude above the thallus surface and are not embedded within the thallus (Fig. 11a). The height of the projection is 92–168 μm and the external D of the conceptacles is 336–661 μm. The chambers are rounded, oval or elongated, with 192–403 μm D (306 μm mean, 95.6 sd.) and 130–175 μm H (158 μm mean, 17.1 sd.). The D/H ratio is 1.2–2.9. The roof filaments are 4–5-celled and are 36–49 μm long. The pore canals are narrow and cylindrical, and 10–15 μm in diameter. The pore canals are lined by 4–5-celled filaments built by cells similar to the rest of the roof cells (Fig. 11f). The position of the upper-most pore canal lining cell to the roof surface suggest that the rosette cells are most likely not sunken.

Remarks: The identification of the fossil *Mesophyllum* and its discrimination from other genera of the order Hapalidiales was a topic of discussions in many scientific papers (Aguirre and Braga 1998; Aguirre et al. 2011; Hrabovský et al. 2015; Hrabovský et al. 2019). Recent diagnosis emendation of this genus provided by Athanasiadis and Ballantine (2014) includes morphological characteristics associated with the reproductive anatomy. What is important is that these characteristics can be used in the identification of fossil *Mesophyllum* species (Hrabovský et al. 2019). The diagnostic characteristics collectively useful for this purpose are the coaxial hypothallus, elongated meristematic cells, non-flared epithallial cells and carposporangial conceptacles with a central pedestal. When specialised pore lining cells are present, they are not markedly elongated at the base (Athanasiadis and Ballantine 2014). Unfortunately, not all of the *Mesophyllum* species bear specialised pore lining cells. In this case, we were not able to strictly distinguish *Mesophyllum* from *Synarthrophyton* because the carposporangial conceptacles of both develop a central pedestal. Moreover, the permanently coaxial hypothallus (Athanasiadis et al. 2004; Athanasiadis and Ballantine 2014) versus patchy coaxial hypothallus indicative of *Mesophyllum* rather than *Synarthrophyton* in some fossils (Basso et al. 1998; Aguirre and Braga 1998; Aguirre et al. 2011) was not observed in studied specimens. Therefore, morphological and reproductive characteristics collectively suggest the presence of the genus *Synarthrophyton*. However, similar vegetative and reproductive characteristics occur in *M. engelhartii.* Actually, this species is characterised by the presence of both non-coaxial and coaxial hypothallial arrangement in the same thallus (Woelkerling and Harvey 1993). We tentatively describe this alga as *M. engelhartii*.

Mesophyllum fructiferum Airoldi, 1932
(Figure 12a-d)

Material: Species description is based on the specimen observed in a thin-section 2019-Sl-2.

Description: Growth form is encrusting (Fig. 12a). No applanate branches or prominent protuberances are present. The thallus is up to 1 mm thick. Numerous large and buried conceptacles are arranged in distinct rows (Fig. 12a). The thallus is pseudoparenchymatous with dorsiventral internal organisation and monomerous construction (Fig. 12b). The hypothallus is coaxial in patches, 50–170 μm and 8–21 filaments thick. The cells are 16–22 μm L (20 μm mean, 1.8 sd.) and 8–10 μm D (9 μm mean, 0.8 sd.). The cells in the perithallus filaments are 6–14 μm L (9 μm mean, 2.1 sd.) and 7–9 μm D (8 μm mean, 0.5 sd.). The perithallus is zoned (Fig. 12c). Lateral cell fusions occur in the hypothallus and perithallus. Meristeme cells, epithallial cells and trichocytes are not observed.

Bi/tetrasporic conceptacles are multiporate and buried. However, their morphology suggests they were protruding above the thallus surface during their maturity (Fig. 12c). The roofs have vanished; however, the contours of the roofs and a few detected pore canals are present (Fig. 12d). The roof filaments are 25–34 μm L, and 3–5-celled. The cells are 5–7 μm L (6 μm mean, 1 sd.) and 5–7 μm D (6 μm mean, 0.7 sd.). The pore canals are cylindrical, 8–13 μm W. The cells in the pore canal filaments are badly visible. Some of them show a better degree of preservation and appear the same as the other roof cells: not specialised "thinner-wider", nor smaller (Fig. 12d). The chambers are large and elongated with rounded corners. The chambers are 351–711 μm D (509 μm mean, 161 sd.) and 156–201 μm H (180 μm mean, 20 sd.) with a D/H ratio of 2.2–3.8. Rosette cells are not sunken.

Remarks: The specimens from Štrba match the morphological diagnosis of the *M. fructiferum* type material (Basso et al. 1998). However, data on pore canal anatomy and the carposporangial conceptacle morphology of the type are missing. Therefore, proving the assessment of the species into the *Mesophyllum* will require further investigation (see remarks about *M. engelhartii*).

Mesophyllum mengaudii (Lemoine) Aguirre, Braga and Bassi, 2011
(Figure 13a-f)

Material: Species description is based on specimens from thin sections 2019-S-4.

Description: Growth form is encrusting layered (Fig. 13(a)) with applanate branches (Fig. 13(b)). The conceptacles may project above the thallus surface. The thallus is 187–494 μm thick, pseudoparenchymatous with dorsiventral internal organisation and monomerous coaxial to non-coaxial construction

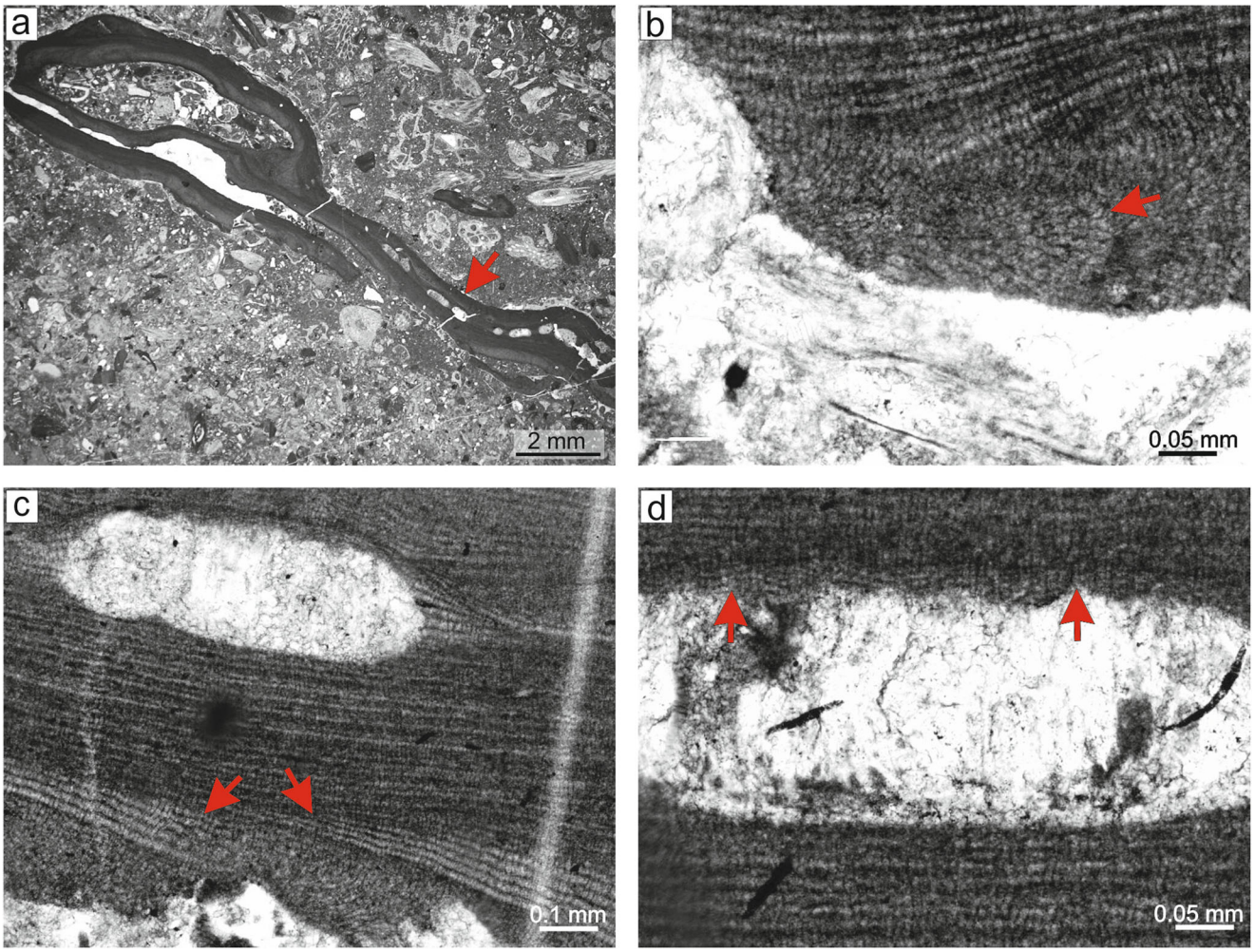

Fig. 12 *Mesophyllum fructiferum* Airoldi, 1932, thin section 2018-Sl-2, bryozoan-coralline algal floatstone; **a** encrusting layered growth form with applanate branches. Note horizontal arrangement of bi/tetrasporic conceptacles (arrow). **b** Monomerous thallus with coaxial (arrow) to non-coaxial ventral core; **c** distinct growth zones developed at the base of the thallus (arrows); **d** bi/tetrasporic conceptacle. Arrows point to the pore canals. Pore canal cells are badly visible

(Fig. 13(b)). The hypothallus is 118–177 μm and 8–13 filaments thick. The cells are 14–31 μm L (22 μm mean, 5.5 sd.) and 5–13 μm D (10 μm mean, 2.2 sd.). Growth zones are present. The cells 6–17 μm L (11 μm mean, 2.6 sd.) and 7–10 μm D (8 μm mean, 0.8 sd.). Lateral fusion of cells is present in the perithallus and hypothallus. Meristeme, epithallial cells and trichocytes are not observed.

The carposporangial conceptacles project above the thallus surface by 168–269 μm (Fig. 13(c)). Its external D is 673–782 μm. The chambers possess a central pedestal (Fig. 13(d)). Chamber D is 518–540 μm (529 μm mean, 14.9 sd.), H from the top of the pedestal to the roof is 158–236 μm (197 μm, 54.9 sd.) and H from the floor to the top of the chamber is 231–244 μm (237 μm mean, 9 sd.). The pore canal is 122 μm L and 56 μm W.

The multiporate sporangial conceptacle external D is 693 μm and projects 195 μm above the thallus surface. The chamber is 416 μm D and 207 μm H. The roof is 53–59 μm thick. The remains of pyritized sporangia are present in the chamber (Fig. 13(e)). They are up to 146 μm L and 38–56 μm D. Roof filaments are 7–8-celled with cells of 6–16 μm L (9 μm mean, 2.8 sd.) and 4–12 μm D (7 μm mean, 2 sd.). The pore canals are about 11 μm W and are lined by 7–8-celled filaments bearing specialised thinner-wider cells or normal cells, like other roof cells. The pore canal lining cells are 5–10 μm L (7 μm mean, 1.5 sd.) and 3–5 μm D (4 μm mean, 0.6 sd.) and are not elongated at the base (Fig. 13(f)).

Remarks: Specimen description matches the diagnosis of the genus *Mesophyllum* (see remarks to *M. engelhartii*). Pore canal cell morphology and carposporangial conceptacle morphology are not known from the type of *M. mengaudii*. Therefore, further investigation of the specimens collected at the type locality is necessary for the confirmation of our

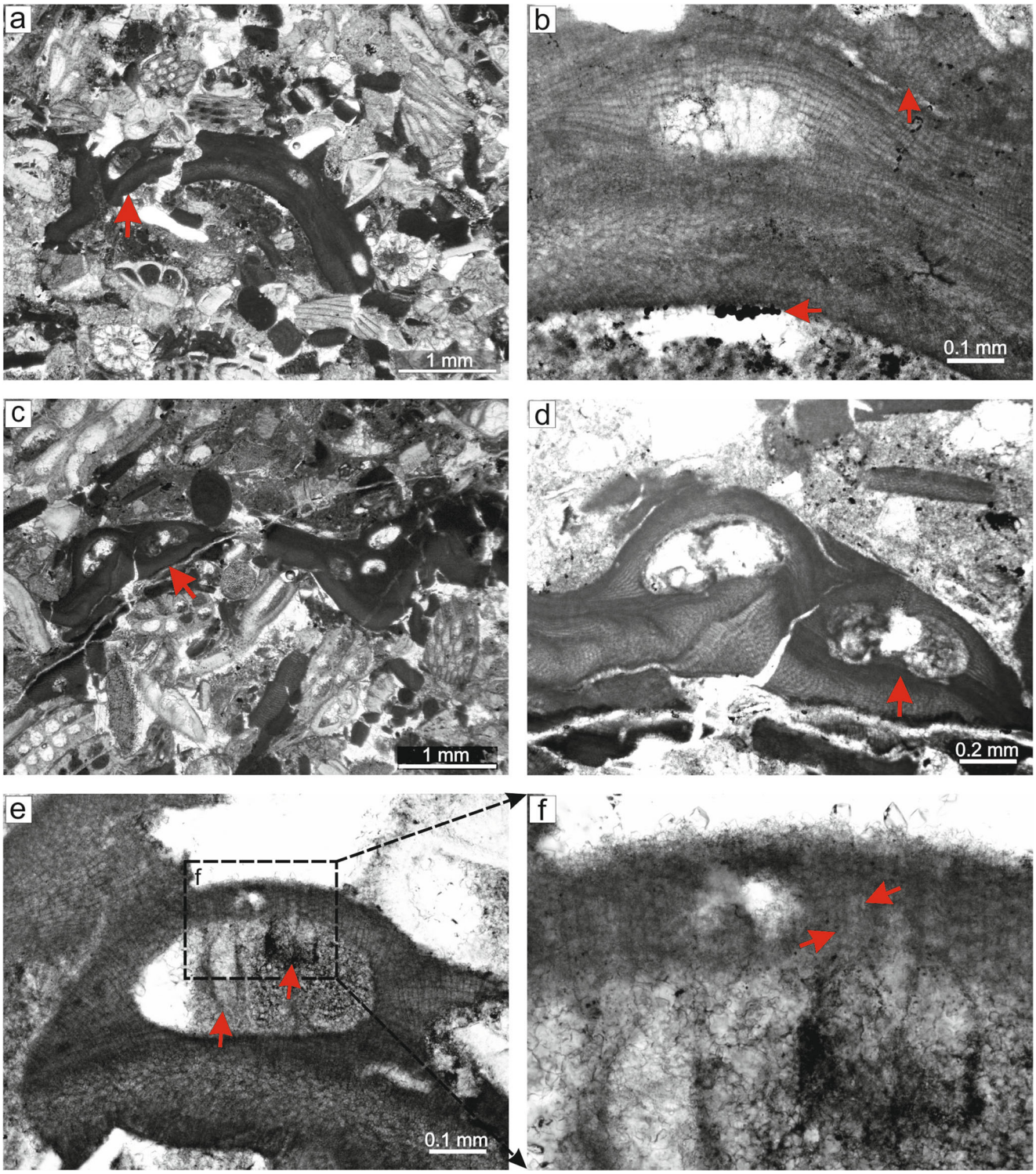

Fig. 13 *Mesophyllum mengaudii* (Lemoine) Aguirre, Braga and Bassi, 2011, thin section 2019-S-4, coralline algal-bryozoan packstone. **a**, **b** Bi/tetrasporic plant; **a** encrusting growth form (arrow); **b** monomerous thallus with non-coaxial to coaxial ventral core marked with an arrow at the top part of the figure. The arrow also points to the development of applanate branches. The arrow at the base points to pyrite framboids. **c**, **d** Gametophyte with carposporangial conceptacles (arrow); **c** encrusting growth form; **d** carposporangil conceptacle with central pedestal (arrow). **e**, **f** Bi/tetrasporic plant; **e** conceptacle with preserved pyritized remains of sporangia (arrows); **f** pore canals lined with specialised thinner-wider cells (arrows)

findings. However, the rest of the morphological characteristics match the type description (Aguirre et al. 2011).

Mesophyllum sp.
(Figure 14a-d)

Material: Species description is based on a specimen from a thin section 2019-S9. Meristematic and epithallial cells are described based on a specimen from a thin section 2019-S2
Description: Growth form is encrusting to lumpy protuberant (Fig. 14a). The thallus is pseudoparenchymatous, with dorsiventral internal organisation and monomerous construction (Fig. 14b). The hypothallus is coaxial in patches (Fig. 14b), 4–10 filaments and 34–71 μm thick. The cells are 11–24 μm L (18 μm mean, 3.6 sd.) and 4–8 μm D (6 μm mean, 1 sd.). The perithallus consists of cells 5–13 μm L (8 μm mean, 1.9 sd.) and 4–8 μm D (6 μm mean, 0.8 sd.). No meristematic and epithallial cells are preserved on this specimen but they are well-visible on another one. On the contrary, the second specimen does not have such well-preserved pore canal lining cells. The meristematic cells are elongated in some spots but mostly the same as the cells that are immediately subtending them. The epithallial cells are rounded or flattened but not flared (Fig. 14c). Trichocytes not observed.

There were multiporate conceptacles protruding above the thallus surface at their maturity (Fig. 14d), but they were subsequently overgrown by the continual meristematic activity of the roof filaments. This caused the roof to vanish in some of them (Fig. 14d). The chambers are 177–326 μm D (234 μm mean, 63.1 sd.) and 103–119 μm H (111 μm mean, 6.7 sd.). The roof is 22–37 μm thick. The pore canal filaments consist of 5 specialised thinner-wider cells that are slightly elongated at the base (Fig. 14d).

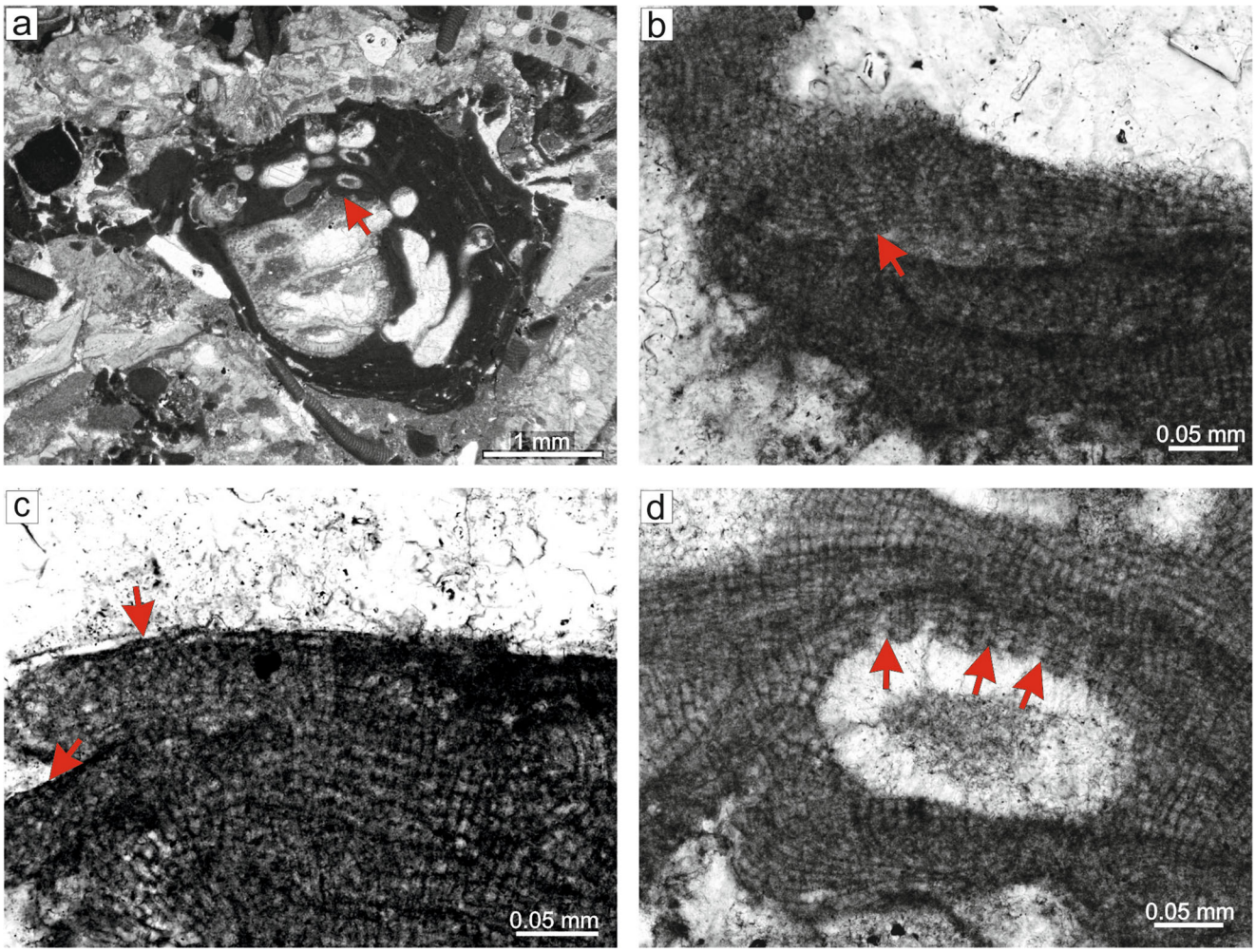

Fig. 14 **a**, **b** *Mesophyllum* sp., thin section 2019-S-9, coralline algal-bryozoan packstone; **a** encrusting lumpy protuberant growth form. The arrow points to the fertile part of the thallus. **b** Coaxial (arrow) to non-coaxial ventral core. **c** *Mesophyllum* sp., thin section 2019-S-2, coralline algal-bryozoan packstone. Epithallial cells (arrows). Meristematic cells are as long as or longer than cells immediately subtending them. **d** *Mesophyllum* sp., thin section of 2019-S-9, coralline algal-bryozoan packstone. Bi/tetrasporic conceptacle with pore canals (arrows). Pore canals are lined with specialised thinner-wider cells

Remarks: The morphological characteristics of the specimen from Štrba match the diagnosis of the genus *Mesophyllum*. The roof morphology and pore canal anatomy match the diagnosis of *M. incisum* (Foslie) Adey, 1970 (Woelkerling and Harvey 1992, 1993) from Southern Australia. However, our specimen bears smaller cells and conceptacles than *M. incisum*. Our specimens have no resemblance with any of the other well-known extant species previously described (Woelkerling and Harvey 1992, 1993; Athanasiadis et al. 2004; Peña et al. 2011; Athanasiadis and Ballantine 2014). In the fossil species, the pore canal cell morphology was proved only recently as a valuable diagnostic characteristic (Hrabovský et al. 2019); therefore, type species needs to be revised accordingly. We classify our specimen as *Mesophyllum* sp.

?Mesophyllum sp.
(Figure 15a-d)

Material: The bi/tetrasporic species description is based on a specimen from a thin section 2020-Sl and the gametophyte from a thin section 2018-S-1.

Description: The growth form is encrusting non-protuberant and without applanate branches (Fig. 15). The thallus is pseudoparenchymatous, dorsiventral and with monomerous construction. The hypothallus is coaxial to non-coaxial, 243–288 μm thick. The cells are 16–39 μm L (30 μm mean, 5.9 sd.) and 7–13 μm D (10 μm mean, 1.7 sd.). The perithallus consists of cells of 9–15 μm L (11 μm mean, 2.2 sd.) and 6–10 μm D (8 μm mean, 1.3 sd.). Cells of the adjacent filaments are laterally joined with fusions (Fig. 15). Overgrowths above the damaged parts of the

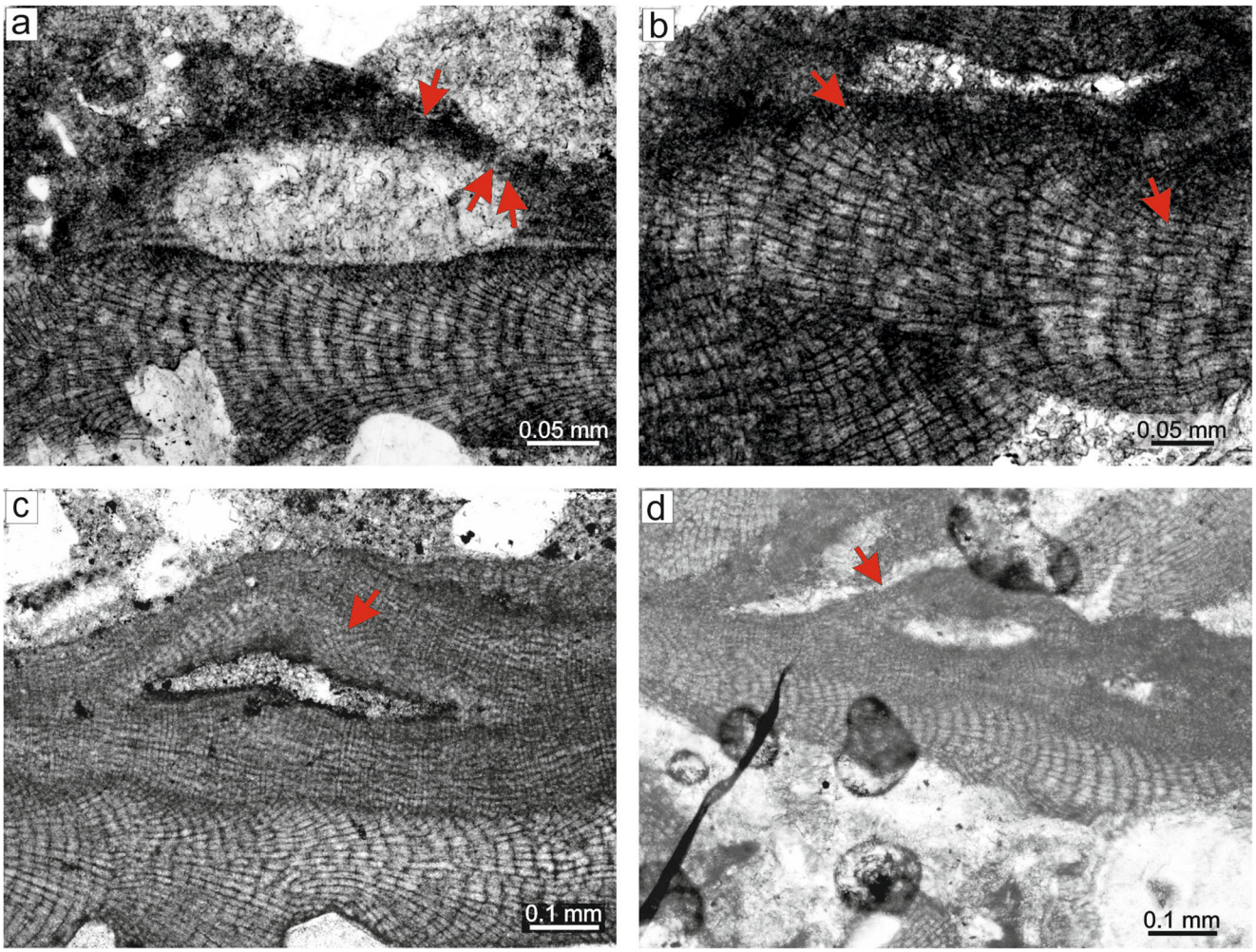

Fig. 15 **a**, **b** *?Mesophyllum* sp., bi/tetrasporic plant, thin section 2020-S-1, coralline algal-bryozoan packstone; **a** fertile portion of the thallus with encrusting growth form. Ventral core is coaxial. Arrows point to the pore canals. Pore canal cells are badly visible. **b** Portion of the thallus where the arrangement of the ventral core filaments is non-coaxial (arrows). Note the development of applanate branches. **c**, **d** *?Mesophyllum* sp. gametophyte, thin section 2018-S-1, coralline algal-bryozoan packstone; **c** conceptacle-like structure resulting from overgrowths over the damaged thallus; **d** *?Mesophyllum* sp. gametophyte bearing the small uniporate conceptacles (arrow).

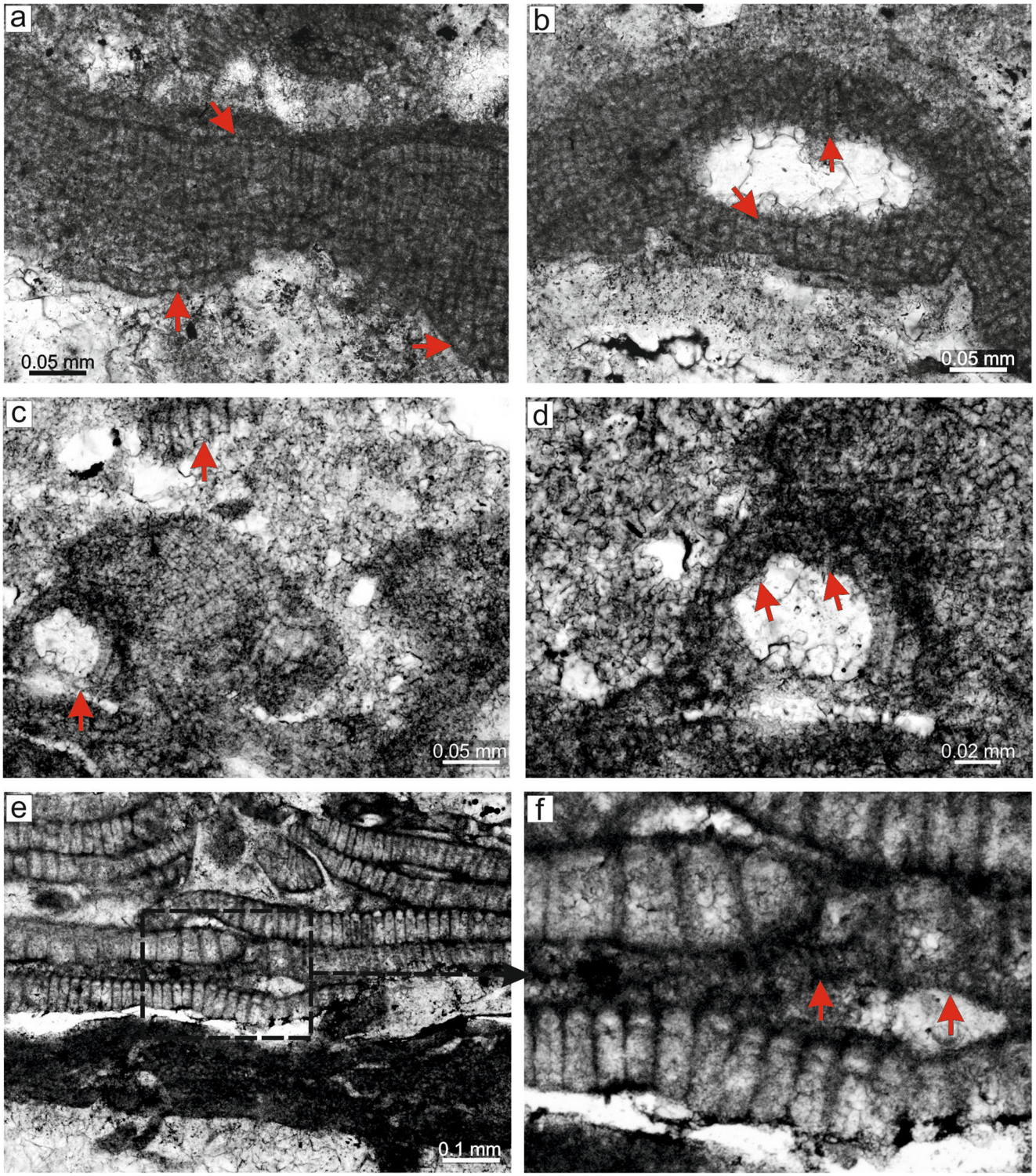

Fig. 16 **a**, **b** *Hydrolithon* sp., thin section 2019-SL-4, coralline algal-bryozoan packstone; **a** dimerous thallus is marked by arrows at the base of the figure and a layer of epithallisl cells (arrow at the top); **b** uniporate bi/tetrasporic conceptacle. Arrow at the base of the figure points to the lateral fusion of the adjacent cells. **c**, **d** *Lithoporella* cf. *minus* Johnson, 1964, fertile thallus, thin section 2020-S-1, coralline algal-bryozoan packstone; **c** dimerous thallus with flattened cells that underlie the bi/tetrasporic conceptacle (arrow at the base). Second arrow at the top of the figure points to the large cells in the fragmentary thallus. **d** roof cells (arrows) that are more or less perpendicularly oriented to the chamber. **e**, **f** *Lithoporella* cf. *minus* Johnson, 1964, sterile thallus, thin section 2019-S-8, coralline algal-bryozoan packstone; **e** great variability of the cell dimensions in sterile thallus; **f** detailed view of the thallus. Arrows point to the small as well as to the enlarged cells within the proposed single filament

thallus are present in some spots (Fig. 15). These overgrowths are similar with conceptacles but differ by those irregular morphology. Meristematic cells and epithallial cells were observed on the gametophytes. The meristematic cells appear locally elongated; elsewhere they are more or less of the same length. The epithallial cells are rounded, 4–5 μm L (4 μm mean, 0.1 sd.) and 8–9 μm D (8 μm mean, 0.5 sd.).

The proposed gametophytes possess conceptacles with chambers of 132–209 μm D and 30–42 μm H (Fig. 15). External D is 407 and conceptacle protrude 86 μm above the thallus surface. The bi/tetrasporic plant bears a single multiporate conceptacle (Fig. 15). Its external diameter is 797 μm and is raised 192 μm above the thallus surface. The cells around the conceptacle are elongated. The chamber is 480 μm D and 172 μm H. The roof consists of 7–8-celled filaments with cells shortening upward. The roof filaments are 54 μm L. The pore canals are badly visible.

Remarks: Although almost the gametophytic and bi/tetrasporic life cycle of this species is known, we do not have enough data to assess it in the genus *Mesophyllum* or in *Melyvonnea*. Therefore, we classify it as ?*Mesophyllum* sp., with a question mark.

Order Corallinales Silva and Johansen, 1986
Family Hydrolithaceae Townsend and Huisman, 2018
Subfamily Hydrolithoideae Kato and Baba in Kato et al., 2011
Genus *Hydrolithon* (Foslie) Foslie, 1909

Type species: *Hydrolithon boergesenii* (Foslie) Foslie, 1909; St. Croix, Virgin Islands, recent.

Hydrolithon sp.
(Figure 16a-b)

Material: Species occurs only in a thin section 2019-SL-4.

Description: Growth form encrusting (Fig. 16(a)). The thallus, up to 0.5 mm thick, is pseudoparenchymatous with dorsiventral internal organisation and dimerous construction (Fig. 16(a)). The primigenous filaments consist of non-palisade cells of 9–18 μm H (14 μm mean, 2.2 sd.) and 8–16 μm L (11 μm mean, 2.1 sd.). The H/L ratio of primigenous cells is 1–1.9. The postigenous cells are 7–19 μm L (12 mean, 2.9 sd.) and 8–14 μm D (11 μm mean, 1.8 sd.). The meristematic cells are mostly elongated, 9–16 μm L (13 μm mean, 2.5 sd.) and 5–9 μm D (7 μm mean, 1.3 sd.). The epithallial cells are rounded, 4–6 μm L (5 μm mean, 0.9 sd.) and 5–8 μm D (6 μm mean, 1 sd.) (Fig. 16(a)). Trichocytes are not observed.

The uniporate conceptacle is 196 μm D and 79 μm H. The pore canal is 73 μm L and 31 μm D. The presumed pore lining cells are badly preserved (Fig. 16(b)).

Remarks: Discrimination among the *Hydrolithon*, *Porolithon* and *Harveylithon* genera in fossil records is problematic without sufficient morphological data, i.e. trichocytes (Rösler et al. 2016). However, Rösler et al. (2016) provided genera diagnosis and included morphological characteristics that are also associated with thallus organisation. Based on their diagnosis, it is possible to exclude *Harveylithon* because this genus includes specimens with monomerous construction and a plumose hypothallus. Specimens with primarily dimerous thallus construction could be classified as *Hydrolithon* although monomerous could be present as well. Monomerous and dimerous thallus constructions occur and are probably more common in the genus *Porolithon*. Because only a dimerous thallus was observed, we identify the specimen as ?*Hydrolithon*.

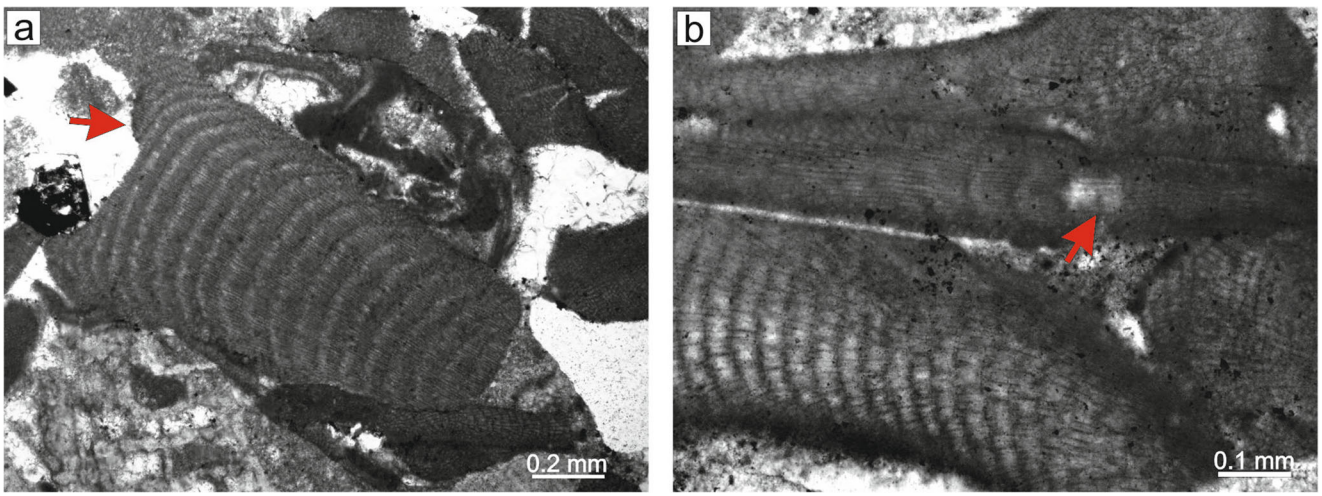

Fig. 17 Geniculate coralline algae from the Štrba locality; **a** *Arthrocardia mengaudi* (Lemoine) Aguirre, Braga et Bassi, 2011 (arrow), thin section 2019-SL-3, coralline algal-bryozoan packstone; **b** *Corallina* sp., thin section 2019-SL-2, coralline algal-bryozoan packstone. Note preserved genicula (arrow)

Subfamily Mastophoroideae Setchell, 1943
Genus *Lithoporella* (Foslie) Foslie, 1909

Type species: *Lithoporella melobesioides* (Foslie) Foslie 1909; South Niladu Island, Maldives, Recent.

Lithoporella cf. *minus* Johnson, 1964
(Figure 16c-f)

Material: Species description is based on two specimens: a sterile one from the thin section of 2019-S8, which has great variability of cell dimension, and a fertile one from the thin section of 2020-S1.
Description: The thallus is entirely bi-stratose and non-protuberant (Fig. 16(c)). Applanate branches are common. The thallus is pseudoparenchymatous with dorsiventral internal organisation and dimerous construction (Fig. 16(c)). The primigenous filaments consist of palisade cells of 8–15 μm H (12 μm mean, 2.4 sd.) and 6–10 μm L (8 μm mean, 1.7 sd.). The H/L ratio of primigenous cells is 0.9–2.2. However, fragments of thallus with cells of up to 32 μm in length occur near the fertile one. Trichocytes are not observed.

The identified conceptacle has a single pore canal of 23 μm L and 27 μm D (Fig. 16(d)). The roof cells are more or less parallel to the length of the pore canal (Fig. 16(d)). However, the cut is improper and our observation needs further confirmation. The conceptacle completely protrudes 77 μm above the thallus surface and its external diameter is 106 μm. The chamber is mostly rounded and 43 μm H and 62 μm D.

There are many thalli with cells of great variability in their morphology (Fig. 16(e)). Some sections consist of multiple fused cells and appear as large squares. The cells are 7–44 μm H (24 μm mean, 13.7 sd.) and 6-18 μm L (12 μm mean, 3.5 sd.). The H/L ratio of the primigenous cells is 0.9–4.3. The adjacent cells are joined laterally through fusion (Fig. 16(f)). One or two epithallial cells are above the primigenous cells (Fig. 16(f)). The epithallial cells are flattened or rounded but not flared, 10–12 μm L (11 μm mean, 1.1 sd.) and 12–15 μm D (14 μm mean, 2 sd.) (Fig. 16(f)).
Remarks: Our results point either to the presence of two separate species, or to the single species with great variety in cell morphology. In the latter option, small and flattened cells occur in the fertile area beneath the conceptacles and around them, while large cells could develop in distant parts of the thalli. The general lack of reproductive characteristics in the Priabonian *Lithoporella* species prevents any straightforward conclusions. It is worth noting that the fertile thallus is no larger than 300 μm. We did not find any arguments that enable us to discriminate the observed specimens. Therefore, we tentatively consider the observed thalli as belonging to a single species. The morphological characteristics of the fertile thallus match with those reported for *L. minus* from the Miocene (Hrabovský 2019; Bucur and Nicorici 1992). The cell dimensions of the fertile thallus match with the type; however, the height of the primigenous cells in the sterile thalli is 15 μm higher than the one reported for the type species (Johnson 1964). Therefore, we consider the specimens to be *L.* cf. *minus*.

Family Corallinaceae Lamouroux, 1812
Subfamily Corallinoideae (Areschoug) Foslie, 1908
Genus *Arthrocardia* Decaisne, 1842

Type species: *Arthrocardia corymbosa* (Lamarck) Decaisne, 1842, Cape of Good Hope, South Africa, Recent.

Arthrocardia mengaudii (Lemoine) Aguirre, Braga et Bassi, 2011
(Figure 17a)

Material: The description is based on a specimen from the thin section of 2019-SL-3.
Description: The complete intergenicula are about 1.5 mm L and 0.7 mm D (Fig. 17a). The medullary cells are 20–47 μm L (32 μm mean, 7.5 sd.) and 7–14 μm D (9 μm mean, 1.5 sd.). The intergenicula are 48–53 filaments thick. Genicula are not preserved and all the specimens are sterile.

Genus *Corallina* Linnaeus, 1758

Type species: *Corallina officinalis* Linnaeus, 1758, Europe, Recent.

Corallina sp.
(Figure 17b)

Material: The description is based on a specimen from the thin section of 2019-SL-2.
Description: The complete intergenicula are about 0.9 mm L and 0.2 mm D (Fig. 17b). The medullary cells are 18–31 μm L (24 μm mean, 4 sd.) and 6–8 μm D (7 μm mean, 0.6 sd.). The intergenicula are 6–15 filaments thick. Genicula are present only in this specimen. It consists of 8 filaments in the section. All the specimens are sterile.

Discussion

Biostratigraphy

Our results from nannoplankton biostratigraphy point to the 17–NP 18 Zone, hence an early Priabonian age of the studied section. This age corresponds with the limestone ages on this locality and adjacent areas (Gross

et al. 1980; Buček et al. 2013), as well as the distant Tichá dolina locality (Gross et al. 1993; Filo et al. 2009), which is inferred from the large foraminifera association. However, some ranges of the calcareous nannoplankton species could suggest a Bartonian age. Our biostratigraphical research did not cover the basal conglomerates in the Štrba locality. However, considering (1) the stratigraphic framework of this locality and adjacent sites, and (2) the similar sedimentary succession of these sites, as well as (3) the position of the section with respect to the direction of the marine transgression, all of which suggest that the Bartonian age of the basal conglomerates is unlikely. On the other hand, the calcareous nannoplankton assemblages lack species of the late Priabonian. This result has further strengthened the arguments about the age of the marine transgression in this part of CCPB.

The data from the biostratigraphical research of nannoplankton are consistent with the results based on the benthic foraminifera that point to the Shallow Benthic Zone (SBZ) 19 (Buček et al. 2013). Since the documented shallow benthic foraminiferal zone and nannoplankton zones overlap at the base of the SBZ19, the deposition of the limestone in Štrba could have occurred at the earliest beginning of the SZB19 zone (early Priabonian).

Endoliths

Microboring organisms in the marine realm include cyanobacteria, rhodophytes, chlorophytes, fungi, Eubacteria, and Archaea (Wisshak 2012). The morphology of tunnels is not sufficient to determine which among them is able to produce the observed borings, due to the similarity of the tunnels produced by fungi hyphae, cyanobacteria and eukaryotic algae (Golubic et al. 2005). The published ranges of diameters of these tubes vary between n.10-1 and n.101 μm (e.g. Golubic et al. 1984, 2005; Tribollet et al. 2011), which agrees with the tunnels observed in Foraminifera and rhodoliths. The tunnels can be branched in different ways and at different frequencies in both fungi and algae. All these morphologies were also recorded in our material. Marked differences were observed between the boring behaviour of phototrophs and heterotrophs: the fungi show a preference to proliferate within shell organic lamellae (Schneider 1976), whereas endolithic algae tend to proliferate within the mineral portion of the shell, apparently unable to digest and penetrate the surrounding organic lamellae (Golubic et al. 1975). In our material, the boring structures were observed in the inorganic material of the mollusk shells, and the direction of the tunnels does not follow the position of the organic lamellae in foraminifera. Therefore, phototrophs are the more probable borers.

In conclusion, we showed the presence of bioeroders in the foraminifera, rhodoliths, mollusks and predators of thecideid brachiopods in the ecosystems of a Štrba section.

Coralline algae

The CRA assemblage in Štrba consists of two geniculate and eleven encrusting species. Some include bi/tetrasporic plants and some gametophytes. The complete life cycle phases are not documented for the studied algae. Gametophytes are present in *L. camarasae*, *M. engelhartii, M. mengaudii* and ?*Mesophyllum* sp. The Hapalidiales is the most diverse order of coralline algae at the Štrba locality, with the highest abundance of the genus *Mesophyllum*. Corallinales and Sporolithales are far less common. In contrast to the Štrba section, the historical collection from the Tichá dolina locality includes two *S. nummuliticum* and *Sporolithon* sp. that bear gametophytes, while hapalidialid specimens are bi/tetrasporic only. Here, the differences in order diversity are not so evident.

Our study provides further evidence for the early Priabonian benthic assemblages with CRA. At least two distinct CRA assemblages inhabited the Central Carpathian Sea during this time interval. The first is characterised by (1) the hapalidialid bearing gametophytes and (2) less diversified corallinoids known from the Štrba locality. The second is characterised by (1) sporolithoid bearing gametophytes and (2) diversified corallinoids found in the Tichá dolina locality. The *Mesophyllum*-dominant assemblage is associated with a greater abundance of suspension feeders, while the *Sporolithon* assemblage is associated with phototrophs. The most striking result to emerge from the data is the distribution of the gametophytes. It is crucial to note that the ability of CRA to produce reproductive structures depends on sea water temperature (Adey 1973). As was pointed out, gametophytes of the *Mesophyllum* genus are probably more sensitive to temperature limits than bi/tetrasporic plants. This is because they are found only in the main area of the genus distribution in the temperate climatic zones, whereas those from the tropics are sterile or bi/tetrasporic plants only (Athanasiadis and Ballantine 2014). However, there is no such extensive research on *Sporolithon*, and further research is necessary to find out whether the inferences of Athanasiadis and Ballantine (2014) could be applied to other genera. Nevertheless, our results suggest that the distribution of warm- and cold-water gametophytes, *Sporolithon* and *Mesophyllum*, respectively, in the early Priabonian CCPB correlates with the distribution of other palaeoclimatic indicators such as corals or nummulites.

Palaeoenvironmental and palaeoecological reconstruction

Basal transgressive conglomerates as well as medium- to thick-bedded bioclastic limestones with wave ripples bearing

abundant large mollusks, and the occurrence of erosional structures suggest a shallow marine environment with high-energy conditions under wave action. Subsequently, accumulations of bryozoans in bryozoan marlstones, interbedded with storm generated sandstone beds suggest deeper settings below the normal wave base (fair-weather wave base) and may reflect deposition in the transition zone between coastal sands and shelf mud sediments. Facies succession thus represents an Upper Eocene transgression above the Triassic base and progressive deepening of the environment in the basin. The largest bulk of the carbonates from the Štrba locality are from shallow water. Based on these results, the stratigraphic succession of the Upper Eocene limestones studied here effectively captures a bathymetric gradient. The estimation of palaeodepth is based on the effects of ecological factors as are the substrate, sedimentation, hydrodynamic energy, nutrients and light penetration (Pérès 1982; Basso 1998). The better understanding of palaeoecological conditions requires the consideration of the microfacies. The microfacies are as follows from the base to the top of the section (Fig. 3): coralline algal-bryozoan packstone, bryozoan-coralline algal floatstone, bryozoan-coralline algal packstone and bryozoan packstone passing into the bryozoan marlstone.

Coralline algal-bryozoan packstone contains a great amount of highly fragmented CRA and bryozoan colonies with large foraminifera. The packstone microfacies is distributed in a variety of littoral settings (Flügel 2004). The dominant components of this microfacies determined in the Štrba locality are CRA crusts in association with geniculate forms. Coralline algal crusts are also common in a variety of recent-sea environments, e.g. mid-littoral (Pérès 1982), infralittoral (Steneck 1986; Fornós and Ahr 2006; Bracchi et al. 2016) and circalittoral (Pérès 1982; Ballesteros 2006). However, this microfacies (1) infills uneven substrate that was flooded during marine transgression, (2) surrounds pebbles derived from surf zone and (3) contains well-preserved nummulites, all suggesting rather shallow-water settings. In general, excess sedimentation is detrimental for the survival of CRA. This requires cleaning agents that are not so intensive so as to cause fatal injuries to corallines, and not so low so as to prevent them from fouling or burial (Steneck 1986; Bosence 1976; Basso and Tomaselli 1994). Therefore, we expect oscillation in the intensity of the physical and/or biological disturbance, allowing active growth of CRA, on the one hand, and their fragmentation, on the other. Because shallow waters are zones of high productivity and hydrodynamics, the grazing of fleshy algae on CRA thalli by herbivores and their mechanic fragmentation by water action is expected (Steneck 1986, 1991 and 1994; Wai and Williams 2006). This mechanism sufficiently explains the generation of biogenic material, as well as the absence of massive encrustations or large biogenic concretions. However, the described palaeoenvironmental settings favoured the development of the two biocoenoses within this microfacies at the Štrba locality: (1) coralline algal crust formed by encrusting species and (2) coralline algal turf formed by geniculate species. The first mentioned include two separate functional groups—thin and thick thalli (Steneck and Detheir 1994). In general, both geniculate and non-geniculate CRA are the first macrophytes colonising the free substrate (Wai and Williams 2006). In the mid-littoral and shallow littoral, the succession in CRA crusts consists of thin thalli overgrown by a thick one (Steneck 1986; Steneck et al. 1991; Adey and Vassar 1975). In the case of the second biocoenosis, geniculate CRA also form distinct biocenosis in the mid- and infralittoral (Pérès 1982; Fornós and Ahr 2006). Geniculate corallines are most abundant in coralline algal-bryozoan packstone and could grow as algal turf made of *Arthrocardia mengaudi*.

Given the above, we propose that the mixing of biocenosis and further packstone microfacies development was caused by the alternation of destructive and active growth phases of biota that generate biogenic sediment, with its subsequent reworking and redeposition with pebbles towards the more stable or sheltered sea bottoms at short distances. This eventually also stopped the phototrophic microendolith activity. In the case of the nummulits, in situ reworking or transport at short distances is suggested by the degree of abrasion of their tests. Pebbles became scarce towards the tops of the microfacies, suggesting a shift of the surf zone, therefore a shift of their landward source. Interparticle pores were subsequently irregularly infiltrated with mud while cement formation occurred in the free pores (Flügel 2004). We exclude diagenetic packstone because solution pressure or microstylolites on the adjacent grains are absent in this microfacies.

Bryozoan-coralline algal floatstone shows a higher concentration of mud. Most likely not all mud was infiltrated into the coralline algal-bryozoan packstone. Some settings enabled its accumulation and the development of a substrate suitable for sea grasses. The variable concentration of hooked and tubular coralline algal structures, as well as the growth of encrusting bryozoans in this microfacies point to the presence of seagrass in Štrba (compare Sola et al. 2013, Beavington-Penney et al. 2004). Therefore, we think that the substrate had nutrient content and was of biogenic origin (Pérès 1982). According to Pérès, seagrasses cause (1) dynamic decrease, (2) dimming out of the sea bottom and (3) the development of suitable substrate for encrusting organisms. At the Štrba locality, the presence of monospecific rhodoliths with loose internal structure and mud concentration, hapalidialid coralline algae with an accessory of *Sporolithon* and growth forms of coralline algae all match with the low-energy and cryptic environment. According to Pérès (1982), the lower limit of the infralittoral is characterised by the vanishing of seagrasses and photophilic plants. This transition is at a water depth of 20–35 m in well-lit sea water (Pérès 1982).

In the case of bryozoan-coralline algal and bryozoan packstone, bioclastic material was accumulated in the front of and around seagrass meadows. This sediment was rich in bryozoa. It is worth noting that most of the bryozoans were re-deposited from the place of their active growth into a place of accumulation (e.g. Bader 2001; Fornós and Ahr 2006). This is also true for other fossils. The exception could be the sparse *Mesophyllum engelhartii* coatings around the bryozoan colony, as well as the sparse monospecific fruticulose *Lithothamnion camarasae* rhodoliths. It should be noted that both of these are represented by a single specimen only. We propose that the accumulation of biogenic material occurred in the wider surroundings of the active production site. We are considering even shallower places than was the accumulation site or laterally distant areas. However, we do not expect the former biocenoses, coralline algal crusts, coralline algal turf or sea grasses meadows to be the source of such high concentrations of bryozoans. The microfacies corresponds with the circa-littoral coastal detritic biocoenosis (Pérès 1982). Its distribution in the recent Mediterranean Sea is mostly controlled by hydrodynamic conditions at the sea bottom and the rate of sedimentation. In the places with low dynamics, there is a prevalence of accumulation of mud above the bioclasts and the development of muddy detritic biocoenosis (Pérès 1982). Rippled structures in the studied biodetrital limestone and sediment texture point to the first point mentioned—the coastal detritic. However, alternation with thin marlstones suggests the possible overlapping with muddy detritic biocoenosis.

Our results point to a decline in irradiance and the transition from circa- to bathy-littoral, according to Pérès (1982) suggested by the decline and subsequent vanishing of coralline algae and the absence of nummulites approximately in the middle of the proposed coastal detritic of the Štrba locality. Generally, the lower limit of the circa-littoral zone is below 100-m water depth (Pérès 1982; Basso 1998; Basso et al. 2016) and corresponds with the maximum depth of the photoautotrophic metaphytes survival (Pérès 1982). This inference is contradictory to the one obtained from the sedimentological data, namely the basal conglomerates and rippled structures that were formed by waves under conditions of fair weather. This occurs in much shallower settings. Given the above, our results point to the shallowing of the photic zone.

Remarkable deepening is observed in the bryozoan marlstone. This environment is characterised by a high rate of sedimentation of fine particles. The sediment is rich in organic matter, indicative of the dark colour of the rocks, as well as the presence of glaucony. The thin sandstones suggest that the sea bottom was affected by events of high intensity and low frequency, such as storms; hence, this part of the succession is interpreted as tempestites.

Palaeoclimate

We found evidence of early Priabonian sea temperatures at the studied locality in the (1) grain associations, (2) coralline algal assemblages, (3) calcareous nannoplankton and (4) unique microendolith.

The documented grain associations in the studied site, rhodalgal and bryomol, are considered to relate to cool water, and are commonly found in shallow-water settings in temperate climatic zones (Carannante et al. 1988; Bader 2001; Nelson et al. 1988; Basso 1998). However, both could develop in tropical and non-tropical settings (Carannante et al. 1988; Halfar et al. 2006). Rhodalgal assemblages can grow in deeper water settings of the tropics where shallow and well-illuminated water favour the growth of chlorophytes and corals (Carannante et al. 1988). However, this is not the case for rhodalgal assemblages at the Štrba locality, because the sedimentological data suggest a shallow-water setting. The presence of rhodalgal grain association in the documented transgressive facies is thus rather indicative of temperate climate. Subsequent bryomol grain association matches with its distribution in recent temperate shallow-water seas where it is commonly found in deeper settings below the rhodalgal (Bader 2001; Hayton et al. 1995). Therefore, both grain associations suggest that temperate climate and cold water influence the growth of benthic assemblages in the Štrba locality.

Another clue for palaeoclimate reconstruction is the presence of the corallines themselves. According to their modern global distribution, the assemblages dominated by Hapalidiales with minor Corallinales and Sporolithales characterise shallow to mid-depth water settings of the mid latitudes (Aguirre et al. 2000; Basso et al. 2009). The argument supporting the temperate climate is the assemblage dominated by *Mesophyllum*. These algae are distributed in the recent temperate seas, i.e. the Northeastern Atlantic (Athanasiadis and Ballantine 2014), Northeastern Pacific (Athanasiadis et al. 2004), Southern Australia and New Zealand (Woelkerling and Harvey 1993). *Mesophyllum* is also known from the tropics or subtropics (Adey et al. 1982; Athanasiadis and Ballantine 2014). However, they are predominantly bi/tetrasporic phases without gametophytes (Athanasiadis and Ballantine 2014).

Furthermore, calcareous nannoplankton is supported in fairly temperate climates because the prevailing *Reticulofenestra bisecta*, *R. stavanensis* and *C. floridanus* indicate temperate water, while *Lanternithus minutus* tolerate even cold water. Moreover, typical warm-water taxa such as *Discoaster* spp. and *Sphenolithus* spp. are nearly missing (temperature preference of species according to Wei and Wise Jr. 1990; Villa et al. 2008; Oszczypko-Clowes and Żydek 2012).

Last but not least, the circular to elliptical structure determined as *Fossichnus solus* are ascribed on thecideid brachiopod. These structures are quite common within

the Quaternary temperate zone. Therefore, it has potential utility as a palaeoecological marker of cold waters in the Eocene (Nielsen et al. 2003).

In summary, cool-water carbonates developed in this part of the CCPB during the early Priabonian. Cold-water benthic assemblages documented to have an extensive accumulation of bryozoan as well as plankton are known from the CCPB and are indicative of the global climate deterioration that is characteristic for the Priabonian (e.g. Soták 2010; Oszczypko-Clowes and Żydek 2012). This event is dated to the uppermost NP18 to NP19-20 nannoplankton zone, while older assemblages commonly contain warm-water and oligotrophic elements such as sporadic hermatypic corals (Schaleková 1962, Gross et al. 1980), nummulites in the extensive nummulitic banks (Gross et al. 1980, Buček et al. 2013), or the CRA reported in this work (at the Tichá dolina locality—see the discussion above). It is generally accepted that such warm-water assemblages have developed under the influence of the Middle Eocene Climatic Optimum spanning from the Lutetian to early Priabonian in the whole SZB19 Zone (Soták 2010). Given the above, the heterogeneous water temperature of the early Priabonian in the Central Carpathian Basin is obvious. Therefore, our results point to factors other than global climatic deterioration as influencing the distribution and growth of benthic assemblages during the early Priabonian at the Štrba locality. One of the most plausible explanations seems to be the upwelling discussed in the next chapter.

Upwelling

What we have observed in the early Priabonian successions is characterised by a few important markers: first, the heterogeneous sea water temperature and nutrient distribution along the CCPB coast that are inferred from the benthic assemblages; second, the opposing palaeobathymetric inferences that are based on palaeontological and sedimentological data; third, the predominance of heterotrophs in the shallow-water settings; and fourth, glaucony in the bryozoan marlstone.

As was suggested by Halfar et al. (2006), carbonates, especially Bryomol, in warm water can "mimic" cool-water assemblages when the cool water and nutrients are carried by upwelling into shallow-water settings. The same pattern was documented for Rhodalgal in the recent Yucatan, where cold-water input from upwelling prevent the development of chlorozoan grain association in the tropics and favour the growth of rhodalgal (Carannante et al. 1988). Also the upwelling favour encrustations of coralline algae above the corals in the Yemen coast (Benzoni et al. 2011). We document upwelling settings in basal conglomerates as well as bedded bioclastic limestone that consist of cool-water assemblages—rhodalgal and bryomol found in the shallow-water environment influenced by fair weather wave action. Our inference is strengthened by the evolution of the CCPB carbonate platform that was determined by the Middle Eocene Climatic Optimum when sea water temperatures were above 20 °C and favoured accumulations of nummulites. According to Soták (2010), such temperatures dominated in the CCPB during the Late Lutetian to early Priabonian, and warm-water carbonate deposition ceased with the latest nummulites in the SBZ20 zone (Soták 2010 p. 395, fig. 4). Palaeotemperatures that were estimated based on the geochemical analyses of nummulit tests from CCPB suggest the average temperature of the sea water was 22 °C (Soták 2010). The situation on the adjacent sites, the position of the Štrba section at the base of SZB19 and a general knowledge of palaeoclimate during this time interval all suggest that cool-water carbonates from the Štrba section were developed on the warm-water carbonate platform, hence are representative of a rather local situation. Moreover, it was discussed in Pérès (1982) that the prolonged action of a single ecological factor would favour the boom of certain organisms at the expense of others, and would consequently cause a shift in biocoenosis spatial distribution. Since suspension feeders such as bryozoans and mollusks exceed the other benthic biota in the bedded bioclastic limestone and marlstones of the Štrba locality, we assume that the reason for their extensive accumulation could be found in the nutrient supply. Moreover, nutrient input and eutrophication are causes of the photic zone shallowing (Pérès 1982) documented here in the bedded bioclastic limestone.

These results offer evidence for coastal upwelling conditions in the Štrba section, with seasonal decrease of the sea water temperature, growth of cool-water coralline algal assemblage in rhodalgal grain association and the expansion of suspension feeders that produced bryomol grain association. It is shown in Smith (1992) that the temperature boundary of the surface water in the upwelling areas is sharp, and that cold upwelled waters can be 8 °C cooler than adjacent warm-surface waters. During the seasons that are free of coastal upwelling, oligotrophic and euphotic warm-water nummulites could thrive on the sea bottom in the warm-water settings. We think that this mechanism would explain why adjacent sites are rich in nummulites but the Štrba section is not. However, their amount in the lithofacies could still reach a few percent. Based on our results, we propose the presence of warm-water organisms such as nummulites together with cool-water *Mesophyllum* gametophytes found in the shallow-water transgressive carbonates to be indicative of a coastal upwelling regime rather than the mixing of assemblages due to the continual deepening and redeposition of carbonate sediments.

One could argue that we have documented mesotrophic conditions in this part of the CCPB sea that are not consistent with the eutrophication characteristics for

upwelling systems. This argument is supported by the fact that the Priabonian CCPB is not characterised by nutrient enrichment but rather by the mesotrophication of the sea water (Soták 2010). However, this restricted concept limits the possible palaeoecological interpretations. Here are a few examples where the identification of coastal upwelling ecosystems in the coastal shallow-water environments is not associated with high eutrophication: (1) coastal upwellings in the Mediterranean Sea do not upwell such amounts of nutrients as are characteristic for the main upwelling centres of the world (Kämpf and Chapman 2016; Cebrián et al. 2000); (2) carbonates from the Mediterranean, Mexican, Pannamian and Peruvian shallow seas grow in zones affected by upwelling; however, these environments do not produce plankton-enriched or fine-grain sediment (Cebrián et al. 2000, Glynn et al. 2007, 2017, Carannante et al. 1988,). Moreover, hydrographic settings in coastal upwelling areas such as eddies or gyres can suppress their effect on primary production (Gruber et al. 2011) and/or they can move the zones of primary production seaward (Gruber et al. 2011; Corsini et al. 2002). In this case, the nutrients are consumed prior to their accumulation on the sea bottom and their content in the upwelled coastal water is lowered (Gruber et al. 2011). Therefore, the absence of the upwelling signal based on the calcareous nannoplankton in the Štrba locality could be artificial, reflecting peculiar hydrographic conditions in the CCPB. Nutrients could also have been carried into the basin by rivers. However, the rivers cannot affect the distribution of cool-water coralline algae or the grain associations in the basin. Given the above, we think that the heterogeneous distribution of the shallow-water sea temperature and nutrients along the CCPB coast is indicative of the seasonal coastal upwelling and hydrographic settings.

Last but not least, the presence of glaucony in bryozoan marlstones is indicative of the nutrient enrichment of the environment. Although its distribution is associated with a variety of depth and temperature environments, nutrient enrichment is of prime importance (Huggett et al. 2017). The boom of the bryozoan and deposition of marlstones above the biogenic or sandy limestone is an event that is documented throughout the CCPB during the Priabonian. It is associated with climate deterioration, the mesotrophication of the sea and the demise of a benthos-producing warm-water carbonate platform (Soták 2010). As was suggested by Soták (2010), the widespread bryomol carbonates and marlstones resulted from the progressive eutrophication of the CCPB, since cooler waters are usually richer in nutrients. The bryozoan marlstone accumulation at the Štrba locality shows slightly earlier onset than that of the other sites. This may be explained as being a result of local upwelling conditions. However, rivers plumes and climate deterioration, as well as coastal upwelling, are agents that may significantly affect nutrient input; thus, discrimination between these factors is not easy. As such, the synergy of all the agents having an effect on the controlled deposition of bryozoan marlstone cannot be rejected (Soták et al. 2010).

Conclusions

We have described a coralline algal assemblage from the southern border of the Central Carpathian Paleogene Basin. The assemblage consists of two geniculate species—*Arthrocardia mengaudi* and *Corallina* sp., and eleven non-geniculate species *Sporolithon nummuliticum*, *Lithothamnion camarasae*, *L.* cf. *corallioides*, *Mesophyllum engelhartii*, *M. fructiferum*, *M. mengaudii*, *Mesophyllum* sp., ?*Mesophyllum* sp., *Phymatolithon* sp., *Lithoporella* cf. *minus* and ?*Hydrolithon* sp. The historical collection of Anna Schaleková was also re-evaluated as we were not able to confirm the presence of lithophylloid coralline algae in her collection. However, what is important is the presence of the oldest record of *Hydrolithon lemoineii*. This paper has stressed the importance of coralline algal gametophytes in palaeoecological interpretations. While warm-water *Sporolithon* gametophytes are known to come from the warm-water limestone of the Tichá dolina site, some temperate *Mesophyllum* gametophytes were observed in the cool-water limestones of the Štrba locality.

In summary, the studied carbonate deposits are of early Priabonian age, namely the SBZ19 and NP17-18 biozones. This time interval is characterised by warm-water carbonate production in the CCPB basin, associated with the extensive accumulation of nummulites. In this paper, we have documented cool-water carbonate production characterised by rhodalgal and bryomol grain association on a warm-water carbonate platform. Sedimentological study suggests that the carbonates are shallow-water and deposited in the environment where carbonate grains were agitated by waves under conditions of fair weather. Our findings support the idea that coastal upwelling determined the distribution of biota in this part of the basin. The seasonal input of cold water decreased the sea water temperature, thus enabling the sexuate reproduction of cool water corallines, the growth of cool-water coralline algal assemblage in rhodalgal grain association and the expansion of suspension feeders. This event was also accompanied by the shallowing of the photic zone as a result of nutrification. During the upwelling-free regime, warm-water nummulites could thrive on the sea bottom. Our interpretations explain why nummulite accumulation was not as extensive as in the adjacent sites, as well as the discrepancies between the depth estimations from the palaeontological and sedimentological data. The depth-level estimation based on

phototrophs is most likely artificial and affected by (1) the expansion of sea grass canopies that shadowed the seafloor and enabled the growth of deep-water coralline algae, (2) the prolonged action of nutrient input that caused the shallowing of the photic zone and subsequent vanishing of deep/cool-water coralline algal assemblage at the depths where they commonly occur in recent seas and (3) the expansion of suspension feeders such as bryozoans and mollusks in the bryomol grain association.

Bryozoan marlstone with glaucony topping the section represents the gradual deepening of the basin and nutrient enrichment. Generally, bryozoan marlstones are considered a marker of global climate deterioration documented in the Priabonian (Soták 2010). However, it is impossible to discriminate between the upwelling, river plumes and climate factors as the sources of nutrients enhancing the expansion of bryozoans and the accumulation of marls.

Taken together, our results suggest that nutrients, sea water temperature and light availability, accompanied with the deepening of the environment due to sea-level rise and the tectonic activity of the basin, all controlled the biotic assemblage and carbonate deposition of the southern part of the Central Carpathian Paleogene Basin during the early Priabonian.

Supplementary Information The online version contains supplementary material available at https://doi.org/10.1007/s12549-021-00488-x.

Acknowledgements This work was carried out within the framework of the VEGA project 2/0014/18 and was partly supported by the Czech Grant Agency project No. GACR 18-05935S. The study was supported by the project PROGRES Q45. We are particularly grateful to doc. Mgr. Natália Hudáčková, PhD, of Comenius University in Bratislava, for providing the historical collection of coralline algae for analysis. We are also grateful to Mgr. Šárka Roušavá of Masaryk University in Brno for the grammar proofreading of the English text. Last but not least, we are grateful for insightful comments and reviews of the manuscript to Daniela Basso and an anonymous reviewer.

Funding This study was financially supported by VEGA project 2/0014/18, GACR 18-05935S, and PROGRES Q45.

Data availability Material is stored in the depository of the Slovak Academy of Science, Bratislava. Historical collection is stored in the depository of the Comenius University in Bratislava.

Declarations

Conflict of interest The authors declare that they have no conflict of interest.

References

Adey, W. H. (1973). Temperature control of reproduction and productivity in a subarctic coralline alga. *Phycologia, 12*(3/4), 111–118.

Adey, W. H., & Vassar, J. M. (1975). Colonization, succession and growth rates of tropical crustose coralline algae (Rhodophyta, Cryptonemiales). *Phycologia, 14*, 55–69.

Adey, W. H., Townsend, R. A., & Boykins, W. T. (1982). The Crustose Coralline Algae (Rhodophyta: Corallinaceae) of the Hawaiian Islands. *Smithsonian Contributions to the Marine Sciences, 15*, 1–74.

Adey, W. H., Athanasiadis, A., & Lebednik, P. A. (2001). Re-instatement of Leptophytum and its type Leptophytum leave: taxonomy and biogeography of the genera Leptophytum and Phymatolithon (Corallinales, Rhodophyta). *European Journal of Phycology, 36*, 191–203.

Aguirre, J., & Braga, J. C. (1998). Redescription of Lemoine's (1939) types of Coralline algal species from Algeria. *Palaeontology, 41*, 489–507.

Aguirre, J., Riding, R., & Braga, J. C. (2000). Diversity of coralline red algae: origination and extinction patterns from the Early Cretaceous to the Pleistocene. *Paleobiology, 26*, 651–667.

Aguirre, J., Braga, J. C., & Bassi, D. (2011). Taxonomic assessment of coralline algal species (Rhodophyta; Corallinales and Sporolithales) described by Pfender, Lemoine, and Miranda from northern Spain type localities. *Annalen des Naturhistorischen Museums in Wien, Serie A, 113*, 267–289.

Andrusov, D. (1937). Rôle des Thallophytes dans la constitution des roches sédimentaires des Carpathes tchécoslovaques. *Věstník Královské České Spolučnosti Nauk, Třída Matematicko-Přírodovědecká, 1938*, 1–32.

Athanasiadis, A. (2001). Lectotypification of *Lithophyllum arcticum* (Corallinales, Rhodophyta) and a study of its relationships within the Melobesioideae. *Nordic Journal of Botany, 21*, 93–112.

Athanasiadis, A., Lebednik, P. A., & Adey, W. H. (2004). The genus *Mesophyllum* (Melobesioideae, Corallinales, Rhodophyta) on the northern Pacific coast of North America. *Phycologia, 43*, 126–165.

Athanasiadis, A., & Ballantine, D. L. (2014). The genera *Melyvonnea* gen. nov. and *Mesophyllum* s.s. (Melobesioideae, Corallinales, Rhodophyta) particularly from the central Atlantic Ocean. *Nordic Journal of Botany, 32*, 385–436.

Bader, B. (2001). Modern bryomol-sediments in a cool-water, high-energy settings: the Inner Shelf off Northern Brittany. *Facies, 44*, 81–104.

Ballesteros, E. (2006). Mediterranean coralligenous assemblages: a synthesis of present knowledge. In R. N. Gibson, R. J. A. Atkonson, & J. D. M. Gordon (Eds.), *Oceanography and Marine Biology – An Annual Review* (pp. 123–195). Boca Raton: CRC Press.

Baráth, I., & Kováč, M. (1995). Systematics of gravity-flow deposits in the marginal Paleogene formations between Markušovce and Kluknava villages (Hornád Depression). *Mineralia Slovaca, Geovestník, 27*, 1–6. [in Slovakian]

Bassi, D. (2005). Larger foraminiferal and coralline algal facies in an Upper Eocene storm-influenced, shallow-water carbonate platform (Colli Berici, north-eastern Italy). *Palaeogeography, Palaeoclimatology, Palaeoecology, 226*, 17–35.

Basso, D. (1995). Living calcareous algae by a paleontological approach: the genus *Lithothamnion* Heydrich nom. cons. from the soft bottoms of the Tyrrhenian Sea (Mediterranean). *Rivista Italiana di Paleontologia e Stratigrafia, 101*, 349–366.

Basso, D. (1998). Deep rhodolith distribution in the Pontian Islands, Italy: a model for the paleoecology of temperate sea. *Palaeogeography, Palaeoclimatology, Palaeoecology, 137*, 173–187.

Basso, D. (2012). Carbonate production by calcareous red algae and global change. In D. Basso & B. Granier (Eds.), *Calcareous algae and global change: from identification to quantification*. *Geodiversitas 34,* 13–33.

Basso, D., & Tomaselli, V. (1994). Palaeoecological potentiality of rhodoliths: a Mediterranean case history. In R. Matteucci et al. (Eds.), *Studies on Ecology and Paleontology of Benthic*

Communities, Bollettino della Societa Paleontologica Italiana, Special Volume 2 (pp. 17–27). Modena: Mucchi.

Basso, D., Fravega, P., Piazza, M., & Vannucci, G. (1998). Revision and re-documentation of M. Airoldi's species of *Mesophyllum* from the Tertiary Piedmon Basin (NW Italy). *Rivista Italiana di Paleontologia e Stratigrafia, 106*, 85–94.

Basso, D., Nalin, R., & Nelson, C. S. (2009). Shallow-water Sporolithon rhodoliths from North Island (New Zealand). *Palaios, 24,* 92–103.

Basso, D., Babbini, L., Ramos-Esplá, A. A., & Salomidi, M. (2016). Mediterranean Rhodolith Beds. In R. Riosmena-Rodríguez, W. Nelson, & J. Aguirre (Eds.), *Rhodolith/Maërl Beds: A Global Perspective* (pp. 281–298). Springer International Publishing.

Beavington-Penney, S. J. (2004). Analysis of the effects of abrasion on the test of *Palaeonummulites venosus*: implication for the origin of Nummulithoclastic Sediments. *Palaios, 19*, 143–155.

Beavington-Penney, S. J., Wright, P., & Woelkerling, W. J. (2004). Recognising macrophyte-vegetated environments in the rock record: a new criterion using 'hooked' forms of crustose coralline red algae. *Sedimentary Geology, 166*, 1–9.

Benzoni, F., Basso, D., Caragnano, A., & Rodondi, G. (2011). *Hydrolithon* spp. (Rhodophyta, Corallinales) overgrow live corals (Cnidaria, Scleractinia) in Yemen. *Marine Biology, 158*, 2419–2428.

Biely, A., Bezák, V., Elečko, M., Kaličiak, M., et al. (1996). *Geological map Map of Slovakia (1:500 000)*. Bratislava: Geological Survey of Slovak Republic.

Bode, A., Varela, M., Prego, R., Rozada, F., & Santos, M. D. (2017). The relative effects of upwelling and river flow on the phytoplankton diversity patterns in the ria of A Coruña (NW Spain). *Marine Biology, 164*, 93.

Bosence, D. W. J. (1976). Ecological studies on two unattached coralline algae from Western Ireland. *Palaeontology, 19*, 365–395.

Bracchi, V., Nalin, R., & Basso, D. (2016). Morpho-structural heterogeneity of shallow-water coralligenous in a Pleistocene marine terrace (Le Castella, Italy). *Palaeogeography Palaeoclimatology Palaeoecology, 454*, 101–112.

Braga, J. C., Bosence, D. W. J., & Steneck, R. S. (1993). New anatomical characters in fossil coralline algae and their taxonomic implications. *Palaeontology, 36*, 535–547.

Bucur, I. I., & Nicorici, E. (1992). Calcareous algae from the Sarmatian deposits in the Simleu Basin (Romania). *Studia Univ Babeş-Bolyai, Geologia, 2*, 3–7.

Buček, S., Filo, I., & Laurinc, D. (2013). Litofaciálne členenie borovského súvrstvia Liptovskej kotliny a západnej časti Popradskej kotliny. In Ľ. Hraško (Ed.), *Aktualizácia geologickej stavby problémových území Slovenska v mierke 1:50 000 (pp. 50)*. Bratislava: Ministerstvo Životného Prostredia Slovenskej Republiky, Štátny Geologický Ústav Dionýza Štúra Geofond archive, archive number: 91733_37.

Carannante, G., Esteban, M., Milliman, J. D., & Simone, L. (1988). Carbonate lithofacies as paleolatitude indicators problems and limitations. *Sedimentary Geology, 60*, 333–346.

Cebrián, E., Ballesteros, E., & Canals, M. (2000). Shallow rocky bottom benthic assemblages as calcium carbonate producers in the Alboran Sea (southwestern Mediterranean). *Oceanologica Acta, 23*, 311–322.

Chalupová, B. (2000). Eocene fish fauna from the Menilite Beds (Huty Formation) of the Central Carpathian Paleogene Basin (Orava region, NW Slovakia). *Slovak Geological Magazine, 6*, 168–171.

Checconi, A., Bassi, D., Carannante, G., & Monaco, P. (2010). Redeposited rhodoliths in the Middle Miocene hemipelagic deposits of Vitulano (Southern Apennines, Italy): Coralline assemblage characterization and related trace fossils. *Sedimentary Geology, 225*, 50–66.

Corsini, G., Grasso, R., & Cipollini, P. (2002). Regional bio-optical algorithms for the Alboran Sea from a reflectance model and in situ data. *Geophysical Research Letters, 29*, 1–4.

Filipek, A., Wysocka, A., & Barski, M. (2017). Depositional setting of the Oligocene sequence of the Western Carpathians in the Polish Spisz region – a reinterpretation based on integrated palynofacies and sedimentological analyses. *Geological Quarterly, 61*, 859–876.

Filo, I., & Siráňová, Z. (1996). The Tomášovce Member – a new lithostratigraphic unit of the Subtatric Group. *Geologicke Práce, Správy, 102*, 41–49. [in Slovakian with English summary]

Filo, I., & Siráňová, Z. (1998). Hornád and Chrasť Member – new regional lithostratigraphic units of the Sub-Tatric Group. *Geologické Práce, Správy, 103*, 35–51. [in Slovakian with English summary]

Filo, I., Buček, S., & Siráňová, Z. (2009). *Litofaciálne členenie borovského súvrstvia podtatranskej skupiny (oravský paleogén)*. Bratislava: Štátny Geologický Ústav Dionýza Štúra.

Flügel, E. (2004). *Microfacies of carbonate rocks. Analysis, Interpretation and Application*. New York: Springer.

Fornós, J. J., & Ahr, W. M. (2006). Present-day temperate carbonate sedimentation on the Balearic Platform, western Mediterranean: compositional and textural variation along a low-energy isolated ramp. In H. M. Pedley & G. Carannante (Eds.), *Cool-Water Carbonates: Depositional Systems and Palaeoenvironmental Controls, Special Publications, 255* (pp. 71–84). London: Geological Society.

Garecka, M. (2005). Calcareous nannoplankton from the Podhale Flysh (Oligocene-Miocene, Inner Carpathians, Poland). *Studia Geologica Polonica, 124*, 353–369.

Gedl, P. (2000). Biostratigraphy of the Podhale Paleogene (Inner Carpathians, Poland) in the light of palynological studies. Part II. Summary and systematic descriptions. *Studia Geologica Polonica, 117*, 155–303.

Ghosh, A. K., Sarma, A., & Sarkar, S. (2013). Diversity of Middle Eocene Coralline Red Algae from the Prang Limestone (Shella Formation) of Jaintia Hills, Meghalaya, NE Himalaya, India with special emphasis on palaeoenvironment. *Chinese Science Bulletin, 58*, 118–125.

Glynn, P. W., & Leyte Morales, G. E. (1997). Coral reefs of Huatulco, West México: reef development in upwelling Gulf of Tehuantepec. *Revista de Biología Tropical, 45*, 1033–1047.

Glynn, P. W., Mones, A. B., Podestá, G. P., Colbert, A., & Colgan, M. W. (2017). El Niño-southern oscilation: effects on Eastern Pacific coral reefs and associated biota. In P. W. Glynn (Ed.), *Coral Reefs of the Eastern Pacific, Coral Reefs of the World 8* (pp. 251–290). Dortrecht: Springer.

Golubic, S., Perkins, R. D., & Lukas, K. J. (1975). Boring microorganisms and microborings in carbonate substrates. In R. W. Frey (Ed.), *The Study of Trace Fossils* (pp. 229–259). Berlin, Heidelberg: Springer.

Golubic, S., Campbell, S. E., & Spaeth, C. (1983). Kunstharzausgüsse fossiler Mikroben-Bohrgänge. *Der Präparator, 29*, 197–200.

Golubic, S., Radtke, G., & Le Campion-Alsumard, T. (2005). Endolithic fungi in marine ecosystems. *Trends in Microbiology, 13*, 229–235.

Gradstein, F. M., Ogg, J. G., Schmitz, M. D., & Ogg, G. M. (2012). *The Geologic Time Scale 2012, 2-Volume Set*. New York: Elsevier.

Gross, P. (2008). *Lithostratigraphy of Western Carpathians: Paleogene – Podtatranská Group*. Bratislava: Štátny Geologický Ústav Dionýza Štúra. [in Slovakian with English summary]

Gross, P., Köhler, E., et al. (1980). *Geology of Liptovská kotlina (depression)*. Bratislava: Štátny Geologický Ústav Dionýza Štúra. [in Slovakian with English summary]

Gross, P., Köhler, E., & Samuel, O. (1984). A new lithostratigraphic division of the Inner-Carpathian Paleogene. *Geologické Práce, Správy, 81*, 113–117. [in Slovakian with English summary]

Gross, P., Köhler, E., Mello, J., Haško, J., Halouzka, R., & Nagy, A. (1993). *Geológia Južnej a Východnej Oravy (Geology of Southern*

and Eastern Orava). Bratislava: Štátny Geologický Ústav Dionýza Štúra.

Gruber, N., Lachkar, Z., Frenzel, H., Marchesiello, P., Münnich, M., McWilliams, J. C., Nagai, T., & Plattner, G. K. (2011). Eddy-induced reduction of biological production in eastern boundary upwelling systems. *Nature Geoscience, 4*, 787–792.

Guerry, A. D., & Menge, B. A. (2017). Grazer impacts on algal community structure vary with the coastal upwelling regime. *Journal of Experimental Marine Biology and Ecology, 488*, 10–23.

Hageman, S. J., Bock, P. E., Bone, Y., & McGowran, B. (1998). Bryozoan growth habits: classification and Analysis. *Journal of Paleontology, 72*, 418–436.

Halfar, J., Strasser, M., Riegl, B., & Godinez-Orta, L. (2006). Oceanography, sedimentology and acoustic mapping of a bryomol carbonate factory in the northern Gulf of California, Mexico. In H. M. Pedley & G. Carannante (Eds.), *Cool-Water Carbonates: Depositional Systems and Palaeoenvironmental Controls, Special Publications* (pp. 197–216). London: Geological Society.

Hayton, S., Nelson, C. S., & Hood, S. D. (1995). A skeletal assemblage classification system for non-tropical carbonate deposits based on New Zealand Cenozoic limestones. *Sedimentary Geology, 100*, 123–141.

Hrabovský, J. (2019). Reproductive phases of Miocene algae from central Paratethys and their bearing on systematics. *Acta Palaeontologica Polonica, 64*, 417–439.

Hrabovský, J., Basso, D., & Doláková, N. (2015). Diagnostic characters in fossil coralline algae (Corallinophycidae: Rhodophyta) from the Miocene of southern Moravia (Carpathian Foredeep, Czech Republic). *Journal of Systematic Palaeontology, 14*, 499–525.

Hrabovský, J., Basso, D., & Coletti, G. (2019). The first identification of fossil Mesophyllum in accordance to the modern taxonomic concepts in coralline algae. *Acta Paleontologica Polonica, 64*, 897–909.

Huggett, J., Adetunj, J., Longstaffe, F., & Wray, D. (2017). Mineralogical and geochemical characterization of warm-water, shallow-marine glaucony from the Tertiary of the London Basin. *Clay Minerals, 52*, 25–50.

Irvine, L. M., & Chamberlain, Y. M. (1994). *Seaweeds of the British Isles. Volume 1 Rhodophyta, Part 2B Corallinales, Hildenbrandiales*. London: Pelagic Publishing.

Iryu, Y., Nakamori, T., Matsuda, S., & Abe, O. (1995). Distribution of marine organisms and its geological significance in the modern reef complex of the Ryukyu Islands. *Sedimentary Geology, 99*, 243–258.

Ishijima, W. (1960). Eocene Coralline Algae from the Kuma Group in the Ishizuchi Range, Shikoku, Japan. *Scientific Report, 4*, 154–161.

Janočko, J., & Jacko, S. (1999). Marginal and deep-sea deposits of Central-Carpathian Paleogene Basin, Spiš Magura region, Slovakia: implication for basin history. *Slovak Geological Magazine, 4*, 281–292.

Johansen, H. W. (1981). *Coralline Algae a First Synthesis*. London, New York: CRC Press.

Johnson, J. H. (1948). Eocene Algae from Florida. *Journal of Paleontology, 22*, 762–766.

Johnson, J. H. (1952). Coralline Algae from the Eocene Atascadero Limestone. *Journal of Paleontology, 26*, 537–543.

Johnson, J. H. (1953). Eocene Coralline Algae from the Meganos Formation, California. *Journal of Paleontology, 27*, 130–136.

Johnson, J. H. (1964). *Eocene Algae from Ishigaki-shima Ryūkyū-rettō*. Washington: United States Government Printing Office.

Johnson, J. H. (1965). Coralline Algae from the Cretaceous and Early Tertiary of Greece. *Journal of Paleontology, 39*, 802–814.

Kázmér, M., Dunkl, I., Frisch, W., Kuhlemann, J., & Ozsvárt, P. (2003). The Palaeogene forearc basin of the Eastern Alps and Western Carpathians: subduction erosion and basin evolution. *Journal of the Geological Society London, 160*, 413–428.

Kämpf, J., & Chapman, P. (2016). *Upwelling Systems of the World. A Scientific Journey to the Most Productive Marine Ecosystems*. Springer International Publishing.

Kováč, M., Plašienka, D., Soták, J., Vojtko, R., Oszczypko, N., Less, G., Ćosović, V., Fügenschuh, B., & Králiková, S. (2016). Paleogene palaeogeography and basin evolution of the Western Carpathians, Northern Pannonian domain and adjoining areas. *Global and Planetary Change, 140*, 9–27.

Köhler, E. (1995). *Paleocénny rífový komlex v Západných Karpatoch. Doctoral Dissertation*. Bratislava: Geological Institute of the Slovak Academy of Sciences.

Kulka, A. (1985). Arni sedimentological model in the Tatra Eocene. *Geological Quarterly, 29*, 31–64.

Le Gall, L., Payri, C. E., Bittner, L., & Saunders, G. W. (2010). Multigene phylogenetic analyses support recognition of the Sporolithales ord. nov. *Molecular Phylogenetics and Evolution, 54*, 302–305.

Lemoine, P. (1934). Algues calcaires de la famille des Coralinacées recueillies dans les Carpathes occidentales par M.D. Andrusov. *Věstník Státního Geologického Ústavu ČSR, 9*, 269–289.

Littler, M. M., Littler, D. S., Blair, S. M., & Norris, J. N. (1985). Deepest known plant life discovered on an uncharted seamount. *Science, 227*, 57–59.

Marshalko, R. (1970). The research of sedimentary textures, structures, and palaeocurrent analysis of basal formations (Central Western Carpathian Paleogene, N of Spišsko-gemerské rudohorie Mts.). *Acta Geologica et Geographica Universitatis Comenianae, 19*, 129–163.

Masotti, I., Aparicio-Rizzo, P., Yevenes, M. A., Gerreaud, R., Belmar, L., & Farias, L. (2018). The influence of river discharge on nutrient export and phytoplankton biomass off the Central Chile Coast (33°-37°S): seasonal cycle and interannual variability. *Frontiers in Marine Science, 5*, 423.

Mišík, M. (1966). *Microfacies of the Mesozoic and Tertiary Limestones of the West Carpathians*. Bratislava: Vydavateľstvo Slovenskej Akademie Vied.

Moussavian, E. (1989). Taxonomische Untersuchungen an "Amphiroa" propria Lemoine (Corallinaceae/Rhodophyta; Maastricht-Thanet). *Münchener Geowissenschaftliche Abhandlungen, 15*, 41–54.

Nelson, C. S., Keane, S. L., & Head, P. S. (1988). Non-tropical carbonate deposits on the modern New Zealand shelf. *Sedimentary Geology, 60*, 71–94.

Nelson, W. A., Sutherland, J. E., Farr, T. J., Hart, D. R., Neill, K. F., Jeong Kim, H., & Su Yoon, H. (2015). Multigene phylogenetic analyses of New Zealand Coralline Algae: *Corallinapetra novozelandiae* gen. et sp. nov. and recognition of the Hapalidiales ord. nov. *Journal of Phycology, 51*, 454–468.

Nielsen, K., Svensson, S., Nielsen, J. K., & Bromley, R. G. (2003). Palaeoecological and ichnological significance of microborings in Quaternary Foraminifera. *Palaeontologica Electronica, 6*(2), 13.

Olszewska, B. W., & Wieczorek, J. (1998). The Paleogene of the Podhale Basin (Polish Inner Carpathians) – micropaleontological perspective. *Przegląd Geologiczny, 46*, 721–728.

Oszczypko-Clowes, M., & Żydek, B. (2012). Paleoecology of the Upper Eocene Lower Oligocene Malcov Basin based on the calcareous nannofossils: a case study of the Leluchów section (Krynica Zone, Magura Nappe, Polish Outer Carpathians). *Geologica Carpathica, 63*, 149–164.

Peña, V., Adey, W. H., Riosmena-Rodríguez, R., Jung, M. Y., Afonso-Carrillo, J., Choi, H. G., & Bárbara, I. (2011). *Mesophyllum sphaericum* sp. nov. (Corallinales, Rhodophyta): a new maërl-forming species from the northeast Atlantic. *Journal of Phycology, 47*, 911–927.

Pérès, J. M., & Picard, J. (1964). Nouveau manuel de bionomie benthique de la Mer Mèditérranée. *Recueil des Travaux de la Station Marine d Endoume-Marseille, 31*, 1–137.

Pérès, J. M. (1982). In O. Kinne (Ed.), *Marine ecology. A Comprehensive, Integrated Treatise on Life in Oceans and Coastal Waters. Volume V: Ocean Management, Part 1* (pp. 9–642). New York: A Wiley Intersience Publication. Chichester.

Pfender, J. (1926). Sur les organisms du Nummulitique de la colline de San Salvador près Camarasa. *Boletín de la Real Sociedad Española de Historia Natural, 26*, 321–330.

Pisera, A. (1985). Paleoecology and lithogenesis of the Middle Miocene (Badenian) algal-vermetid reefs from the Roztocze Hills, southeastern Poland. *Acta Palaeontologica Polonica, 35*, 89–155.

Rasser, M. (1994). Facies and palaeoecology of rhodoliths and acervulinid macroids in the Eocene of the Krappfeld (Austria). *Beiträge zur Paläontologie, 19*, 191–217.

Rasser, M. (2001). Paleoecology and Taphonomy of *Polystrata alba* (Red Alga) from the Late Eocene Alpine Foreland: A New Tool for the Reconstruction of Sedimentary Environments. *Palaios, 16*, 601–607.

Rasser, M., & Piller, W. E. (1994). Re-documentation of Paleocene coralline algae of Austria, described by Lemoine (1930). *Beiträge zur Paläontologie, 19*, 219–225.

Rasser, M., & Piller, W. E. (1999). Application of neontological taxonomic concepts to Late Eocene coralline algae (Rhodophyta) of the Austrian Molasse Zone. *Journal of Micropalaeontology, 18*, 67–80.

Roduit, N. (2001) *JMicrovision: Image analysis toolbox for measuring and quantifying components of high-definition images. Version 1.3.1*. https://jmicrovision.github.io (accessed 10 December 2019).

Rösler, A., Perfectti, F., Peña, V., & Braga, J. C. (2016). Phylogenetic relationships of Corallinaceae (Corallinales, Rhodophyta): taxonomic implications for reef-building corallines. *Journal of Phycology, 52*, 412–431.

Samuel, O., & Fusán, O. (1992). Reconstruction of subsidence and sedimentation of Central Carpathian Paleogene. *Západné Karpaty, Séria Geológia, 16*, 7–46. [in Slovakian with English summary]

Samuel, O., Borza, K., & Köhler, E. (1972). *Microfauna and Lithostratigraphy of the Paleogene and adjacent Cretaceous of the Middle Váh Valley (West Carpathian)*. Bratislava: Geologický Ústav Dionýza Štúra.

Sarkar, S., & Rao, G. M. N. (2018). Coralline red algae from late Palaeocene – earliest Eocene carbonates of Maghalaya, N – E India: palaeocommunity and trophic-level implications. *Carbonates and Evaporites, 33*, 767–781.

Schaleková, A. (1962). *Fytogénne vápence mezozoika a terciéru Slovenska. Dissertation*. Bratislava: Comenius University.

Schaleková, A. (1963). Die Algenfloren der Kretazischen und Paläogenen Kalksteine der Slowakei. *Geologický Sborník, 14*, 165–167.

Schaleková, A. (1964). New informations on the calcareous algae in the bioherm limestones of the Paleocene-Eocene in the Western and Central Slovakia. *Geologický Sborník, 15*, 57–73.

Schneider, J. (1976). *Contributions to Sedimentary Geology 6: Biological and inorganic factors in the destruction of limestone coasts*. Stuttgart: E. Schweizerbart'sche Verlagsbuchhandlung.

Seneš, J., & Ondrejčíková, A. (1991). Proposal for the terminology of fossil marine benthic shelf ecosystems. *Geologica Carpathica, 42*, 231–240.

Shweta, S. G., & Kantimati, G. K. (2018). Natural casts of Early Eocene Entobia from the Kachchh Basin, India. *Ichnos, 25*(4), 261–268.

Silva, P. C., & Johansen, H. W. (1986). A reappraisal of the Order Corallinales (Rhodophyceae). *British Phycological Journal, 21*, 245–254.

Sliva, Ľ. (2005). *Sedimentary facies of the Central Carpathian Paleogene Basin from Spišská Magura. Dissertation*. Bratislava: Department of Geology and Paleontology – Faculty of Natural Sciences CU. [in Slovakian]

Smith, R. L. (1992). Coastal upwelling in the modern ocean. In C. P. Summerhayes, W. L. Prell, & K. C. Emeis (Eds.), *Upwelling Systems: Evolution Since the Early Miocene* (pp. 9–28). London: The Geological Society.

Sola, F., Braga, J. C., & Aguirre, J. (2013). Hooked and tubular coralline algae indicate seagrass beds associated to Mediterranean Messinian reefs (Poniente Basin, Alméria, SE Spain). *Palaeogeography, Palaeoclimatology, Palaeoecology, 374*, 218–229.

Soták, J. (1998). Sequence stratigraphy approach to the Central Carpathian Paleogene (Eastern Slovakia): eustasy and tectonics as controls of deep-sea fan deposition. *Slovak Geological Magazine, 4*, 185–190.

Soták, J. (2010). Paleoenvironmental changes across the Eocene-Oligocene boundary: insights from the Central-Carpathian Paleogene Basin. *Geologica Carpathica, 61*, 393–418.

Soták, J., Pereszlenyi, M., Marschalko, R., Milička, J., & Starek, D. (2001). Sedimentology and hydrocarbon habitat of the submarine-fan deposits of the Central Carpathian Paleogene Basin (NE Slovakia). *Marine and Petroleum Geology, 18*, 87–114.

Soták, J., Gedl, P., Banská, M., & Starek, D. (2007). New stratigraphic data from the Paleogene formations of the Central Western Carpathians at the Orava region: results of integrated micropaleontological study in the Pucov section. *Mineralia Slovaca, 39*, 89–106. [in Slovakian with English summary]

Starek, D., & Fuksi, T. (2017a). Distal turbidite fan/lobe succession of the Late Oligocene Zuberec Fm. - architecture and hierarchy (Central Western Carpathians, Orava-Podhale basin). *Open Geosciences, 9*, 385–406.

Starek, D., & Fuksi, T. (2017b). Statistical analysis as a tool for identification of depositional palaeoenvironments in deep-sea fans (Palaeogene formations, Central Western Carpathians, north Slovakia). *Acta Geologica Slovaca, 9*, 149–162.

Starek, D., Andreyeva-Grigorovich, A. S., & Soták, J. (2000). Suprafan deposits of the Biely Potok Formation in the Orava region: sedimentary facies and nannoplankton distribution. *Slovak Geological Magazine, 6*, 188–190.

Starek, D., Sliva, L., & Vojtko, R. (2004). The channel-levee sedimentary facies and their synsedimentary deformation: a case study from Huty Formation of the Podtatranská skupina Group (Western Carpathians). *Slovak Geological Magazine, 10*, 177–182.

Starek, D., Sliva, Ľ., & Vojtko, R. (2012). Eustatic and tectonic control on late Eocene fan-delta development (Orava Basin, Central Western Carpathians). *Geological Quarterly, 56*(1), 67–84.

Starek, D., Soták, J., Jablonský, J., & Marschalko, R. (2013). Large-volume gravity flow deposits in the Central Carpathian Paleogene Basin (Orava region, Slovakia): evidence for hyperpyclan river discharge in deep-sea fans. *Geologica Carpathica, 64*, 305–326.

Starek, D., Šimo, V., Antolíková, S., & Fuksi, T. (2019). Turbidite sedimentology, biostratigraphy and paleoecology: a case study from the Oligocene Zuberec Fm. (Liptov Basin, Central Western Carpathians). *Geologica Carpathica, 70*, 279–297.

Steneck, R. S. (1986). The Ecology of Coralline Algal Crusts: convergent patterns and adaptative strategies. *Annual Review of Ecology, Evolution, and Systematics, 17*, 273–303.

Steneck, R. S., Hacker, S. D., & Dethier, M. N. (1991). Mechanisms of competitive dominance between crustose coralline algae: an herbivore-mediated competitive reversal. *Ecology, 72*, 938–950.

Steneck, R. S., & Detheir, M. N. (1994). A functional group approach to the structure of algal-dominated communities. *OIKOS, 69*, 476–498.

Steinmetz, J. C. (1979). Calcareous nannofossils from the North Atlantic Ocean, Leg 49, deep sea drilling project. *Deep Sea Drilling Project Initial Reports, 49*, 519–531.

Šurka, J., Sliva, Ľ., & Soták, J. (2012). Facial development of the Borové Formation in the area of Biely Potok at the town of Ružomberok and at Komjatná village (Western Carpathians, Slovakia). *Mineralia Slovaca, 44*, 267–278.

Teichert, S., Woelkerling, W., Rüggeberg, A., Wisshak, M., Piepenburg, D., Meyerhöfer, M., Form, A., Büdenbender, J., & Freiwald, A.

(2012). Rhodolith beds (Corallinales, Rhodophyta) and their physical and biological environment at 80°31' N in Nordkappbukta (Nordaustlandet, Svalbard Archipelago, Norway). *Phycologia, 54*, 371–390.

Temelkov, B., & Andreev, T. (2005). *Recent Bivalve ecology applied to the reconstruction of paleocommunities*. Proceedings of the Balkan Scientific Conference of Biology in Plovdiv (Bulgaria) from 19th till 21st May 2005, 436–442.

Townsend, R. A., Chamberlain, Y. M., & Keats, D. W. (1994). *Heydrichia woelkerlingii* gen. et sp. nov., a newly discovered non-geniculate red alga (Corallinales, Rhodophyta) from Cape Province, South Africa. *Phycologia, 33*, 177–186.

Tribollet, A., Radtke, G., & Golubic, S. (2011). Bioerosion. In J. Reitner & V. Thiel (Eds.), *Encyclopedia of Geobiology* (pp. 117–134). Dordrecht: Springer.

Verheij, E. (1993). The genus *Sporolithon* (Sporolithaceae fam. nov., Corallinales, Rhodophyta) from the Spermonde Archipelago, Indonesia. *Phycologia, 32*, 184–196.

Villa, G., Fioroni, C., Pea, L., Bohaty, S., & Persico, D. (2008). Middle Eocene—late Oligocene climate variability: Calcareous nannofossil response at Kerguelen Plateau, Site 748. *Marine Micropaleontology, 69*, 173–192.

Vokes, H. E. (2017). A new species of *Spondylus* (Mollusca, Bivalvia) from the Eocene of Alabama. *Tulane Studies in Geology and Paleontology, 23*, 127–129.

Wai, T.-C., & Williams, G. A. (2006). Effect of grazing on coralline algae in seasonal, tropical, low-shore rock pools: spatio-temporal variation in settlement and persistence. *Marine Ecology Progress Series, 326*, 99–113.

Wei, W., & Wise Jr., S. W. (1990). Biogeographic gradients of Middle Eocene-Oligocene calcareous nannoplankton in the South Atlantic Ocean. *Palaeogeography, Palaeoclimatology, Palaeoecology, 79*, 29–61.

Westwalewicz-Mogilska, E. (1986). A new look at the genesis of the Podhale Flysh. *Przegląd Geologiczny, 34*, 690–698. [in Polish with English summary]

Wieczorek, J. (1989). The Hecho model for Podhale flysh? *Przegląd Geologiczny, 37*, 419–422. [in Polish]

Wilson, S. T., Hawco, N. J., Armbrust, E. V., Barone, B., Björkman, K. M., Boysen, A. K., Burgos, M., Burrell, T. J., Casey, J. R., DeLong, E. F., Dugenne, M., Dutkiewicz, S., Dyhrman, S. T., Ferrón, S., Follows, M. J., Foreman, R. K., Funkey, C. P., Harke, M. J., Henke, B. A., Hill, C. N., Hynes, A. M., Ingalls, A. E., Jahn, O., Kelly, R. L., Knapp, A. N., Letelier, R. M., Ribalet, F., Shimabukuro, E. M., Tabata, R. K. S., Turk-Kubo, K. A., White, A. E., Zehr, J. P., John, S., & Karl, D. M. (2019). Kilauea lava fuels phytoplankton bloom in the North Pacific Ocean. *Science, 365*, 1040–1044.

Wisshak, M. (2012). Microbioerosion. In D. Knaust & R. G. Bromley (Eds.), *Trace Fossils as Indicators of Sedimentary Environments: Developments in Sedimentology 64* (pp. 231–243). Amsterdam: Elsevier.

Woelkerling, W. J., & Harvey, A. (1992). *Mesophyllum incisum* (Corallinaceae, Rhodophyta) in Southern Australia: Implications for generic and specific delimitation in the melobesioideae. *Brithish Phycological Journal, 27*, 381–399.

Woelkerling, W. J., & Harvey, A. (1993). An account of Southern Australia Species of *Mesophyllum* (Corallinaceae, Rhodophyta). *Australian Systematic Botoany, 6*, 571–637.

Woelkerling, W. J., Irvine, L. M., & Harvey, A. S. (1993). Growth-forms in Non-geniculate Coralline Red Algae (Corallinales, Rhodophyta). *Australian Systematic Botoany, 6*, 277–293.

Wright, V. P. (1992). A revised classification of limestones. *Sedimentary Geology, 76*, 177–185.

Young, J. R., Bown, P. R., Lees, J. A. (2019). *Nannotax3 website. International Nannoplankton Association*. URL: http://www.mikrotax.org/Nannotax3

Zágoršek, K. (1992). Priabonian (Late Eocene) Cyclostomata Bryozoa from the Western Carpathians (Czecho-Slovakia). *Geological Carpathica, 43*, 235–247.

Zágoršek, K. (1996). Eocene Coilostega Bryozoa from the Western Carpathians (Slovakia). *MIneralia Slovaca, 28*, 523–534.

Zágoršek, K. (1997). Eocene Anascan Bryozoa from new localities in the Western Carpathians, Slovakia. *Geologica Carpathica, 48*, 401–409.

Zágoršek, K., & Kázmér, M. (1999). Late Eocene Bryozoan faunas in the Alpine-Carpathian region – a comparison. *Acta Paleontologica Romaniae, 2*, 493–504.

Zágoršek, K., & Vávra, N. (2000). A New method for the extraction of Bryozoans from hard rocks from the Eocene of Austria. *Jahrbuch der Geologischen Bundesanstalt, 142*(2), 249–258.

Zágoršek, K., Holcová, K., & Trasoň, T. (2008). Bryozoan event from Middle Miocene (Early Badenian) lower neritic sediments from the locality Kralice and Oslavou (Central Paratethys), Moravia part of the Carpathian Foredeep. *International Journal of Earth Sciences, 97*, 835–850.

Žuljević, A., Kaleb, S., Peña, V., Despalatović, M., Cvitković, I., De Clerck, O., Le Gall, L., Falace, A., Vita, F., Braga, J. C., & Antolić, B. (2016). First freshwater coralline alga and the role of local features in a major biome transition. *Scientific Reports, 6*, 19642.